

**WIRELESS BROADBAND  
SINGLE-CARRIER SYSTEMS  
WITH MMSE TURBO  
EQUALIZATION RECEIVERS**

**KIMMO  
KANSANEN**

Faculty of Technology,  
Department of Electrical and  
Information Engineering,  
University of Oulu

OULU 2005





*KIMMO KANSANEN*

**WIRELESS BROADBAND SINGLE-  
CARRIER SYSTEMS WITH MMSE  
TURBO EQUALIZATION RECEIVERS**

Academic Dissertation to be presented with the assent of  
the Faculty of Technology, University of Oulu, for public  
discussion in Raahensali (Auditorium L10), Linnanmaa,  
on December 12th, 2005, at 9 a.m.

OULUN YLIOPISTO, OULU 2005

Copyright © 2005  
University of Oulu, 2005

Supervised by  
Professor Tadashi Matsumoto

Reviewed by  
Professor Ralf Müller  
Professor Xiaodong Wang

ISBN 951-42-7932-8 (nid.)  
ISBN 951-42-7933-6 (PDF) <http://herkules.oulu.fi/isbn9514279336/>  
ISSN 0355-3213 <http://herkules.oulu.fi/issn03553213/>

OULU UNIVERSITY PRESS  
OULU 2005

# **Kansanen, Kimmo, Wireless broadband single-carrier systems with MMSE turbo equalization receivers**

Faculty of Technology, University of Oulu, P.O.Box 4000, FIN-90014 University of Oulu, Finland,  
Department of Electrical and Information Engineering, University of Oulu, P.O.Box 4500, FIN-  
90014 University of Oulu, Finland

2005

Oulu, Finland

## ***Abstract***

Broadband single-carrier modulated signals experience severe multipath distortion when propagating through the physical medium. Correcting the distortion with channel equalization is the foremost task of the detector. Prior information about the transmitted signals in the form of channel decoder feedback can significantly enhance equalization accuracy. An algorithm that iteratively performs channel decoding and equalization with prior information is generally denoted a turbo equalizer. This thesis focuses on turbo equalization with prior information using the principle of interference cancellation followed by minimum mean squared error (MMSE) filtering. Receiver algorithms, receiver convergence, and coding and modulation in the context of MMSE turbo equalization are studied.

Computationally efficient versions of the receiver algorithm through approximate time-average filtering, matched filtering, square-root time-variant filtering and frequency-domain filtering are studied. The frequency-domain turbo equalizer (FDTE) is found to exhibit both superior convergence and low computational complexity among the compared equalizer algorithms.

Multi-dimensional extrinsic information transfer (EXIT) charts are introduced for the purpose of tracking the convergence of the turbo equalization of layered MIMO transmissions. Generic properties of the equalizer EXIT functions defining the equalizer convergence are analyzed. The principles for detector ordering, maximum sum-rate code design and maximum rate symmetric design are derived from the properties of the multidimensional EXIT functions.

Semi-analytical EXIT charts are developed for the convergence analysis of the FDTE. The effects of channel parameters and the channel code are analyzed with semi-analytical methods. A new approach for the design of irregular low-density parity-check (LDPC) codes using a convergence outage principle is proposed. A performance gain is demonstrated in a single-input multiple output (SIMO) channel over non-optimized regular LDPC codes and irregular LDPC codes optimized for the AWGN channel. The outage convergence based design, which takes advantage of the semi-analytical convergence analysis method, is also extended to layered MIMO transmissions.

Quadrature amplitude modulation using multilevel bit-interleaved coded modulation (MLBICM) is studied as an alternative to regular bit-interleaved coded modulation (BICM) for highly bandwidth-efficient transmission in MMSE turbo equalized systems. A linear bit-to-symbol mapping is introduced that enables the use of a computationally efficient MMSE turbo equalizer at the receiver. The proposed coded modulation is compared with BICM in channel measurement data based simulations and found to exhibit superior robustness against changes in spatial channel parameters. An automatic repeat request (ARQ) configuration using one ARQ controller for each equally performing group of code levels is proposed. The configuration takes advantage of the unequal error protection (UEP) property of the coded modulation. The semi-analytical convergence analysis is extended to the multilevel modulated case and applied in a channel measurement based convergence evaluation. The construction of the MLBICM is found to have an inherently better convergence behavior than BICM. Finally, the outage convergence based channel code design is extended to the layered MIMO multilevel signalling case.

*Keywords:* convergence analysis, equalization, fading channels, MIMO, multilevel coding



*To Oili, Omppu and Masse*



## Preface

This work has been conducted at the telecommunications laboratory and Centre for Wireless Communications (CWC), University of Oulu, Finland. I was accepted to the laboratory to write my diploma thesis on multiuser detectors for CDMA with two persons now professors, Markku Juntti and Matti Latva-aho. I want to thank them and Prof. Pentti Lappänen for giving me the opportunity to work in the laboratory which has evolved into the exceptional research unit for wireless communications it is now.

After graduation I continued working on CDMA multiuser detection with Prof. Juntti. During that time I learnt to value his advice. When Tadashi Matsumoto arrived in Oulu we soon realized so much common interests in research that he became my thesis supervisor. His encouragement and enthusiasm provided me with the necessary push to complete the work in this thesis. His commitment to his work and his personal efforts to bring it forward are seconded by no-one I know. I want to thank the two reviewers of my thesis, Prof. Ralf Müller from Norwegian University of Science and Technology, Trondheim, Norway, and Prof. Xiaodong Wang, Columbia University, New York, United States for their thorough work and the thoughtful comments that helped improve the quality of manuscript considerably in some important parts. I am also grateful to Zach Shelby for proofreading the manuscript.

A number of colleagues have been invaluable both in scientific and work related matters, as well as in maintaining my sanity during the work. Kari Hooli, with whom I shared a room for years, deserves a warm thank you both as a friend and as a model of work ethic and self-discipline. Djordje Tujkovic deserves a thank you for his friendship, but also for showing that impossible things are merely hard. I have enjoyed the time working with Esa Kunnari, Nenad Veselinovic, Mariella Särestöniemi and Juha Karjalainen, as well as the discussions with Prof. Keijo Ruotsalainen, the mathematician to call when you need one. I have had the pleasure to guide the diploma thesis of Fan Jianke and Kai Kiiskilä. It has also been a pleasure to co-operate with Christian Schneider from Reiner Thomä's group at TU Ilmenau, Germany, and Benjamin Ng from Dave Falconer's group at Carleton University, Ottawa, Canada. The supporting efforts of Jari Sillanpää, Timo Äikäs, Pirjo Kumpumäki, Pekka Nissinaho, Hanna Saarela and Elina Komminaho have made life and work relatively painless, if such a thing is possible at a university. All of the staff at telecommunication laboratory and CWC receive a warm thanks for the friendly work environment. I have been here since 1997 and have yet to see a grumpy face being maintained for very long. From

the side of industrial sponsors, discussions with Kari Horneman, Jukka-Pekka Nuutinen, Jaakko Vihriälä and Jorma Lilleberg have been inspiring and informative.

This work was funded by the Academy of Finland, Elektrobit, the European Union, Finnish Defence Forces, Instrumentointi, Nokia and the National Technology Agency of Finland (Tekes). The further financial support of Infotech Oulu graduate school, Tekniikan edistämissäätiö, Tauno Tönningin säätiö, Nokia Oyj:n säätiö and Jenny ja Antti Wihurin rahasto is gratefully acknowledged.

While working with this thesis I have found that I have a desire to have things done right, and have hopefully improved on actually doing that in the course of work. I can also clearly see that I have inherited this desire from my parents. When seeing this thesis, I hope they will get a warm fuzzy feeling of proudness in return for all they have given me.

Finally, my family deserves the greatest acknowledgement. Our children Oili and Osmo have time and again disconnected me from any thesis related worries the moment I come home. Their unconditional affection is heart-warming and their company has taught me some of the small wonders of the world I have forgotten. Our furry family members never fail to greet me with enthusiasm. All of this is held together by my loving wife Masse, who has yet to complain about my working habits. Her support has been my solid ground to stand on.

Oulu, November 9th 2005

Kimmo Kansanen

## Symbols and abbreviations

$a_{V(i)}$	ratio of variable nodes of degree $d_{V(i)}$
$b_{k,m}(n)$	$m$ th encoded bit of $n$ th symbol on transmit antenna $k$
$\mathbf{b}_k(n)$	vector of encoded bits within the $n$ th symbol of transmit antenna $k$ ( $M \times 1$ )
$\mathbf{b}_k$	vector of encoded bits within transmitted frame of transmit antenna $k$ ( $MN \times 1$ )
$\mathbf{b}$	vector of encoded bits within transmitted frame ( $KMN \times 1$ )
$\bar{b}_{s_i}(m)$	$m$ th bit of the bit vector mapped to symbol $s_i$
$B$	symbol mapper
$\mathbf{B}_k$	diagonal matrix with $ \hat{s}_k(n) $ , $n \in \{1 \dots N\}$ on the diagonal ( $N \times N$ )
$\mathcal{B}^{-1}$	symbol de-mapping function
$\mathcal{B}$	symbol estimation function
$c_i$	check node decoder $i$
$\mathbb{C}$	set of complex numbers
$C_{\text{MAC}}$	multiple access capacity
$C_{UI}$	uniform input channel capacity
$\mathcal{C}_k$	convergence set of transmit antenna $k$
$C_B(\mu_{k,a}, B)$	Constellation constrained capacity of constellation used by the mapper $B$
$C_{B_k^j}(\mu_{k,a}, B)$	Constellation constrained capacity of a sub-constellation of mapper $B$ when the $j$ th bit takes on the value $k \in \{-1, 1\}$
$\mathcal{C}_0$	point of EXIT set corresponding to no prior information
$\mathcal{C}_1$	point of EXIT set corresponding to full prior information
$\mathcal{C}_k^0$	subset of EXIT set corresponding to no prior information of transmission $k$
$\mathcal{C}_k^1$	subset of EXIT set corresponding to full prior information on transmission $k$
$d_C$	check node degree

$d_{V^{(i)}}$	variable node degree $i$
$\mathbf{D}_k$	diagonal matrix with $\alpha_k(n)$ , $n \in \{1 \dots N\}$ on the diagonal ( $N \times N$ )
$\mathbb{E}$	set of real numbers in range $[0, 1]$
$E_b/N_0$	bit energy per noise power ratio
$E_b/N_0^*$	estimated bit energy per noise power ratio threshold where the LDPC code reaches design outage
$f$	frequency index
$f_d$	EXIT function of decoder giving the mutual information of decoder input that results in a given mutual information of decoder extrinsic output
$f_d^q$	EXIT function of decoder for code level $q$ giving the mutual information of decoder input that results in a given mutual information of decoder extrinsic output
$f_e$	EXIT function of equalizer giving the mutual information of equalizer extrinsic output given the corresponding mutual information of equalizer prior information input
$f_e^q$	EXIT function of equalizer giving the mutual information of equalizer extrinsic output for code level $q$ given the corresponding mutual information of equalizer prior information input
$\mathbf{f}_d$	vector EXIT function of decoder ( $K \times 1$ )
$\mathbf{f}_e$	vector EXIT function of equalizer ( $K \times 1$ )
$f_{d,\text{opt}}$	EXIT function of an optimal code
$f_{e,o_k}({}^0\mathbf{I}_d(I_{d,o_k}))$	order-projected EXIT function of antenna indicated by ordering index $o_k$ given full knowledge of all preceding antennas in the ordering
$f_{e,k}(g_p)$	EXIT function of antenna $k$ along the path defined by the curve $g_p$
$f_{g_p,k}(I_{d,k})$	the function giving the value of $f_{e,k}$ along the path $g_p(t)$ as projected to the dimension $I_{d,k}$
$f_C$	EXIT function of LDPC check node decoders
$f_V$	EXIT function of LDPC variable node decoders
$f_{V,e}$	combined EXIT function of equalizer and LDPC variable node decoders
$\mathbf{F}$	DFT/FFT transform matrix ( $N \times N$ )
$\mathbf{F}_K$	block DFT/FFT matrix with $K N \times N$ diagonal blocks ( $KN \times KN$ )
$\mathcal{F}_{cdf}(I_d, I)$	cumulative distribution function of EXIT function values with prior information $I_d$
$\mathcal{F}_{cdf}^q(\mathbf{I}_d, I)$	cumulative distribution function of EXIT function values with prior information $I_d$ for code level $q$
$g_d(t)$	a multidimensional “diagonal” spatial curve, whose points at each point $t$ are equally distant from all basis
$g_p(t)$	a multidimensional spatial curve denoting the curve of convergence of an optimized system through the EXIT space $\mathbb{E}^K$ from $\mathcal{C}^0$ to $\mathcal{C}^1$
$h_{k,j,l}(n)$	channel response of $l$ th multipath between transmit and receive an-

	tennas $k$ and $j$ for the $n$ th symbol
$\mathbf{h}_{k,j}(n)$	multipath channel response vector between transmit and receive antennas $k$ and $j$ for the $n$ th symbol ( $L \times 1$ )
$\bar{\mathbf{h}}_{k,j}(n)$	zero-padded multipath channel response vector between transmit and receive antennas $k$ and $j$ for the $n$ th symbol ( $(N + L - 1) \times 1$ )
$\mathbf{H}_{k,j}$	channel matrix between transmit antenna $k$ and receive antenna $j$ for one frame ( $(N + L - 1) \times N$ )
$\mathbf{H}_k$	channel matrix between transmit antenna $k$ and all receive antennas for one frame ( $(J(N + L - 1) \times N$ )
$\mathbf{H}$	channel matrix ( $(J(N + L - 1) \times KN$ )
$\mathbf{H}_{c,k}$	block-circulant channel matrix between transmit antenna $k$ and all receive antennas for one frame ( $JN \times N$ )
$\mathbf{H}_c$	block-circulant channel matrix ( $JN \times KN$ )
$\tilde{h}_{k,j}(f)$	channel response at frequency $f$ between transmit and receive antennas $k$ and $j$
$\mathbf{h}_k(n)$	channel vector for symbol $n$ ( $(J(N + L - 1) \times 1$ )
$\mathbf{H}'$	channel matrix with spatially uncorrelated entries ( $(J(N + L - 1) \times KN$ )
$\mathbf{I}^K$	identity matrix ( $K \times K$ )
$\mathbf{I}_d$	decoder extrinsic output mutual information vector ( $K \times 1$ )
$\mathbf{I}_{d,q}$	decoder extrinsic output mutual information vector for code level $q$ ( $K \times 1$ )
$I_{e,q}(\mathbf{I}'_d   \mathbf{H}_A)$	equalizer extrinsic output mutual information vector for code level $q$ given channel matrix $\mathbf{H}_A$ ( $K \times 1$ )
$\mathcal{I}(\cdot; \cdot)$	mutual information between arguments
$I_{d,k}$	mutual information between decoder $k$ extrinsic information output and transmitted encoded bits of transmit antenna $k$
$I_{e,k}$	mutual information between equalizer (de-mapper) output and transmitted encoded bits of transmit antenna $k$
$I'_{e,k}$	mutual information between equalizer (de-mapper) output and transmitted encoded bits of transmit antenna $k$ at fixed point of detector iteration
$I'_{a,k}$	mutual information between decoder <i>a posteriori</i> likelihoods on encoded bits and transmitted encoded bits of transmit antenna $k$ at fixed point of detector iteration
$I'_{a,k,GAD}$	mutual information between decoder <i>a posteriori</i> likelihoods on encoded bits and transmitted encoded bits of transmit antenna $k$ given full prior information
$I_{\text{th}}$	threshold mutual information to reach a desired performance
$\bar{\mathbf{I}}_d$	vector of basis vectors in the EXIT-space $\mathbb{E}$ ( $K \times 1$ )
$I_V$	mutual information at the output of LDPC variable node decoders
$I_C$	mutual information at the output of LDPC check node decoders

$\mathbf{I}_d^0(I_{d,k})$	shorthand for $\mathbf{I}_d = [\mathbf{1}^{k-1}, I_{d,k}, \mathbf{0}^{K-k}]$ signifying full prior information on preceding $k - 1$ transmissions, prior information $I_{d,k}$ for the desired $k$ th transmission, and no prior information on the last $K - k$ transmissions
$\mathbf{I}_d^0(I_{d,o_k})$	corresponding notation with absolute indexes replaced by the ordered indexes
$\mathbf{I}_d^0(I_{d,k})$	corresponding notation with no prior information on other transmissions
$\mathbf{I}_d^1(I_{d,k})$	corresponding notation with full prior information on other transmissions
$j$	receive antenna index
$j$	imaginary unit
$J$	number of receive antennas
$\mathbf{J}$	EXIT function Jacobian at some point in the EXIT set $\mathbb{E} (K \times K)$
$\mathcal{J}$	function giving the mutual information between a binary random variable and its likelihood at the output of an AWGN channel
$k$	transmit antenna index
$K$	number of transmit antennas
$l$	channel multipath index
$L$	number of channel multipaths between each pair of transmit and receive antennas
$L_{k,s_i}^e(n)$	likelihood of symbol hypothesis $s_i$ for symbol $n$ of transmit antenna $k$
$\mathcal{L}_{k,q,a}$	effective SNR of the frequency-domain MMSE turbo equalizer signal estimate for multilevel coding level $q$ of transmit antenna $k$
$\mathcal{L}_{k,a}$	effective SNR of equivalent Gaussian channel at the output of the frequency-domain MMSE turbo equalizer
$\mathcal{L}_k$	effective SNR of the $k$ th transmit antenna signal estimate
$\mathcal{L}_k^{[GAD]}$	effective SNR of the $k$ th transmit antenna signal estimate with perfect prior information on all signals
$m$	bit index within a symbol
$M$	number of bits per symbol
$n$	symbol index
$N$	frame length in symbols
$N_{prefix}$	cyclic prefix length in symbols
$\bar{o}$	ordering vector containing a permutation of indexes $1 \dots K (K \times 1)$
$\bar{o}_k$	vector containing the first $k$ indexes of the ordering vector $\bar{o} (k \times 1)$
$P_a$	<i>a priori</i> probability
$P(\xi_k^d b)$	conditional probability of decoder extrinsic output log-likelihood ratios given transmitted encoded bit
$P_{out}$	outage probability

$\mathbf{P}_{k,k'}$	inner product matrix between signal eigenbases $\Phi_k$ and $\Phi_{k'}$ ( $N \times N$ )
$\mathcal{P}$	power allocation strategy
$Q$	number of code levels in multilevel code
$\mathcal{Q}$	feasible set of power allocation strategies
$\mathbf{r}$	received signal vector ( $J(N + L - 1) \times 1$ )
$\tilde{\mathbf{r}}$	residual after interference cancellation ( $J(N + L - 1) \times 1$ )
$\tilde{\mathbf{r}}$	residual after interference cancellation for multilevel coded transmission ( $J(N + L - 1) \times 1$ )
$\check{\mathbf{r}}$	residual after cancellation and addition of stabilizing noise ( $J(N + L - 1) \times 1$ )
$\bar{\mathbf{r}}(n)$	residual pre-filtered with previous step ( $n - 1$ ) covariance inverse estimate
$R$	channel code rate
$R_k$	channel code rate of transmission $k$
$\mathbf{R}$	channel code rate vector
$\mathbb{R}$	set of real numbers
$\mathbb{R}_+$	set of non-negative real numbers
$S$	set of complex symbol points in the symbol mapping $B$
$S_1^m$	set of complex symbol points in $S$ having the $m$ th bit "1"
$S_{-1}^m$	set of complex symbol points in $S$ having the $m$ th bit "-1"
$s_i$	$i$ th element in the set $S$
$s_k(n)$	transmitted symbol $n$ of transmit antenna $k$
$\mathbf{s}_k$	vector of transmitted symbols within a frame for transmit antenna $k$ ( $N \times 1$ )
$\mathbf{s}$	vector of transmitted symbols within a frame ( $KN \times 1$ )
$\underline{s}_k(n)$	MLBICM symbol of transmit antenna $k$ for symbol interval $n$
$\underline{\mathbf{s}}_k$	MLBICM symbol vector for the frame of transmit antenna $k$ ( $N \times 1$ )
$\underline{\mathbf{s}}$	MLBICM symbol vector for the frame ( $KN \times 1$ )
$\mathcal{S}$	subset of transmitters
$T$	symbol duration
$\mathbf{u}_k(n)$	residual filter for transmit antenna $k$ symbol $n$
$\mathbf{u}_k^{[\text{MF}]}$	residual filter of matched filter approximation for transmit antenna $k$ symbol $n$
$\mathbf{u}_k^{[\text{TA}]}$	residual filter of time average approximation for transmit antenna $k$ symbol $n$
$\underline{\mathbf{u}}_k(n)$	residual filter for transmit antenna $k$ symbol $n$ common to all levels of multilevel coding
$\mathbf{U}(n)$	inverse of residual covariance matrix $\Sigma_{\tilde{\mathbf{r}}}(n)$
$\mathbf{U}_p$	matrix containing the rows and columns from the second to the last in $\mathbf{U}(n)$

$\mathbf{u}_p$	vector containing the elements from the second to the last in the first column of $\mathbf{U}(n)$
$u_p$	the first element in $\mathbf{U}(n)$
$\mathbf{U}_n$	matrix containing the rows and columns from the first to the second last in $\mathbf{U}(n+1)$
$\mathbf{u}_n$	vector containing the elements from the first to the second last in the first column of $\mathbf{U}(n+1)$
$u_n$	the last element in $\mathbf{U}(n+1)$
$\mathbf{V}$	matrix of eigenvectors (eigenbasis) of the frequency-domain covariance matrix of the residual ( $JN \times JN$ )
$v_i$	variable node decoder $i$
$\mathbf{w}$	vector of noise samples ( $JN \times 1$ )
$\tilde{\mathbf{w}}$	vector of uncorrelated Gaussian noise samples used for stabilization of the iterative inverse
$w_e$	noise process of an equivalent Gaussian channel
$\mathbf{W}_p$	Cholesky factorization of $\mathbf{U}(n)$
$\mathbf{W}_f$	Cholesky factorization of $\mathbf{U}(n+1)$
$x_k(n)$	equalizer output for time instant $n$ , transmit antenna $k$
$x_{k,m}(n)$	equalizer output for time instant $n$ , transmit antenna $k$ , level $m$ of multilevel coding
$\mathbf{x}_{k,a}$	frequency-domain equalizer output vector for transmit antenna $k$
$\mathbf{z}$	linear symbol mapper for one symbol
$z_m$	linear symbol mapper weight for bit $m$
$\mathbf{Z}$	linear symbol mapper matrix for a frame
$\alpha_k(n)$	intermediate computation result in the MMSE turbo algorithm
$\alpha_k^{[\text{MF}]}$	intermediate computation result in the matched filter turbo algorithm
$\alpha_k^{[\text{TA}]}$	intermediate computation result in the time average MMSE turbo algorithm
$\underline{\alpha}_k(n)$	intermediate computation result in the MMSE turbo algorithm for multilevel coded QAM
$\beta_k(n)$	intermediate computation result in the MMSE turbo algorithm
$\beta_k^{[\text{MF}]}$	intermediate computation result in the matched filter turbo algorithm
$\beta_k^{[\text{TA}]}$	intermediate computation result in the time average MMSE turbo algorithm
$\underline{\beta}_k(n)$	intermediate computation result in the MMSE turbo algorithm for multilevel coded QAM
$\bar{\gamma}_k$	average effective SNR of prior information relative to residual filter output for the frequency-domain MMSE turbo equalizer
$\bar{\gamma}_k^{[\text{MF}]}$	average effective SNR of prior information relative to residual filter output for the frequency-domain matched filter approximation

$\bar{\gamma}_{k,o_k} \left( \begin{smallmatrix} 0 \\ 1 \end{smallmatrix} \mathbf{I}_d(I_{d,o_k}) \right)$	$\bar{\gamma}_k$ with full prior information on previous $k$ transmissions in the ordering $\bar{o}$
$\vartheta$	channel power delay profile in dB ( $L \times 1$ )
$\delta_k$	variance of symbol estimates of $k$ th transmit antenna
$\Delta$	frequency domain symbol residual covariance matrix ( $KN \times KN$ )
$\Delta_k$	$k$ th diagonal block of the symbol residual covariance matrix ( $N \times N$ )
$\eta_k(n)$	intermediate computation result vector in a square-root MMSE turbo equalizer
$\Theta$	product matrix of unitary rotation matrices
$\Lambda$	covariance matrix of symbol residual ( $KN \times KN$ )
$\bar{\lambda}_{k,q}$	average symbol residual variance for transmit antenna $k$ , multilevel coding level $q$
$\bar{\lambda}_k$	average symbol residual variance for transmit antenna $k$
$\underline{\Lambda}$	covariance matrix of the symbol residual for multilevel modulation ( $KN \times KN$ )
$\lambda_f$	forgetting factor
$\lambda_f(n)$	time-varying forgetting factor for time-step $n$
$\mu_k(n)$	expected value of equalizer output conditioned on the symbol $n$ of transmit antenna $k$ , or the amplitude of the equivalent Gaussian channel of transmit antenna $k$ at the output of the MMSE turbo equalizer
$\mu_{k,a}$	amplitude of the equivalent Gaussian channel of transmit antenna $k$ at the output of the frequency-domain MMSE turbo equalizer
$\mu_{k,q,a}$	amplitude of the equivalent Gaussian channel of the code level $q$ of transmit antenna $k$ at the output of the frequency-domain MMSE turbo equalizer
$\mu_{k,a} \left( \begin{smallmatrix} 0 \\ 0 \end{smallmatrix} \mathbf{I}_d(0) \right)$	amplitude of the equivalent Gaussian channel of transmit antenna $k$ at the output of the frequency-domain MMSE turbo equalizer with no prior information
$\mu_{k,a} \left( \begin{smallmatrix} 1 \\ 1 \end{smallmatrix} \mathbf{I}_d(1) \right)$	amplitude of the equivalent Gaussian channel of transmit antenna $k$ at the output of the frequency-domain MMSE turbo equalizer with full prior information on all transmissions
$\mu_{o_k,a} \left( \begin{smallmatrix} 1 \\ 1 \end{smallmatrix} \mathbf{I}_d(I_{d,o_k}) \right)$	amplitude of the equivalent Gaussian channel of transmit antenna $k$ at the output of the frequency-domain MMSE turbo equalizer with full prior information on the previous $k$ transmissions in the ordering $\bar{o}$
$\nu_k(n)$	variance of equalizer output for symbol $n$
$\xi_k^e$	equalizer output (log-)likelihood information for antenna $k$
$\xi_k^d$	decoder output (log-)likelihood information for antenna $k$
$\xi_{k,m}^d(n)$	decoder output (log-)likelihood information for multilevel coded bit $m$ of antenna $k$
$\Xi_k(f)$	frequency-domain channel response matrix for frequency $f$ between transmit antenna $k$ and all receive antennas ( $J \times 1$ )

$\Xi(f)$	frequency-domain channel response matrix for frequency $f$ ( $J \times K$ )
$\Xi'$	frequency-domain channel response matrix with uncorrelated random entries ( $JN \times KN$ )
$\Pi$	interleaving
$\Pi^{-1}$	de-interleaving
$\rho_{i,j}$	receive side spatial correlation between antennas $i,j$
$\tilde{\rho}$	receive side spatial correlation exponent basis
$\varrho_{i,j}$	transmit side spatial correlation between antennas $i,j$
$\tilde{\varrho}$	transmit side spatial correlation exponent basis
$\sigma_0^2$	variance of noise
$\sigma_{e,k}^2$	variance of noise of the equivalent Gaussian channel of antenna $k$
$\Sigma_p$	matrix containing the rows and columns from the second to the last in the residual covariance matrix computed in the previous step
$\sigma_p$	vector containing the elements from the second to the last in the first row of the residual covariance matrix computed in the previous step
$\sigma_p$	the first element in the residual covariance matrix computed in the previous step
$\bar{\Sigma}$	matrix containing the rows and columns from the first to the second to last in the residual covariance matrix computed in the current step
$\sigma_p$	vector containing the elements from the first to the second to last in the last row of the residual covariance matrix computed in the current step
$\sigma_p$	the last element in the residual covariance matrix computed in the current step
$\Sigma_r$	covariance matrix of received signal ( $J(N+L-1) \times J(N+L-1)$ )
$\hat{\Sigma}_r^{[\text{TA}]}$	time-average estimated covariance matrix of received signal
$\Sigma_{\tilde{r}}$	covariance matrix of residual after cancellation ( $J(N+L-1) \times J(N+L-1)$ )
$\Sigma_{\tilde{r}}$	covariance matrix of residual with multilevel coded transmission ( $J(N+L-1) \times J(N+L-1)$ )
$\hat{\Sigma}_{\tilde{r}}^{[\text{TA}]}$	time-average estimated covariance matrix of residual after cancellation
$\hat{\Sigma}_{\tilde{r}}^{[\text{MF}]}$	diagonal approximated covariance matrix of residual after cancellation ( $J(N+L-1) \times J(N+L-1)$ )
$\Sigma_{\mathbf{h}_{k,j}}$	covariance matrix of channel multipath response between one transmit and one receive antenna ( $L \times L$ )
$\Sigma_{\text{vec}(H)}$	full channel covariance matrix ( $JK(N+L-1) \times JK(N+L-1)$ )
$\bar{\Sigma}_R$	receive side spatial covariance matrix for one symbol ( $J \times J$ )
$\Sigma_R$	receive side spatial covariance matrix for the frame ( $JN \times JN$ )
$\varsigma_f$	frequency-wise SINR of frequency-domain MMSE turbo equalizer given prior information

$\bar{\zeta}_f$	average frequency-wise SINR of frequency-domain MMSE turbo equalizer given prior information
$\bar{\Sigma}_T$	transmit side spatial covariance matrix for one symbol ( $K \times K$ )
$\Sigma_T$	transmit side spatial covariance matrix for the frame ( $KN \times KN$ )
$\Sigma_{\mathbf{H}\hat{\mathbf{b}}}$	covariance matrix of estimated received signal ( $J(N+L-1) \times J(N+L-1)$ )
$\Upsilon$	diagonal matrix with eigenvalues of the received signal covariance matrix $\Sigma_r$ on the diagonal ( $JN \times JN$ )
$\Upsilon_k$	diagonal matrix with eigenvalues of the channel matrix of transmit antenna $k$ on the diagonal ( $JN \times JN$ )
$v_{k,i}$	$i$ th eigenvalue of the channel matrix of transmit antenna $k$
$\tilde{\Upsilon}$	diagonal matrix with the eigenvalues of the residual covariance matrix $\Sigma_{\tilde{r}}$ on the diagonal ( $JN \times JN$ )
$\bar{v}_i$	$i$ th eigenvalue of the covariance matrix of the residual $\Sigma_{\tilde{r}}$
$\Phi$	matrix of eigenvectors (eigenbasis) of received signal frequency-domain covariance matrix ( $JN \times JN$ )
$\phi(i)$	$i$ th eigenvector of received signal frequency-domain covariance matrix ( $JN \times 1$ )
$\Phi_k$	matrix of eigenvectors (eigenbasis) of $k$ th antenna's frequency-domain channel covariance matrix ( $JN \times JN$ )
$\phi_k(i)$	$i$ th eigenvector of $k$ th antenna's frequency-domain channel covariance matrix ( $JN \times 1$ )
$\chi_{2k}^2$	chi-squared random variable with $2k$ degrees of freedom
$\Psi_k$	frequency-domain residual filter for transmit antenna $k$ ( $N \times JN$ )
$\Omega_p$	matrix containing the rows and columns from the second to the last in $\mathbf{W}_p$
$\omega_p$	vector containing the elements from the second to the last in the first column of $\mathbf{W}_p$
$\omega_p$	the first element in $\mathbf{W}_p$
$\Omega_f$	matrix containing the rows and columns from the first to the second to last in $\mathbf{W}_{\text{smbbox}f}$
$\omega_f^H$	vector containing the elements from the first to the second to last in the last row of $\mathbf{W}_f$
$\omega_f^*$	the last element in $\mathbf{W}_f$
$\bar{\Omega}$	Cholesky factorization of $\bar{\Sigma}^{-1}$
3GPP	Third Generation Partnership Project
AMC	adaptive coding and modulation
ARQ	automatic repeat request
BCJR	Bahl-Cocke-Jelinek-Raviv algorithm
BEC	binary erasure channel
BICM	bit interleaved coded modulation

BP	block partitioning
BPSK	binary phase shift keying modulation
bps	bits per second
CCC	constellation constrained capacity
CDMA	code division multiple access
CDD	cyclic delay diversity
CIR	channel impulse response
CND	check node decoders
DFT	discrete Fourier transform
EXIT	extrinsic information transfer
FDE	frequency-domain equalizer
FDTE	frequency-domain (minimum mean squared error) turbo equalizer
FEC	forward error correction
FER	frame error rate
FFT	fast Fourier transform
GAD	genie aided detection with perfect prior information
GSM	global system for mobile communications (originally Groupe Spécial Mobile)
IDFT	inverse discrete Fourier transform
IFFT	inverse fast Fourier transform
ISI	inter-symbol interference
ISM	industrial-scientific-medical band
LMMSE	linear minimum mean squared error
L-ARQ	layered multi-controller automatic repeat request scheme
LDPC	low-density parity check
LOS	line of sight
M-PSK	M-level phase-shift keying
MAP	maximum <i>a posteriori</i>
MF	matched filter
MFB	matched filter bound
MIMO	multiple input – multiple output
MLBICM	multilevel BICM
MMSE	minimum mean squared error
MMSE-DFE	minimum mean squared error decision feedback equalizer
MRC	maximum ratio combining
NLOS	non line of sight
OFDM	orthogonal frequency-division multiplexing
PAPR	peak-to-average power ratio
PDP	time-domain channel power delay profile
P/S	parallel to serial conversion

PSK	phase shift keying modulation
QAM	quadrature amplitude modulation
QPSK	quadrature phase shift keying modulation
RA	repeat accumulate (code)
RLS	recursive least squares
S-ARQ	single controller automatic repeat request scheme
S/P	serial to parallel conversion
SC/MMSE	soft canceling MMSE equalizer
SFISFO	soft input – soft output
SISO	single input – single output
SIMO	single input – multiple output
SNR	signal to noise ratio
SOVA	soft output Viterbi algorithm
TPeff	throughput efficiency
UMTS	universal mobile telephone system
UCA	uniform circular array
UEP	unequal error protection
ULA	uniform linear array
VND	variable node decoders
$\mathbf{1}^N$	a vector of ones ( $N \times 1$ )
$\mathbf{0}^N$	a vector of zeros ( $N \times 1$ )
$\otimes$	Kronecker product
$(\cdot)^T$	transpose of the argument
$(\cdot)^*$	conjugate of the argument (element-wise for vectors and matrices)
$(\cdot)^H$	Hermitean (conjugate transpose) of the argument
$(\cdot)^{-1}$	inverse of the argument
$(\cdot) \bullet (\cdot)$	(vector) dot product of the arguments
$\nabla \times (\cdot)$	curl of the argument vector field
$ \cdot $	absolute value
$\ \cdot\ _2$	Euclidean vector norm
$\det(\cdot)$	determinant of the argument
$\zeta(\cdot)$	eigenvalues of the argument matrix
$\zeta_i(\cdot)$	$i$ th eigenvalue of the argument matrix
$\hat{(\cdot)}$	estimate of the argument
$\text{circ}(\cdot)$	circulant operation, where circularly shifted copies the argument vector are placed on the consecutive columns of the result matrix
$\text{diag}(\cdot)$	(vector argument) diagonal matrix with the argument vector at the main diagonal
$\text{diag}(\cdot)$	(matrix argument) the main diagonal of the argument as a vector
$\text{tr}\{\cdot\}$	trace of the argument matrix

$\text{vec}(\cdot)$  a vector with the columns of the argument matrix stacked (from left to right)

$\mathbf{A}_{[i,j]}$  the  $i$ th element on the  $j$ th column of matrix  $\mathbf{A}$

$(\cdot)_8$  octal number

# Contents

Abstract	
Preface	
Symbols and abbreviations	
Contents	
1 Introduction . . . . .	23
2 Preliminaries . . . . .	25
2.1 Review of earlier and parallel work . . . . .	25
2.1.1 Channel equalization . . . . .	25
2.1.2 Turbo methods . . . . .	26
2.1.3 Turbo equalization . . . . .	27
2.1.4 Channel coding and modulation . . . . .	28
2.2 Aims and outline of the thesis . . . . .	29
2.3 The author's contribution to the publications . . . . .	29
2.4 System model . . . . .	30
2.5 Fundamental limits . . . . .	34
3 Receiver algorithms . . . . .	37
3.1 MMSE MIMO turbo equalizer . . . . .	37
3.2 Recursive square-root filtering . . . . .	41
3.3 Time-average approximation . . . . .	45
3.4 Matched filter approximation . . . . .	47
3.5 Frequency-domain filtering . . . . .	49
3.6 Computational complexity comparison . . . . .	57
3.7 Summary and discussion . . . . .	59
4 Convergence analysis . . . . .	61
4.1 Mutual information and EXIT charts . . . . .	61
4.2 Multi-dimensional EXIT charts . . . . .	67
4.2.1 Approximate rate interpretations from EXIT functions . . . . .	70
4.2.2 Symmetric design . . . . .	74
4.3 Semianalytical EXIT charts . . . . .	77
4.3.1 Accuracy verification . . . . .	79
4.4 EXIT function characteristics . . . . .	82
4.4.1 Single transmit and single receive antenna . . . . .	82

4.4.2	EXIT function slope with single transmit and single receive antenna	84
4.4.3	Spatial separation of multiple antennas	86
4.4.4	EXIT function orientation	87
4.4.5	EXIT function slope with multiple transmit antennas	88
4.5	Summary and discussion	89
5	Fading channels	91
5.1	Convergence in fading channels	91
5.1.1	Considered channel codes	92
5.1.2	Interleaving	93
5.1.3	Channel delay spread	94
5.1.4	Spatial correlation in MIMO channels	98
5.2	Coding for fading channels	99
5.2.1	Code design using the combined EXIT function	103
5.2.2	Numerical evaluation	105
5.2.3	Code design for layered MIMO transmission	106
5.3	Summary and discussion	107
6	Multilevel coding and modulation	108
6.1	Multilevel coded QAM	108
6.2	MMSE turbo equalization of block-partitioned QAM	110
6.2.1	Numerical evaluations	112
6.3	Evaluation in the real field	113
6.3.1	Measurement scenario and propagation characterization	113
6.3.2	Measurement data based performance results	116
6.4	Convergence analysis	121
6.5	Analytical evaluation in the real field	123
6.6	Outage based code design for MLBICM 16-QAM	127
6.7	Summary and discussion	129
7	Conclusions and future work	131
7.1	Conclusions	131
7.2	Future work	132
	References	132
	Appendices A-D	

# 1 Introduction

In the last two decades the wireless communications sector in academia and industry has gone through major changes. The myriad of new results in the areas of channel coding, multiuser detection, multi-antenna communications and network information theory have brought the possibilities promised by communication systems to a new level. Together with this increasing understanding of the fundamental characteristics of systems, a continuous array of advances in implementation techniques has made it conceivable, that a major portion of the advances promised by theory could be realizable in implementations. For the theoretician, implementation complexity seems no longer to be a reason to avoid topics.

Another change in the sector has been the steady rise of commercial systems and products to the side of their military counterparts, with a corresponding surge in research targeting the area. It is significant, that research effort is spent on increasing the quality of life of the common man outside of societal crisis, even though the preparation for and prevention of crisis is necessary. A practical outcome of the rise of commercial systems is the increased average price-awareness of systems suppliers, system operators, and of course the final recipient of the total bill, the customer. Many persons would be more than happy to have almost *any* country's military budget to spend on their telecommunication costs, but that is usually not the case. Thus, the commercial necessity of low costs and the theoretical results promising more with an increasing complexity and price must be carefully balanced in order to bring the theoretical promises into the hands of the customer, thereby filling its ultimate practical purpose.

New systems require new spectrum to operate in, and available spectrum has proved in the past to be a scarce resource. The situation is emphasized with the fact, that new systems are envisioned to operate with as high as 100MHz of bandwidth. Such frequency allocations seem to currently be available only by considering frequencies well beyond the current UMTS bands around 2GHz. A system's centre frequency has a major influence on the propagation loss experienced by the system, thereby influencing the maximum distance reachable by any single link. Cellular systems having a higher centre frequency are forced to employ a higher density of access points to reach the same coverage than a comparable system with a lower centre frequency. This effect is already visible between the GSM, GSM1800 and UMTS systems where the minimum practical cell size decreases from the first to the last. The higher density of access points requires a higher initial investment

to build the system. The system bandwidth is another factor limiting system coverage: in order to guarantee reliable transmission, a required received energy per information bit must be achieved. However, the maximum transmission power of the system is limited by the regulation concerning radio emissions. Thereby the maximum throughput of the system is dictated by the channel propagation loss, which is effectively dependent on the transmission distance. If the system is to provide high data rate services, it can either do that in limited areas around access points or increase the access point density. Some systems operating on the industrial-scientific-medical (ISM) frequency bands provide the possibility for micro-operators to provide services to customers, often as an additional service to existing customers of a seemingly unrelated business. Cost-effectiveness is a necessity for the equipment of such systems, as the operator often does not obtain any direct additional revenue from the operation of the system. It is conceivable that such systems proliferate in the future due to the distributed nature of investment required to build up the system and will at minimum provide competition to traditional operators, if not directly supersede traditional cellular systems.

A logical conclusion of the above is that it is increasingly difficult, but extremely necessary for commercial success, to find low-complexity solutions to the implementation of new systems. From the point of view of the customer, terminal price is one of the important cost factors in using the system. Even if the operator provides the terminal, in practice the cost will be forwarded to the customer as higher access fees. A significant portion of the cost of the terminal is due to the transmitter power amplifier, a fact which is further emphasized by the introduction of multiple transmit antennas requiring dedicated amplifiers in all but the simplest transmitter configurations. Power amplifier cost is highly dependent on its peak power requirement, giving a clear cost advantage to systems employing modulations with a low peak-to-average power ratio (PAPR). This fact encourages the use of single-carrier over multi-carrier modulation, which exhibits very high PAPR and dictates the use of a combination of highly linear power amplifiers, pre-distortion, clipping compensation and amplifier backoff to mitigate the problem. While a terminal transmitting single-carrier modulation can operate its power amplifier with high efficiency in saturation, usually the linear amplifiers used with multi-carrier modulation exhibit lower efficiency and, thus, generate more heat and draw more power from the supply in comparison. The last two issues are especially important in portable, battery operated devices. The modulator in a single-carrier transmitter is in many cases simpler than in its multi-carrier counterparts due to the absence of frequency-domain processing [1, 2].

The complexity and cost advantage of the single-carrier transmitter is partly compensated for by the requirement of equalization at the receiver. Simple serial transmission over a channel with delay spread introduces intersymbol interference (ISI), which must be corrected at the receiver. This thesis deals with the efficient equalization of single-carrier signals by using turbo methods, the analysis of such equalizers, and the evaluation and design of channel coding for such systems.

## 2 Preliminaries

### 2.1 Review of earlier and parallel work

In this section the existing literature relevant to the topic is reviewed. The section begins with an overview of the development of channel equalization methods until the development of turbo methods. These are examined with an emphasis on turbo equalization, but also key contributions made on the topics of turbo channel decoding and turbo multiuser detection are considered. Many problems, research methods and solutions in the latter areas are applicable, and have been applied, in turbo equalization. Especially the topics of turbo multiuser detection and turbo MIMO detection are closely related.

The attention is then turned to turbo equalization, especially in the context of multiple input multiple output (MIMO) scenarios. A more detailed literature review is made on equalizer algorithms, their application with multilevel modulation, and channel coding for turbo equalization. Then, a review of the current knowledge on the performance limits of turbo equalization and convergence of turbo equalizers is made.

#### 2.1.1 Channel equalization

Maximum likelihood (ML) equalization was first presented in a formal manner in [3]. The equalizer consists of a noise whitening matched filter followed by a Viterbi algorithm. The complexity of the algorithm is exponential in the channel memory length. In the case of coded systems, the computational complexity becomes exponential in the product of channel and encoder memory lengths. As a result, the ML equalizer becomes prohibitively complex for practical systems. The most noteworthy of suboptimal equalizers are the linear minimum mean squared error (LMMSE) equalizer and the nonlinear minimum mean squared error decision feedback equalizer (MMSE-DFE) algorithms. Both can be considered standard textbook material, and the estimation-theoretic background, the algorithm descriptions and references to original work can be found in e.g. [4, 5]. The MMSE-DFE equalizer is more closely related to iterative equalizers based on turbo methods than the linear equalizers above. An overview of earlier results and a study of achievable rate with MMSE-DFE can be found in [6, 7]. In [8] it is argued that the MMSE-DFE of [6, 7] can-

not reach capacity due to the mismatch between the assumed equalizer output distribution based on perfect post-cursor removal and the actual equalizer output where residual interference is present. The authors of [9] show that if optimal prediction is used for feedback estimation and the residual interference covariance is correctly taken into account in the feedback filter, channel capacity can be reached.

### 2.1.2 Turbo methods

The method of iteratively decoding a concatenated channel code exchanging soft information using the principle currently referred to as *turbo*, was first presented in [10] (later published as [11]). Although the contributions of [11] included a new principle for the design of error control codes, a more interesting contribution from the point of view of this work was the decoding principle. The decoder avoided the prohibitive complexity of the optimal decoder by iteratively decoding the component codes of the concatenated code. In each iteration *prior* information in the form of likelihood values was used from the other component decoder by the symbol-by-symbol optimal Bahl-Cocke-Jelinek-Raviv (BCJR) [12] decoders. Each component decoder provided the *prior* information to the other component decoder. The optimality of the approach was later proved by the authors of [13] under the assumption of independent encoded bits, that results in the bit-wise probability computed with the BCJR algorithm also providing the correct codeword level probability. In practice, (large) interleavers can be used to provide independence between coded bits.

The decoding approach made possible the efficient decoding of many types of codes and gave rise to a new class of high performance channel codes. For the topic of this thesis, most relevant are the results on serially concatenated channel codes, which consist of an outer and an inner code separated by an interleaver. The frequency selective channel can be seen as such a system, where the propagation channel acts as the inner code. Serial concatenated codes are thoroughly presented in [14]. The serial concatenated approach is exploited in [15] to analyze iterative demodulation and decoding.

At the time when the turbo principle was found, much work was devoted to studying multiuser detection [16, 17, 18], especially for CDMA systems. The turbo principle can directly be applied to multiuser detection by considering the multi-access channel as the inner code to be decoded. Turbo multiuser detection is considered in [19, 20, 21] for narrowband (non-spread) systems. CDMA systems are considered in [22, 23, 24, 25, 26], whereas systems with arbitrary waveforms (with CDMA as a special case) are considered in [27]. There is a considerable amount of results on the iterative detection in uncoded CDMA [28, 29, 30] and MIMO systems [31], but such systems are not the focus of this thesis. For this thesis, the most relevant contribution can be found in [32, 33], where a sub-optimal algorithm combining an interference canceller with an minimum mean squared error (MMSE) filter was proposed for turbo multiuser detection.

### 2.1.3 Turbo equalization

The idea of applying the turbo principle to channel equalization was first presented in [34]. The authors used a soft-output Viterbi algorithm (SOVA) for soft-in-soft-out channel equalization and decoding. Soft information in the form of likelihood ratios was exchanged between the equalizer and the decoder. In [35] turbo equalization with a maximum *a posteriori* (MAP) equalizer was considered with turbo codes, and the equivalent Gaussian channel model for the equalizer outputs was introduced.

The soft canceling MMSE (SC/MMSE) algorithm originally introduced in [32][33] for the turbo detection of CDMA was applied to turbo equalization in [36], where M-PSK modulations were considered. In parallel, the authors of [37] found the same algorithm. An extension of the algorithm for arbitrary modulations was given in [38] and [39, 40]. In the latter, the authors showed the significance of symbol mapping to the convergence properties and asymptotic performance of the equalizer. An extension of the MMSE turbo algorithm to multiple-input-multiple-output (MIMO) setups was presented in [41, 42].

The MMSE turbo equalizer algorithm [37] employs an MMSE filter, whose taps are computed using an optimality criterion defined on a per-symbol basis. Various techniques to reduce the complexity required to compute the optimal filter taps for each symbol have been proposed. The authors of [36] propose a recursive matrix inverse updating procedure to compute the filter coefficients for consecutive symbols, or alternatively utilize an MMSE filter computed using a time-averaged interference covariance matrix. A modified recursion is proposed for time-varying channels in [43]. The authors of [44] propose a square-root extending window algorithm to compute the equalizer outputs. A matched filter approximation, which makes a Gaussian approximation of the remaining interference and replaces the interference covariance matrix with an approximate diagonal matrix is proposed in [45]. Frequency-domain approaches for MMSE turbo equalization are proposed in [38] and [46] for single-input-single-output (SISO) and MIMO systems, respectively.

In MIMO systems, the MMSE turbo detector can be configured in multiple ways. The simplest configuration consists of an antenna-wise MMSE filter producing a symbol estimate, followed by a decoder for the used coded modulation [39]. If joint-antenna or space-time channel coding is used, the equalizer can provide an estimate of the signal sum of the transmit antennas, followed by ML decoding of the space-time code [47]. In principle, any components of the received signal can be chosen so that the MMSE provides an estimate of their sum, and a suitable joint estimator provides further processing for their separation [47, 48]. Such approaches are reported in [49] for joint multipath detection and [50] for joint detection of space-time BICM transmissions.

In reality a wireless receiver consists of a multitude of signal processing functions operating in unison. From the viewpoint of the equalizer, the most significant of these is the channel estimator. All coherent receivers in general, and equalizers in particular, rely on accurate channel state information in their processing. A number of contributions [51, 52, 53, 54] deal with the topic of using turbo iterations to improve the channel estimation accuracy.

In some multiple access systems, for example cellular systems, receivers may have to tolerate interference from signals that are not meant to be detected by the receiver in question. In such cases the receiver must have means to suppress such interference effectively.

For the MMSE turbo equalizer, such methods are presented in [55, 47, 56].

### *2.1.4 Channel coding and modulation*

Forward error correction (FEC) coding, usually referred to as channel coding, is crucial in turbo equalization, as the technique requires the co-operation of an equalizer algorithm and the channel decoder. Different channel codes and interleaving schemes have been studied in the context of turbo equalization [57, 58, 59, 60, 61] with the main emphasis on link performance simulations. Unfortunately without further analysis such results are mainly indicative and provide little information on how to predict link behavior in different channel scenarios and with different channel codes. A more analytical approach is taken in [60, 61, 62], where it is found that the asymptotic performance of the equalizer, with perfect prior information, depends entirely on the utilized coding and modulation scheme. The mapping used with bit-interleaved coded modulation (BICM) [63] is optimized for iterative de-mapping and turbo equalization in [64]. The difference between average bit-wise mutual information provided by the de-mapper [65] in the cases of no and full prior information is used as a mapping selection tool.

Asymptotic behavior is only useful if the equalizer converges to, or close to the limit of perfect prior information. Without a method to analyze the turbo equalizer behavior during convergence, any approach to transmission optimization is essentially somewhat ad-hoc. A useful tool for the convergence analysis of iterative detection algorithms is extrinsic information transfer (EXIT) charts [66] that track the evolution of mutual information in the algorithm. It simplifies density evolution [67] by assuming a known distribution (usually Gaussian) of the exchanged soft values. The EXIT functions describing how each soft-input-soft-output (SfISfO) block transforms input metrics into output metrics were initially obtained through numerical simulations [66]. In general, mutual information of the soft information is considered to be the most robust metric to analyze algorithm convergence [68]. Numerically obtained EXIT functions for the MMSE turbo equalizer have been used in e.g. [39, 69, 70] for convergence analysis in selected fixed channels. The main result is that the convergence characteristic defined by the EXIT function of the equalizer is dependent on the channel. Rate arguments related to EXIT functions in e.g. [71, 72, 73] demonstrate that to maximize the transmission rate, one should match the code to the channel. An optimal outer code would match the EXIT function exactly. This requires, however, that the code structure exhibits enough degrees of freedom to shape the code EXIT function to realize this matching.

Low-density parity check (LDPC) codes are one family of such codes. Outer LDPC coding in combination with turbo equalization has been considered in [74] for magnetic recording channels and in [75] for wireless channels. The necessity of optimizing the LDPC code to match the channel and the equalizer was first demonstrated in [76, 77, 78]. Related work on CDMA systems in [79, 80, 81] show corresponding results.

Due to the dependence of the equalizer EXIT function and the channel, wireless channels have essentially random EXIT functions. In such cases the code optimization for static channels in [78] is no longer very useful. Furthermore, the method for obtaining the equalizer EXIT function through simulations is too computationally intensive for practical

applications. A more analytical approach for the computation of the equalizer EXIT function is required as a basis of the code design. Recently, such approaches for evaluating MMSE turbo equalizers and iterative detectors have been proposed in e.g. [82, 83, 84]. Such methods can not only aid in the transmission design, but also in the performance evaluation given a particular design.

## 2.2 Aims and outline of the thesis

Turbo equalizers are promising significant performance gains for single-carrier broadband systems operating over frequency-selective MIMO channels. Many potential algorithms for turbo equalization have been proposed, with the MMSE turbo equalizer (sometimes denoted as SC/MMSE) being the main topic of this thesis.

The aims of the thesis are threefold. Firstly, new approaches in the equalizer signal processing reducing the complexity of the MMSE turbo equalizer are studied. These include new approximate and recursive methods for equalizer algorithm execution, presented in Chapter 3. Secondly, the convergence properties of the equalizer are studied analytically to enable the evaluation of the equalizer convergence in fading channels and optimization of the channel code in Chapters 4 and 5. Thirdly, multilevel modulation is studied in Chapter 6 for robust and efficient high bandwidth-efficiency transmission over frequency-selective MIMO channels with MMSE turbo equalization receivers. The results of the previous chapters are applied in the analysis and design of the multilevel coded system.

## 2.3 The author's contribution to the publications

This thesis is written as a monograph, but its content is based on eight original publications. The author was the main contributor to [85, 86, 87] and [88, 89, 90], and developed the main ideas in them. The other authors provided ideas, comments, help, and in the case of [87], also simulation results. In [91], the author provided the equalizer convergence analysis and developed the convergence outage approach in co-operation with the other authors. In [92], the author provided the results concerning the performance of frequency-domain turbo equalization with punctured convolutional codes.

All simulation software for the numerical results was produced by the author, with the following exceptions. All results with turbo codes, including the simulation of EXIT charts for turbo codes, have used turbo encoding and decoding software by Mikko Vehkaperä. All simulated channels with a nontrivial correlation structure were produced with the channel simulator by Esa Kunnari. All the results in [87] have been produced by Christian Schneider with software not produced by the author. The used channel measurement data was provided by the Ilmenau University of Technology, Germany. Also, in [91], the software used to produce the numerical examples was co-authored by the author and Rainer Wohlgenannt, whose LDPC encoding and decoding software was used in the simulations and who also performed the EXIT function fitting based code optimization for the turbo equalizer.

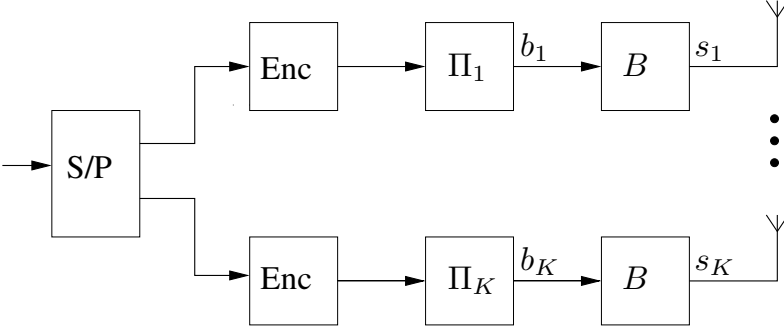


Fig. 1. BICM encoder and modulator.

## 2.4 System model

In this section the mathematical model suitable for the presentation of a single-carrier system, with either multiple users each with a single transmit antenna, or one user with multiple transmit antennas in a layered configuration, is presented. The complex baseband expressions for the transmitted signal, the propagation channel and the received signal model are given.

The system employs  $K$  transmit and  $J$  receive antennas. The transmission is BICM with  $M$  bits per symbol, and each transmit antenna sends an independently encoded and modulated symbol stream. The information bits, taking the values  $\{-1, 1\}$  with equal probability, are encoded by a binary channel code, interleaved with a transmit antenna specific random interleaver  $\Pi_k$  and segmented into groups of  $M$  bits each and the segments used for constructing each of the  $N$  transmitted symbols in a frame. The segmented bits for each frame can be expressed in vector form as

$$\mathbf{b} = [\mathbf{b}_1^T, \dots, \mathbf{b}_k^T, \dots, \mathbf{b}_K^T]^T \in \{-1, 1\}^{KMN}, \quad (1)$$

where the bits transmitted through the  $k$ th transmit antenna are given by

$$\mathbf{b}_k = [\mathbf{b}_k^T(1), \dots, \mathbf{b}_k^T(n), \dots, \mathbf{b}_k^T(N)]^T \in \{-1, 1\}^{NM} \quad (2)$$

with each segment  $\mathbf{b}_k(n)$  of  $M$  bits for antenna  $k$  given by

$$\mathbf{b}_k(n) = [b_{k,1}(n), \dots, b_{k,m}(n), \dots, b_{k,M}(n)]^T \in \{-1, 1\}^M. \quad (3)$$

Each group is mapped into a complex symbol  $s_k(n)$  with time duration  $T$  using a symbol mapper  $B : \mathbf{b}_k(n) \rightarrow s_k(n)$  consisting of a set of  $2^M$  complex points labeled with the binary input vector  $\mathbf{b}_k(n)$ . The transmitted symbols can be arranged into a vector

$$\mathbf{s} = [\mathbf{s}_1^T, \dots, \mathbf{s}_k^T, \dots, \mathbf{s}_K^T]^T \in S^{KN}, \quad (4)$$

with

$$\mathbf{s}_k = [s_k(1), \dots, s_k(n), \dots, s_k(N)]^T \in S^N. \quad (5)$$

In this thesis the constellation is normalized so that  $\mathbb{E} \left\{ |s_k(n)|^2 \right\} = 1$ .

The space-time multipath channel matrix  $\mathbf{H}$  with  $L$  separable paths between each pair of transmit and receive antennas,  $K$  transmitter and  $J$  receiver antennas is given as

$$\mathbf{H} = [\mathbf{H}_1, \dots, \mathbf{H}_k, \dots, \mathbf{H}_K] \in \mathbb{C}^{J(N+L-1) \times KN} \quad (6)$$

$$\mathbf{H}_k = [\mathbf{H}_{k,1}^T, \dots, \mathbf{H}_{k,j}^T, \dots, \mathbf{H}_{k,J}^T]^T \in \mathbb{C}^{J(N+L-1) \times N} \quad (7)$$

$$\mathbf{H}_{k,j} = [\bar{\mathbf{h}}_{k,j}(1), \dots, \bar{\mathbf{h}}_{k,j}(n), \dots, \bar{\mathbf{h}}_{k,j}(N)] \in \mathbb{C}^{(N+L-1) \times N}, \quad (8)$$

where  $\bar{\mathbf{h}}_{k,j}(n) = [\mathbf{0}^{(n-1)T}, \mathbf{h}_{k,j}^T(n), \mathbf{0}^{(N-n+1)T}]^T$  incorporates the multipath channel response between transmit and receive antennas  $k$  and  $j$  at time  $n$ , given by

$$\mathbf{h}_{k,j}(n) = [h_{k,j,1}(n), \dots, h_{k,j,l}(n), \dots, h_{k,j,L}(n)]^T \in \mathbb{C}^L, \quad (9)$$

with the vector  $\mathbf{0}^q$  denoting an all-zeros vector of length  $q$ . For notational convenience when dealing with symbol estimators, the space-time channel for each transmitted symbol is defined as

$$\mathbf{h}_k(n) = [\bar{\mathbf{h}}_{k,1}^T(n), \dots, \bar{\mathbf{h}}_{k,j}^T(n), \dots, \bar{\mathbf{h}}_{k,J}^T(n)]^T \in \mathbb{C}^{J(N+L-1)} \quad (10)$$

The channel multipath coefficients between each pair of transmit and receive antennas are assumed independent complex Gaussian and, thus, distributed according to  $h_{k,j,l} \sim \mathcal{N}(0, \Sigma_{\mathbf{h}_{k,j}})$ , with the covariance matrix given by

$$\Sigma_{\mathbf{h}_{k,j}} = \mathbb{E} \{ \mathbf{h}_{k,j}(n) \mathbf{h}_{k,j}^H(n) \} \quad (11)$$

$$= \text{diag} \left\{ 10^{-\boldsymbol{\vartheta}/10} \right\} \in \mathbb{R}_+^{L \times L}, \quad (12)$$

where  $\boldsymbol{\vartheta}$  denotes the power-delay-profile vector of the channel given in decibels. The full covariance matrix of the channel is assumed to adhere to the Kronecker model [93, 94] so that

$$\Sigma_{\text{vec}(\mathbf{H})} = \mathbb{E} \{ \text{vec}(\mathbf{H}) \text{vec}(\mathbf{H}^H) \} \quad (13)$$

$$= \Sigma_R \otimes \Sigma_T \in \mathbb{C}^{JK(N+L-1) \times JK(N+L-1)}, \quad (14)$$

where  $\text{vec}(\cdot)$  denotes the operator for stacking the matrix column into a vector, and  $\Sigma_R$  and  $\Sigma_T$  are the receive and transmit side spatial correlation matrices, respectively. By assuming the spatial correlation is equal between all multipath components, the detailed structure of the receive side correlation matrix can be expressed as

$$\Sigma_R = \bar{\Sigma}_R \otimes \mathbf{I}^{N+L-1} \in \mathbb{C}^{J(N+L-1) \times J(N+L-1)}, \quad (15)$$

where the correlation for one symbol is given by

$$\bar{\Sigma}_R = \begin{bmatrix} 1 & \cdots & \rho_{1,j}^* & \cdots & \rho_{1,J}^* \\ \vdots & \ddots & \vdots & & \vdots \\ \rho_{j,1} & \cdots & 1 & \cdots & \rho_{k,J}^* \\ \vdots & & \vdots & \ddots & \vdots \\ \rho_{J,1} & \cdots & \rho_{J,j} & \cdots & 1 \end{bmatrix} \in \mathbb{C}^{J \times J}. \quad (16)$$

Correspondingly, the transmit side spatial correlation matrix can be expressed as

$$\mathbf{\Sigma}_T = \bar{\mathbf{\Sigma}}_T \otimes \mathbf{I}^{N+L-1} \in \mathbb{C}^{K(N+L-1) \times K(N+L-1)}, \quad (17)$$

where the correlation for one symbol is given by

$$\bar{\mathbf{\Sigma}}_T = \begin{bmatrix} 1 & \cdots & \varrho_{1,k}^* & \cdots & \varrho_{1,K}^* \\ \vdots & \ddots & \vdots & & \vdots \\ \varrho_{k,1} & \cdots & 1 & \cdots & \varrho_{k,K}^* \\ \vdots & & \vdots & \ddots & \vdots \\ \varrho_{K,1} & \cdots & \varrho_{K,k} & \cdots & 1 \end{bmatrix} \in \mathbb{C}^{K \times K}. \quad (18)$$

In (16) and (18),  $\rho_{i,j}$  and  $\varrho_{i,j}$  denote the cross-correlation between the  $i$ th and  $j$ th receive and transmit antennas, respectively. Even though this model has some shortcomings in terms of modeling accuracy [95, 96], it provides the means to demonstrate the effects of transmit and receive side spatial correlation with a relatively simple model. With the model, the channel matrix (6) can be expressed as the product

$$\mathbf{H} = \mathbf{\Sigma}_R^{1/2} \mathbf{H}' \mathbf{\Sigma}_T^{H/2}, \quad (19)$$

where  $\mathbf{H}'$  is a channel matrix with spatially uncorrelated entries, and  $\mathbf{\Sigma}_R = \mathbf{\Sigma}_R^{1/2} \mathbf{\Sigma}_R^{H/2}$  and  $\mathbf{\Sigma}_T = \mathbf{\Sigma}_T^{1/2} \mathbf{\Sigma}_T^{H/2}$  are the Cholesky decompositions of the receive and transmit side spatial correlation matrices, respectively.

In some cases a cyclic transmission is used to enable low-complexity frequency-domain processing at the receiver, and a cyclic prefix is prepended to the encoded symbol stream so that the total transmitted symbol block length becomes  $N + N_{prefix}$  and

$$[s_k(1), \dots, s_k(N_{prefix})] = [s_k(N+1), \dots, s_k(N+N_{prefix})]. \quad (20)$$

If the channel remains static over the frame and  $N_{prefix} > L-1$ , the channel matrix, after the removal of the prefix, has a block-circulant structure with the last  $J(L-1)$  rows added to the first  $J(L-1)$  rows, and a DFT/FFT operation can be utilized at the receiver to convert the channel matrix into a block matrix with  $J \times K$  blocks, so that each block is a  $N \times N$  diagonal matrix. In the sequel, the matrix structure will be denoted as ‘‘diagonal-block’’. An  $N \times N$  DFT matrix operator  $\mathbf{F}$  with  $[\mathbf{F}]_{i,j} = N^{-\frac{1}{2}} e^{-j\frac{2\pi}{N}(i-1)(j-1)}$ ,  $j = \sqrt{-1}$ ,  $i, j = 1 \dots N$  is defined for the Fourier transformation. If the block-circulant channel matrix is denoted by

$$\mathbf{H}_c = [\mathbf{H}_{c,1}^T, \dots, \mathbf{H}_{c,k}^T, \dots, \mathbf{H}_{c,K}^T]^T, \quad (21)$$

where each of the  $\mathbf{H}_{c,k}$  is a block-circulant matrix constructed from  $\mathbf{H}_k$ , the block-circulant channel matrix can be expressed as the product

$$\mathbf{H}_c = \mathbf{F}_J^H \mathbf{\Xi} \mathbf{F}_K \in \mathbb{C}^{JN \times KN}, \quad (22)$$

where the block-Fourier matrices

$$\mathbf{F}_K = \mathbf{I}_K \otimes \mathbf{F} \in \mathbb{C}^{KN \times KN} \quad (23)$$

$$\mathbf{F}_J = \mathbf{I}_J \otimes \mathbf{F} \in \mathbb{C}^{JN \times JN} \quad (24)$$

are utilized. The diagonal-block frequency-domain channel matrix is then given by

$$\Xi = [\Xi_1, \dots, \Xi_k, \dots, \Xi_K] \in \mathbb{C}^{JN \times KN}, \quad (25)$$

where

$$\Xi_k = [\Xi_{k,1}, \dots, \Xi_{k,j}, \dots, \Xi_{k,J}]^T \in \mathbb{C}^{JN \times N}, \quad (26)$$

with

$$\Xi_{k,j} = \text{diag} \left\{ \tilde{h}_{k,j}(1), \dots, \tilde{h}_{k,j}(f), \dots, \tilde{h}_{k,j}(N) \right\} \in \mathbb{C}^{N \times N}, \quad (27)$$

where  $f = 1 \dots N$  enumerates the frequency bins and  $\tilde{h}_{k,j}(f)$  is the channel response at frequency  $f$  between transmit and receive antennas  $k$  and  $j$ . For convenience, the spatial response matrix between the transmit and receive antennas at frequency  $f$  is defined as

$$\Xi(f) = [\Xi_1(f), \dots, \Xi_k(f), \dots, \Xi_K(f)] \in \mathbb{C}^{J \times K}, \quad (28)$$

where

$$\Xi_k(f) = [\tilde{h}_{k,1}(f), \dots, \tilde{h}_{k,j}(f), \dots, \tilde{h}_{k,J}(f)]^T \in \mathbb{C}^J. \quad (29)$$

Since the receive and transmit side correlation matrix Cholesky decompositions are lower triangular block matrices with diagonal blocks, where each block is a product of the identity matrix and a complex scalar, it can be easily shown that<sup>1</sup>  $\mathbf{F}_J \Sigma_R^{1/2} \mathbf{F}_J^H = \Sigma_R^{1/2}$  and  $\mathbf{F}_K \Sigma_T^{1/2} \mathbf{F}_K^H = \Sigma_T^{1/2}$ . The channel matrix can then be expressed by

$$\mathbf{H}_c = \mathbf{F}_J^H \Sigma_R^{1/2} \Xi' \Sigma_T^{H/2} \mathbf{F}_K \in \mathbb{C}^{JN \times KN}, \quad (30)$$

where  $\Xi'$  denotes a frequency-domain channel matrix of a spatially uncorrelated channel, and the dimensions of  $\Sigma_R^{1/2}$  and  $\Sigma_T^{1/2}$  have been matched to the circulant channel dimension. Constant spatial correlation over multipaths is transformed into constant spatial correlation over the frequency bins.

When the symbols given by (4) pass through the channel, the received signal vector  $\mathbf{r}$ , embedded in circularly symmetric complex Gaussian noise, is given by

$$\mathbf{r} = \mathbf{H}\mathbf{b} + \mathbf{w} \in \mathbb{C}^{J(N+L-1)}, \quad (31)$$

where the noise covariance is given by  $\mathbf{E} \{ \mathbf{w}\mathbf{w}^H \} = \mathbf{I}\sigma_0^2 = \mathbf{I}N_0MJJR/K$  with  $N_0$  denoting the power spectral density of receiver. The signal-to-noise ratio (SNR) and the energy per bit ratio  $E_b/N_0$  are related as

$$\text{SNR}_{[dB]} = E_b/N_0[dB] + 10 \log_{10} (R \log_2 M). \quad (32)$$

---

<sup>1</sup>This can be demonstrated for the  $2 \times 2$  case by  $\begin{pmatrix} \mathbf{F} & \mathbf{0} \\ \mathbf{0} & \mathbf{F} \end{pmatrix} \begin{pmatrix} a\mathbf{I} & \mathbf{0} \\ b\mathbf{I} & c\mathbf{I} \end{pmatrix} \begin{pmatrix} \mathbf{F}^H & \mathbf{0} \\ \mathbf{0} & \mathbf{F}^H \end{pmatrix} = \begin{pmatrix} \mathbf{F} & \mathbf{0} \\ \mathbf{0} & \mathbf{F} \end{pmatrix} \begin{pmatrix} a\mathbf{F}^H & \mathbf{0} \\ b\mathbf{F}^H & c\mathbf{F}^H \end{pmatrix} = \begin{pmatrix} \mathbf{F}a\mathbf{F}^H & \mathbf{0} \\ \mathbf{F}b\mathbf{F}^H & \mathbf{F}c\mathbf{F}^H \end{pmatrix} = \begin{pmatrix} a\mathbf{I} & \mathbf{0} \\ b\mathbf{I} & c\mathbf{I} \end{pmatrix}.$

## 2.5 Fundamental limits

Throughout the thesis, it is assumed that the transmitter has no channel state knowledge and the receiver has full channel state knowledge. The channel is also assumed to be fully correlated (in time) within a transmitted block and independent between blocks, i.e. *non-ergodic*. In such a case, the channel capacity is a random variable conditioned on the channel realization and the traditional Shannon capacity is zero [97]. However, mutual information between the channel inputs and outputs, conditioned on the channel realization, is given by

$$\mathcal{I}(\mathbf{b}; \mathbf{r}|\mathbf{H}) = \log_2 \det \left[ \mathbf{I} + \frac{1}{K\sigma_0^2} \mathbf{H}\mathbf{H}^H \right] \text{ bps/Hz.} \quad (33)$$

Since the channel state is not known by the transmitter, the antennas are assumed to transmit uncorrelated signals that have an even power allocation over the spectrum. In channels with spatial correlation, this results in a loss, and (33) represents a capacity lower bound. A typical metric derived from the random mutual information of a non-ergodic channel is the *outage capacity* giving the maximum rate supportable with some desired probability so that it does not exceed the capacity conditioned on the channel state

$$P(\mathcal{I}(\mathbf{b}; \mathbf{r}|\mathbf{H}) \leq R) = P_{out}. \quad (34)$$

If the channel is frequency-selective, it is more intuitive to express the mutual information using the frequency-domain channel matrix as

$$\mathcal{I}(\mathbf{b}; \mathbf{r}|\mathbf{\Xi}) = \log_2 \det \left[ \mathbf{I} + \frac{1}{K\sigma_0^2} \mathbf{\Xi}\mathbf{\Xi}^H \right] \quad (35)$$

$$= \sum_{f=1}^N \log_2 \det \left[ \mathbf{I} + \frac{1}{K\sigma_0^2} \mathbf{\Xi}(f)\mathbf{\Xi}^H(f) \right] \text{ bps/Hz} \quad (36)$$

which is equal to (33) since the DFT preserves channel eigenvalues and the overhead due to the prefix disappears at the limit of an infinite block length. The equality of between (36) and (35) is due to the structure of  $\mathbf{\Xi}$  which makes it possible to express the determinant as a product of frequency-wise determinants.

Since the considered system employs dedicated signalling for each transmit antenna, it can also be viewed as a multi-user system. For a multi-user system, where each user employs a single transmit antenna, the channel mutual information region is given by the set of rate vectors [98]

$$C_{\text{MAC}} = \bigcup_{\mathcal{P} \in \mathcal{Q}} \left\{ \mathbf{R} : \mathbf{R}(\mathcal{S}) \leq \int_{1/2T}^{1/2T} \log_2 \left( 1 + \frac{\sum_{k \in \mathcal{S}} \mathcal{P}_k(f) \text{tr} \{ \mathbf{\Xi}_k(f)\mathbf{\Xi}_k^H(f) \}}{K\sigma_0^2} \right) df \right. \\ \left. \forall \mathcal{S} \subset \{1, \dots, K\} \right\}, \quad (37)$$

where  $\mathbf{R} = [R_1, \dots, R_k, \dots, R_K]$  and the power allocation policy  $\mathcal{P}_k$  of each user  $k$

belongs to a feasible set  $\mathcal{Q}$  defined by

$$\mathcal{Q} = \left\{ \mathcal{P} : \int_{1/2T}^{1/2T} \mathcal{P}_k(f) df \leq 1 \forall k \right\}. \quad (38)$$

The region of the set  $\mathcal{Q}$  is a convex set, whose boundary points can be achieved by using joint water filling in the frequency-domain and successive decoding [99, 98]. However, if water filling is not performed, the rate region is a  $K$ -dimensional polyhedron [100]. In the special case of two transmit antennas, the rate region is a pentagon.

The above capacity expressions assume Gaussian signaling. A frequency-selective channel fed with symbols drawn (with uniform probability) from a discrete constellation is referred to as a finite state ISI channel with  $2^{ML}$  states. A closed-form expression for the capacity  $C_{UI}$  of such channels is not available, but numerical methods to compute the capacity are given in [101, 102] and [103] for SISO and MIMO channels, respectively.

One practical and widely used performance metric is the matched filter bound, where *all* interference has been removed by a genie. The corresponding SNR is defined as

$$\mathcal{L}_k^{[GAD]} = \sigma_0^{-2} \|\Xi_k\|_2^2, \quad (39)$$

which also corresponds to the capacity upper bound given in [104]. The expression in (39) assumes knowledge of all interfering signals including the current desired symbol. The matched filter bound is usually computed as the performance of a given channel code at the SNR given by (39).

Capacity and asymptotic figures like the matched filter bound are useful in demonstrating the limits of any design one may construct. They rarely, however, by themselves, provide much information on how to approach the limits. In the case of turbo methods, such information is available in the form of EXIT chart analysis and the related area properties of the EXIT function [71, 105, 72] of the equalizer and the decoder. In [105] it is observed, that if prior information is modeled as if being the output of a Gaussian channel and the employed equalizer is the optimal symbol-wise MAP equalizer, then

$$C_{UI} \approx \int_0^1 I_e(I_d) dI_d, \quad (40)$$

where  $C_{UI}$  denotes the channel capacity assuming inputs drawn from a discrete alphabet with uniform probability, and

$$I_d = \lim_{N \rightarrow \infty} \frac{1}{N} \mathcal{I}(\mathbf{b}; \xi^d) \in [0, 1] \quad (41)$$

$$I_e = \lim_{N \rightarrow \infty} \frac{1}{N} \mathcal{I}(\mathbf{b}; \xi^e) \in [0, 1] \quad (42)$$

are the mutual information between the transmitted data and the decoder and equalizer outputs,  $\xi^d$  and  $\xi^e$ , respectively. Another result in [71] for the outer code gives that

$$R = 1 - \int_0^1 I_d(I_e) dI_e, \quad (43)$$

when the prior information is generated by a binary erasure channel (BEC), but holds also approximately for Gaussian channel generated prior information, as well. These results show that to approach the uniform input capacity  $C_{UI}$  of the ISI channel, a good strategy is to match the outer code EXIT function to the equalizer EXIT function.

The result in (40) assumes optimal decoding (i.e. symbol-by-symbol MAP with interleaving and infinite block size), and does not directly apply to suboptimal decoding such as MMSE turbo equalization. Due to the sub-optimality of MMSE turbo equalization, it can be deduced that the MMSE turbo equalizer exhibits a loss with respect to channel capacity. This can also be empirically supported by considering comparisons between MMSE turbo and optimal MAP equalization e.g. in [69], where the MAP equalizer EXIT function always lies above the MMSE turbo equalizer's corresponding function.

## 3 Receiver algorithms

The minimum mean squared error turbo equalizer is one of the most promising sub-optimal algorithms for iterative channel equalization and signal detection. The primary objective of the study in this chapter is to search for approaches to decrease the computational complexity for realistic implementations. A secondary objective is to gain familiarity with the algorithm and its behavior in general to enable further studies in the following chapters.

The MMSE turbo equalizer algorithm for BICM-coded MIMO systems is presented, and a square-root recursion utilizing the Cholesky decomposition for computing the equalizer coefficients is developed. A version of the equalizer algorithm employing an approximate time-average MMSE filter is developed and combined through switching with a channel matched filter algorithm. A frequency-domain turbo equalizer (FDTE) is derived, compared with the previous algorithms, and evaluated with a range of coding and modulation configurations. Finally, algorithm complexities are evaluated.

### 3.1 MMSE MIMO turbo equalizer

The equalizer structure consists of an SfISfO equalizer block and an SfISfO channel decoder block for each transmit antenna separated by interleaving and de-interleaving, as depicted in Fig. 2. The equalizer block performs soft interference cancellation using the channel decoder feedback. An MMSE filter is then defined for the filtering of the residual and for the computation of the extrinsic symbol likelihoods at the output of the equalizer block. The bit likelihoods are computed with a soft de-mapper that treats the equalizer output as the output of an equivalent Gaussian channel [32, 35]. The computations proceed as follows. The first two moments of the soft symbol estimates are obtained using

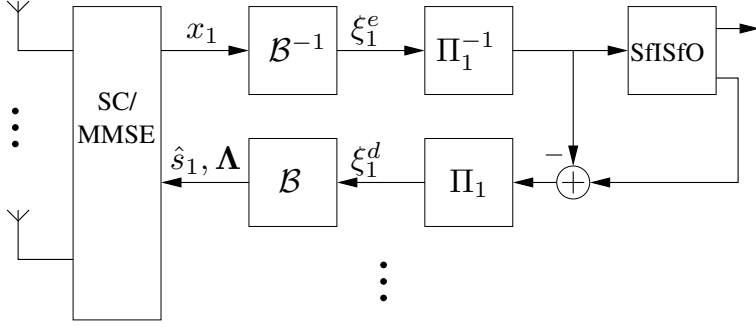


**Fig. 2. Turbo equalizer, demodulator and decoder for BICM.**

channel decoder feedback  $\xi_{k,m}^d$  for each  $k, m$  and  $n$  as

$$\begin{aligned}\hat{s}_k(n) &= \text{E} \{s_k(n)\} \\ &= \sum_{s_i \in \mathcal{S}} s_i P_a(s_k(n) = s_i)\end{aligned}\quad (44)$$

$$\text{E} \left\{ |\hat{s}_k(n)|^2 \right\} = \sum_{s_i \in \mathcal{S}} |s_i|^2 P_a(s_k(n) = s_i), \quad (45)$$

where  $P_a$  is the symbol *a priori* probability. Assuming the feedback consists of independent bit likelihoods,  $P_a$  can be computed as [32]

$$P_a(s_k(n) = s_i) = 2^{-M} \prod_{m=1}^M \left[ 1 - 2\bar{b}_{s_i}(m) \tanh \left( \frac{\xi_{k,m}^d(n)}{2} \right) \right], \quad (46)$$

where  $\xi_{k,m}^d(n)$  is the extrinsic log-likelihood ratio of bit  $b_{k,m}(n)$  provided by the decoder and  $\bar{b}_{s_i}(m)$  is the  $m$ th bit in the symbol hypothesis  $s_i$ . The log-likelihood ratio of bit  $n$  of transmit antenna  $k$  is defined by

$$\xi_{k,m}^d(n) = \ln \left( \frac{P(b_{k,m}(n) = -1)}{P(b_{k,m}(n) = 1)} \right). \quad (47)$$

This estimation of the symbol mean and variance is denoted in Fig. 2 by  $\mathcal{B}$ . The *a priori* symbol mean given by (44) is then used to cancel signal components estimated with *a priori* information from the received signal to provide a residual as

$$\tilde{\mathbf{r}} = \mathbf{r} - \mathbf{H}\hat{\mathbf{s}}, \quad (48)$$

where the desired signal component has also been canceled to be able to utilize the residual for all  $k$ . The MMSE minimization problem

$$\arg \min_{\mathbf{u}_k(n)} |s_k(n) - \mathbf{u}_k(n)^H (\tilde{\mathbf{r}}(n) + \mathbf{h}_k(n)\hat{s}_k(n))|^2, \quad (49)$$

is then solved for each  $n$  and  $k$  to compute the filter taps  $\mathbf{u}_k(n)$ . In (49),  $\tilde{\mathbf{r}}(n)$  consists of  $J$  ranges of samples of  $\tilde{\mathbf{r}}$ , indexed as  $nj \dots nj + L - 1$ , where  $j \in \{1 \dots J\}$ . The filter input in (49) consists of the desired signal component added to the windowed residual (48). If the feedback  $\hat{\mathbf{s}}$  is adequately randomized by interleaving, it can be assumed to be uncorrelated, in which case the symbol residual covariance matrix reduces to a diagonal matrix given by

$$\mathbf{\Lambda} = \text{diag} \left\{ \mathbb{E} \left\{ |\mathbf{s}(n)|^2 \right\} - |\hat{\mathbf{s}}(n)|^2 \right\}, \quad (50)$$

with which the covariance matrix of the residual (48) is given by

$$\mathbf{\Sigma}_{\tilde{\mathbf{r}}} = \mathbf{H}\mathbf{\Lambda}\mathbf{H}^H + \sigma_0^2\mathbf{I}. \quad (51)$$

With (51), the filter coefficients for estimating symbol  $n$  can be formulated as

$$\mathbf{u}_k(n)^H = \mathbf{h}_k^H(n)\mathbf{\Sigma}_{\tilde{\mathbf{r}}}^{-1}(n), \quad (52)$$

where  $\mathbf{\Sigma}_{\tilde{\mathbf{r}}}(n)$  contains the rows and columns of  $\mathbf{\Sigma}_{\tilde{\mathbf{r}}}$  indexed in a manner identical to the samples in (49). After decomposing the filter output to the desired component and the residual, and invoking the matrix inversion lemma, two intermediate variables are computed as

$$\alpha_k(n) = \mathbf{u}_k(n)^H \mathbf{h}_k(n) \quad (53)$$

$$\beta_k(n) = \left( 1 + \alpha_k(n) |\hat{\mathbf{s}}_k(n)|^2 \right)^{-1}, \quad (54)$$

to be utilized in the computation of the filter output as

$$x_k(n) = \beta_k(n) \left( \alpha_k(n) \hat{\mathbf{s}}_k(n) + \mathbf{u}_k(n)^H \tilde{\mathbf{r}}(n) \right). \quad (55)$$

A block diagram illustrating the algorithm is given in Fig. 3. Notice that in (52) the covariance matrix inverse is common to all  $k$ , and can be re-used for all  $k$ , and that the difference between filters of transmit antennas is due to the transmit antenna-wise channel responses. If the equalizer output (55) is seen as the output of an equivalent AWGN channel having  $s_k(n)$  as input, the equivalent channel variance can be computed as

$$\nu_k(n) = \mu_k(n) (1 - \mu_k(n)), \quad (56)$$

where

$$\mu_k(n) = \alpha_k(n) \beta_k(n). \quad (57)$$

Since the elements of the diagonal matrix  $\mathbf{\Lambda}(n)$  are not constant the MMSE solution is time-variant and Eqs. (52) – (56) have to be computed for each  $n$ . The time-variance is due to the filter being conditioned on each desired symbol estimate. Due to this, the algorithm is often referred to as the *conditioned MMSE* filter [26]. Algorithms that remove the conditioning are presented in Sections 3.3 – 3.5. The extrinsic bit log-likelihood can be computed by using *a priori* information as [65]

$$\xi_{k,m}^e(n) = \ln \frac{\sum_{s_i \in S_{-1}^m} P(s_k(n) = s_i) e^{L_{k,s_i}^e(n)}}{\sum_{s_i \in S_1^m} P(s^m = s_i) e^{L_{k,s_i}^e(n)}}, \quad (58)$$

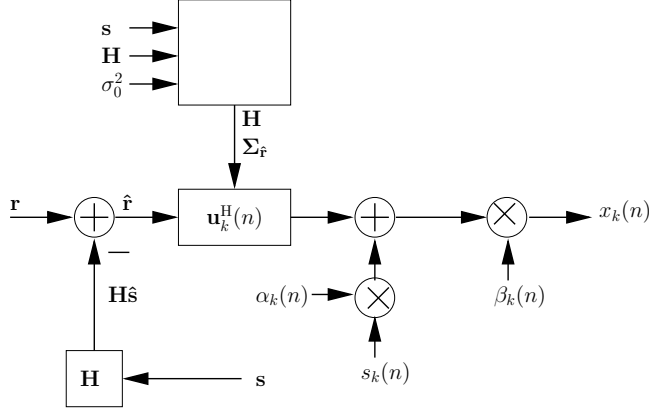


**Fig. 3. A block diagram of the conditioned MMSE turbo equalizer for transmit antenna  $k$ .**

where  $S_1^m$  and  $S_{-1}^m$  define the subsets of  $S$  where the bit  $b_m$  takes the values 1 and  $-1$ , correspondingly, and  $L_{k,s_i}^e(n)$  is the *a priori* likelihood of symbol point  $s_i$  based on information of all data bits within the segment other than  $m$ , given by

$$L_{k,s_i}^e(n) = \log \sum_{\substack{m'=1 \\ m' \neq m}}^M e^{\xi_{k,m}^d(n)}. \quad (59)$$

The de-mapping is denoted in Fig. 2 as  $\mathcal{B}^{-1}$ . The benefit of using *a priori* information in de-mapping depends heavily in the mapping function used [64], and is very small for Gray mappings. For this reason, prior information is not used for de-mapping in the work presented in this thesis. The probability of each mapping point  $s_i$  in (58) is computed with the equalizer output as

$$P(s_k(n) = s_i) = \frac{1}{\nu_k(n)\pi} e^{-\frac{|x_k(n) - \alpha_k(n)\beta_k(n)s_i|^2}{\nu_k(n)}}, \quad (60)$$

which approximates the equalizer output as Gaussian distributed with mean  $\mu_k(n)$  and variance  $\nu_k(n)$ . After the equalization of each frame, de-interleaving, and SfISfO channel decoding are performed, and the extrinsic log-likelihood information of both encoded transmitted bits and information bits is computed. The former is then re-interleaved, fed back to the equalizer and utilized in another equalization iteration in the computation of (44)–(45) and (58). During the first iteration, when no *a priori* information of the transmitted bits is available, the symbol residual covariance matrix reduces to an identity matrix, and the equalizer reduces to a linear MMSE equalizer.

### 3.2 Recursive square-root filtering

An equalizer operating with a sliding window can utilize the memory within the window to reduce computational complexity. A recursive covariance matrix inverse update algorithm to compute the time variant coefficients was introduced in [36] and modified for time-variant channels in [43]. The recursion avoids the repeated inversion of the symbol-wise interference covariance matrix and reduces the dominating complexity order of the algorithm from  $O(J^3L^3)$  to  $O(J^2L^2)$ , i.e., from cubic to square order complexity.

In general, square root algorithms, where the signal covariance matrix is replaced by its square-root, are desirable due to their numerical properties regarding stability and roundoff error [106, 107, 108, 109]. In this section a square-root form of the recursion given in [36] utilizing the Cholesky factorization is developed to enable the further development of computationally efficient implementations of the receiver. A similar approach for an extending window algorithm is presented in [44]. Given accurate channel estimates, the equalizer can be applied in time-variant channels as well as static channels.

A matrix partitioning approach for recursive updating of  $\Sigma_{\bar{r}}^{-1}(n)$  was proposed in [36]. The approach utilizes the fact that  $\Sigma_{\bar{r}}(n)$  is a shifted version of  $\Sigma_{\bar{r}}(n-1)$  with new components only in the last row and column. In cases where the received signal is oversampled in space or time, the covariance matrix has a block structure, and the recursion must be executed multiple times per output symbol to match the oversampling ratio.

The interference covariance matrix for the previous time step  $n$  is partitioned as [36]

$$\Sigma_{\bar{r}}(n) = \begin{pmatrix} \sigma_p & \sigma_p^H \\ \sigma_p & \Sigma_p \end{pmatrix} \quad (61)$$

and for the subsequent time step  $n+1$  as

$$\Sigma_{\bar{r}}(n+1) = \begin{pmatrix} \bar{\Sigma} & \sigma_f \\ \sigma_f^H & \sigma_f \end{pmatrix}. \quad (62)$$

These are the two consecutive sub-matrices of the global covariance matrix when the equalizer sliding window is moved forward. The sliding window principle is illustrated in Fig. 4.

Also the inverses of  $\Sigma_{\bar{r}}(n)$  and  $\Sigma_{\bar{r}}(n+1)$  are partitioned as

$$\mathbf{U}(n) = \begin{pmatrix} u_p & \mathbf{u}_p^H \\ \mathbf{u}_p & \mathbf{U}_p \end{pmatrix} \quad (63)$$

$$\mathbf{U}(n+1) = \begin{pmatrix} \mathbf{U}_f & \mathbf{u}_f \\ \mathbf{u}_f^H & u_f \end{pmatrix}. \quad (64)$$

Notice that on the right hand side of the definitions (61) – (64) the time step index  $n$  has been omitted for clarity. The recursion will be derived for a single step update and is directly applicable for any step  $n$ . In cases with multiple receiver samples per symbol, the computation of new covariance components must be modified accordingly, but the update is otherwise identical.

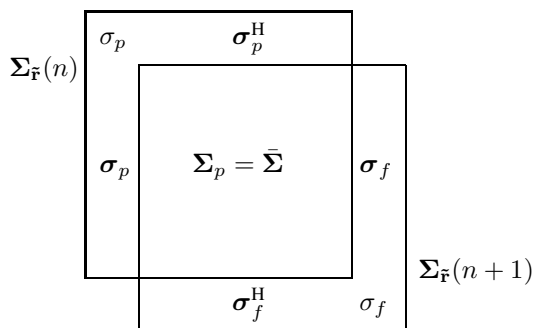


**Fig. 4. Covariance matrix partitioning for consecutive symbols.**

The objective is to compute  $\mathbf{U}(n+1)$  from  $\mathbf{U}(n)$  by using the common components  $\bar{\Sigma} = \Sigma_p$  of the consecutive covariance matrices  $\Sigma_{\bar{r}}(n)$  and  $\Sigma_{\bar{r}}(n+1)$ . In [36], this is shown to be achieved by the following equations

$$\bar{\Sigma}^{-1} = \mathbf{U}_p - \frac{\mathbf{u}_p \mathbf{u}_p^H}{u_p} \quad (65)$$

$$u_f = \left( \sigma_f - \sigma_f^H \bar{\Sigma}^{-1} \sigma_f \right)^{-1} \quad (66)$$

$$\mathbf{u}_f = -u_f \bar{\Sigma}^{-1} \sigma_f \quad (67)$$

$$\mathbf{U}_f = \bar{\Sigma}^{-1} + u_f^* \bar{\Sigma}^{-1} \sigma_f \sigma_f^H \bar{\Sigma}^{-H}, \quad (68)$$

where the new covariance components are given by

$$\begin{pmatrix} \sigma_f \\ \sigma_f \end{pmatrix} = \Sigma_{\bar{r}}(n+1) \begin{pmatrix} \mathbf{0} \\ 1 \\ \mathbf{0}^{J-j} \end{pmatrix}, \quad (69)$$

which is easily computed using (51). Spatial oversampling is taken into account in (69) in the last  $J-j$  zeros of the rightmost vector, effectively choosing each of the last  $J$  rows of the covariance matrix as  $j$  is incremented over the updates from 1 to  $J$ . The first all-zeros vector in the same term is assumed to “stretch” accordingly to keep the notation convenient. In the following, a recursive update for the interference covariance matrix inverse will be defined utilizing the Cholesky factorization.

The Cholesky factorizations of  $\mathbf{U}(n)$  and  $\mathbf{U}(n+1)$  are defined as the lower-triangular matrices

$$\mathbf{W}_p = \begin{pmatrix} \omega_p & \mathbf{0}^H \\ \omega_p & \Omega_p \end{pmatrix} \quad (70)$$

$$\mathbf{W}_f = \begin{pmatrix} \Omega_f & \mathbf{0} \\ \omega_f^H & \omega_f^* \end{pmatrix}, \quad (71)$$

respectively. The task is to derive equations that compute  $\mathbf{W}_f$  recursively from  $\mathbf{W}_p$  and then utilize it to compute the equalizer outputs (55)–(56).

The Cholesky factorization for the inverse of the common section of the two consecutive covariance matrices is defined as

$$\bar{\Sigma}^{-1} = \bar{\Omega}\bar{\Omega}^H. \quad (72)$$

In Appendix 1 it is shown that this factorization can be found simply by choosing the correct sub-matrix from  $\mathbf{W}_p$  and that

$$\bar{\Omega} = \Omega_p. \quad (73)$$

As detailed in Appendix 1, when (72) is applied into (66)–(68), a new set of equations given in terms of the factorization are obtained, which can be put into the form of pre- and post-arrays [110]. With these arrays  $\mathbf{W}_f$  can be computed as

$$\mathbf{W}_f = \begin{pmatrix} \bar{\Omega} & -\sqrt{u_f}\bar{\Omega}\bar{\Omega}^H\sigma_f \\ \bar{\mathbf{0}}^H & \sqrt{u_f} \end{pmatrix} \Theta, \quad (74)$$

where  $\Theta$  is a matrix representing a series of unitary rotations that annihilate the last column of the pre-array. A presentation on unitary rotations can be found e. g. in [110]. In case the last diagonal element of the pre-array is non-real, the rotations  $\Theta$  must apply phase correction [110]. Notice the new covariance components must be pre-filtered with  $\bar{\Omega}\bar{\Omega}^H$  to compute the pre-array.

Finally, Eqs. (53) and (55) can be computed as

$$\alpha_k(n) = \boldsymbol{\eta}_k^H(n)\boldsymbol{\eta}_k(n) \quad (75)$$

$$x_k(n) = \beta_k(n) \left( \alpha_k(n)\hat{b}_k(n) + \boldsymbol{\eta}_k^H(n)\mathbf{W}_f^H\tilde{\mathbf{r}}(n) \right), \quad (76)$$

where  $\boldsymbol{\eta}_k(n) = \mathbf{W}_f^H\mathbf{h}_k(n)$  and  $\beta_k(n)$  as given in (54). With the aid of (56) the extrinsic likelihood output of the equalizer can be computed.

The algorithm has been derived as a functional equivalent to the original algorithm in [36]. Their performances with unlimited precision arithmetic are, thus, expected to be the same, given identical filter dimensions. The benefits of the algorithm are related to practical implementation. Unitary rotation based algorithms are known to be numerically stable and robust to rounding error [111]. The proposed algorithm requires a pre-filtering stage for the new covariance components and one sequence of unitary rotations to update the Cholesky decomposition of the interference covariance matrix inverse. Fig. 5 outlines the equalizer structure, which consists of a block computing channel estimates and new covariance matrix components. Another block updates the square-root decomposition and multiplies the residual  $\tilde{\mathbf{r}}$  and the channel vector with the new decomposition. The post-processing for each  $k$  then obtains the metrics needed in the likelihood computation. For a pipelined systolic array implementation, a detailed study of the causality constraints of the algorithm should be performed, but is beyond the scope of this thesis. An efficient pipelined implementation may be difficult to construct due to the time-variance of the algorithm.

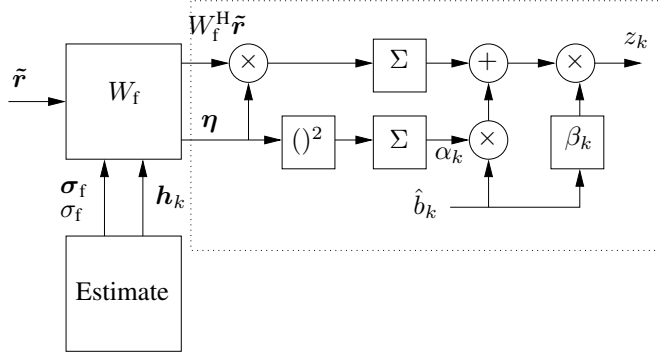


**Fig. 5. Square-root equalizer block diagram, where the dotted line encloses post-processing for transmitter antenna  $k$ .**

In many realistic cases the receiver cannot construct a complete or accurate system model to accurately compute (69). If the system model is constructed by relying on channel estimation, the system model accuracy is limited by the accuracy of the estimation algorithm. Additionally, channel estimation error reduces the accuracy of interference cancellation resulting in higher residual interference than with precise channel estimates. In multiuser and multi-cell scenarios the received signal may contain interference which the receiver may be unable to estimate. In such cases the signal model in (69) is insufficient to compute the interference covariance matrix. As a means to partly overcome this problem, another approach to compute the desired covariance matrix is to estimate the received signal covariance and the estimated signal covariance as

$$\hat{\Sigma}_{\mathbf{r}}^{[\text{TA}]}(n) \approx \frac{1}{N} \sum_{n=1}^N \mathbf{r}(n) \mathbf{r}^H(n) \quad (77)$$

$$\Sigma_{\mathbf{H}\hat{\mathbf{b}}} = \mathbf{H} (\mathbf{I} - \Lambda) \mathbf{H}^H, \quad (78)$$

and define the residual interference covariance as the difference given by

$$\Sigma_{\tilde{\mathbf{r}}}(n) = \Sigma_{\mathbf{r}}^{[\text{TA}]}(n) - \Sigma_{\mathbf{H}\hat{\mathbf{b}}}(n). \quad (79)$$

The symbol indexing with  $n$  within (77) – (79) corresponds to the symbol indexing in (49).

All unknown components and receiver noise are included in  $\mathbf{R}(n)$ , as well as the residual interference due to inaccurate channel estimation. The accuracy of the estimator in Eq. (77) is limited mainly by the coherence time of the received signal. In cases where channel coherence time is shorter than the received frame, windowed averaging or sequential estimation with a forgetting factor can be applied.

### 3.3 Time-average approximation

From the previous sections it becomes relatively clear that the time-variant filter computation imposes a significant computational complexity burden on the receiver. Calculating the inverse of (61) dominates the complexity of the algorithm by exhibiting cubic complexity with the number of filter coefficients, which grows quickly prohibitive as the number of equalized channel taps or the number of receiver antennas increases. Further complexity reduction by means of approximate filtering becomes, thus, a topic of some interest.

Originally, the approach utilising a covariance matrix time average has been proposed for SISO channel equalization in [36], and applied in numerous studies. In the MMSE turbo equalizer algorithm considered in this section the symbol-wise matrix inversion computed for the MMSE equalizer is replaced by a frame-wise average. The resulting algorithm is equivalent to the *unconditional MMSE* filter [26]. A simple method for computing the inverse by using the matrix inversion lemma utilising the residual signal at the output of the soft interference canceller is presented.

The time-averaged covariance matrix of the residual interference is given by

$$\hat{\Sigma}_{\tilde{\mathbf{r}}}^{[\text{TA}]}(n) = \frac{1}{N} \sum_{n=1}^N \tilde{\mathbf{r}}(n) \tilde{\mathbf{r}}^H(n). \quad (80)$$

When the residual signal  $\tilde{\mathbf{r}}$  is used for the computation of the covariance matrix, the need for estimating the receiver noise level is removed due to the noise being included in the residual. The inverse of the sum of outer products in (80) can easily be computed utilising the matrix inversion lemma in a similar fashion as the covariance inverse matrix is propagated in the recursive least squares (RLS) algorithm. The iteration must be normalised since inaccuracies in  $\hat{\Sigma}_{\tilde{\mathbf{r}}}(n)$  will introduce a bias to the likelihood computation in (59). The covariance inverse is computed by iterating over  $n$

$$\check{\mathbf{r}}(n) = \tilde{\mathbf{r}}(n) + \tilde{\mathbf{w}} \quad (81)$$

$$\bar{\mathbf{r}}(n) = \hat{\Sigma}_{n-1}^{-1} \check{\mathbf{r}}(n) \quad (82)$$

$$\hat{\Sigma}_n^{-1} = \lambda_f^{-1} \hat{\Sigma}_{n-1}^{-1} - \frac{\lambda_f^{-2} \bar{\mathbf{r}}(n) \bar{\mathbf{r}}^H(n)}{(1 - \lambda_f)^{-1} + \lambda_f^{-1} \bar{\mathbf{r}}(n) \bar{\mathbf{r}}^H(n)} \quad (83)$$

$$n = 1 \dots N, \quad (84)$$

with the initialisation  $\hat{\Sigma}_0^{-1} = \epsilon^{-1} \mathbf{I}$ , where  $\epsilon$  is a small positive constant and  $\lambda_f$  is the forgetting factor. Diagonal weighting to stabilise the iteration can be added with the Gaussian noise vector  $\tilde{\mathbf{w}}$  to the residual. In some cases a fixed forgetting factor is not desirable, and a time-varying factor can be applied so that for each input step  $n$ , the forgetting factor in (81) – (83) is defined by

$$\lambda_f(n) = \begin{cases} 1 & n = 1 \\ \frac{n-1}{n} & n = 2 \dots N. \end{cases} \quad (85)$$

The approximation requires the coherence time of the channel to be large compared to

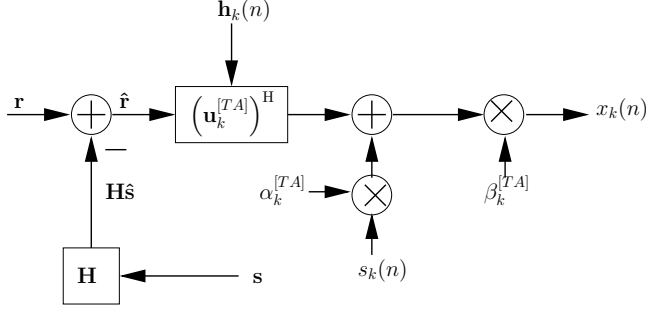


**Fig. 6. A block diagram of the unconditioned MMSE turbo equalizer for antenna  $k$ .**

the symbol duration to be able to accurately compute the matrix inverse. For a wideband system with a reasonable mobility this assumption can be considered to hold. The benefit of the averaging is in performing one square order complexity matrix inversion lemma iteration instead of one cubic order complexity matrix inverse per received symbol. Due to the time-averaging, also Eqs. (52), (53) and (54) become unconditioned on the current symbol and are given by

$$\left(\mathbf{u}_k^{[\text{TA}]}\right)^{\text{H}} = \mathbf{h}_k^{\text{H}}(n) \left(\hat{\Sigma}_{\tilde{\mathbf{r}}}^{[\text{TA}]}(n)\right)^{-1} \quad (86)$$

$$\alpha_k^{[\text{TA}]} = \left(\mathbf{u}_k^{[\text{TA}]}\right)^{\text{H}} \mathbf{h}_k(n) \quad (87)$$

$$\beta_k^{[\text{TA}]} = \left(1 + \alpha_k^{[\text{TA}]} \sum_{n=1}^N |\hat{s}_k(n)|^2\right)^{-1}. \quad (88)$$

In the first equalization iteration when no prior information is available on the transmitted symbols, the equalizer algorithm is a standard linear MMSE equalizer. Only by changing the input signal from the receiver signal  $\mathbf{r}$  to the interference residual  $\tilde{\mathbf{r}}$  the algorithm can be applied to all cancellation iterations without further modifications. A block diagram of the algorithm for one transmit antenna is depicted in Fig. 6, where it is emphasized, that the filtering unit requires no other information than the residual and the desired channel response.

The performance of the time-average filtering is tested through simulations in two MIMO setups, a 2-by-2 case and a 4-by-4 case using BPSK modulation. The channel is assumed to be known to the receiver, the information frame length is 300 bits, and the code is a 1/2-rate convolutional code with a constraint length of 3 (i.e.  $N = 600$ ) and generator polynomials  $(5, 7)_8$ . The channel has 10 Rayleigh fading taps with equal average power and the equalizer employs a filter of length  $JL$ . The equalizer performs four iterations in the 2-by-2 case and five iterations in the 4-by-4 case. In the matrix inverse iterations Gaussian noise at a level -3dB relative to the received signal power is added to provide stabilising diagonal weighting. The suitable level to stabilise the algorithm was

found empirically. The forgetting factor for the inverse iteration is set to 0.99.

In the remainder of the thesis the following simulation configurations are used, unless otherwise stated. The bit interleaver is randomly generated for each transmitted frame. The propagation channel state remains constant over each transmitted frame and is independently generated for consecutive frames. The employed channel decoder utilizes the bit-wise optimal MAP (or BCJR) algorithm [12].

The performance reference of the simulations is the matched filter bound of the channel given the channel code, which is equivalent to the performance of  $JL$ th order diversity reception without interference. Since the techniques to generate approximate performance references in static channels are relatively complex [112], the MFB performance has been simulated with a  $JL$ th order receive diversity system with a spatially uncorrelated flat Rayleigh fading channel.

The simulation results given in Fig. 7 and 8 show that time-average filtering provides a significant iteration gain up to the third iteration, i.e., the third receiver iteration is the last one to provide significant gain from the previous stage. The performance of the 2-by-2 system is within 0.5-1dB from the MFB while the performance gap of the 4-by-4 system to the optimal performance is somewhat larger. The 4-by-4 system's loss from the MFB is smaller at high SNRs, which implies convergence issues at small SNRs.

### 3.4 Matched filter approximation

A further simplification of the MMSE turbo equalization algorithm can be achieved through the use of simple channel matched filtering in place of the MMSE filter. Such an approach is proposed in [45], and combined with the time-average approximation through switching in [69]. The time-average approximation evaluated in Section 3.3 does not provide much iteration gain after three iterations and the third iteration gain is smaller than that of the previous iterations. On the other hand, if the *a priori* information from the decoders is good enough, even a simpler approximation will suffice to improve the detector performance [38]. It is thus proposed, that a matched filter approximation is performed after the first two iterations of time-average approximate filtering that provide the most gain.

The matched filter approximation provided below is an enhanced version of that proposed in [45]. The original proposal of [45] utilized a pilot symbol based estimation of receiver noise level as a basis for the computation of the symbol likelihood metrics. The algorithm in [69] considered an MMSE filter with all interference removed, and a known receiver noise level, which effectively results in a channel matched filter. The proposed method computes the interference from (partially) canceled signals and Gaussian noise, and approximates their sum as Gaussian. The combined noise and interference power is estimated directly from the residual signal  $\tilde{\mathbf{r}}$  as

$$\hat{\Sigma}_{\tilde{\mathbf{r}}}^{[\text{MF}]} \approx \frac{1}{JN} \text{tr} \{ \tilde{\mathbf{r}} \tilde{\mathbf{r}}^H \} \mathbf{I} \quad (89)$$

$$= \frac{1}{JN} \|\tilde{\mathbf{r}}\|_2^2 \mathbf{I}. \quad (90)$$

The approximated residual signal  $\tilde{\mathbf{r}}$  covariance matrix is diagonal, and the multiplication

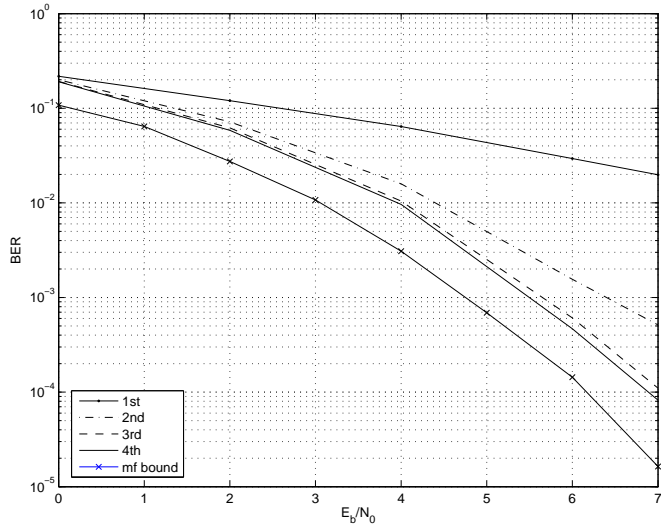


**Fig. 7. 2-by-2 system BER with time-average approximation.**

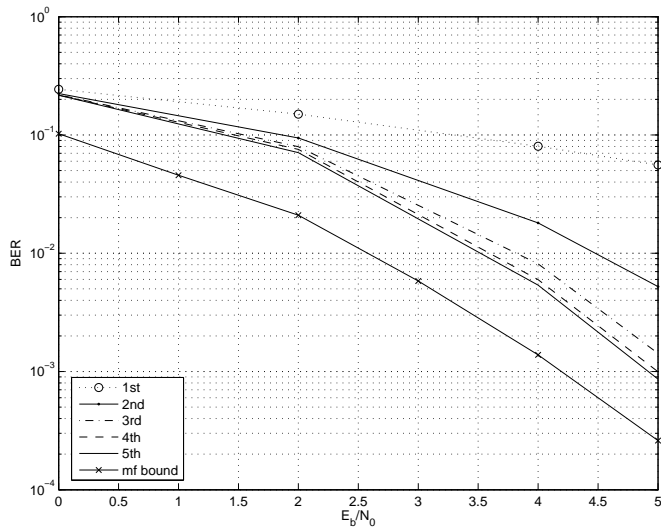


**Fig. 8. 4-by-4 system BER with time-average approximation.**

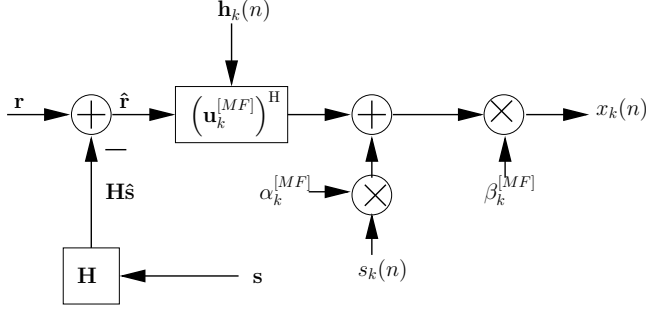


**Fig. 9. A block diagram of the MMSE turbo equalizer matched filter approximation for antenna  $k$ .**

with the matrix inverse can be reduced to a scalar multiplication. The modified algorithm with the MF approximation is identical to the algorithm in Section 3.1 except for Eqs. (52), (53) and (54), which are replaced by

$$\mathbf{u}_k^{[\text{MF}]}(n) = JN \|\tilde{\mathbf{r}}\|_2^{-2} \mathbf{h}_k(n) \quad (91)$$

$$\alpha_k^{[\text{MF}]}(n) = JN \|\tilde{\mathbf{r}}\|_2^{-2} \|\mathbf{h}_k(n)\|_2^2 \quad (92)$$

$$\beta_k^{[\text{TA}]} = \left( 1 + \alpha_k^{[\text{MF}]} \sum_{n=1}^N |\hat{s}_k(n)|^2 \right)^{-1}. \quad (93)$$

Obviously, Eq. (91) constitutes a channel matched filter for the symbol of interest. A block diagram of the algorithm is depicted in Fig. 9. The structure of the algorithm is very similar to the time average algorithm, but the filter computation is much simpler than that of the time average algorithm.

The combined algorithm executing two iterations of time-average approximate filtering and subsequently switching into matched filtering is tested with 2-by-2 and 4-by-4 MIMO configurations. The transmission and channel parameters are identical to those utilised in Section 3.3. Both cases show the MF approximation can provide further gain when the prior information is reliable. At high signal-to-noise ratios ( $\geq 4\text{dB}$ ) the performance after a total of five iterations is very close to the MFB. In practice, the fourth iteration is the last one to provide any significant iteration gain. At low signal-to-noise ratios the algorithm cannot converge to the MRC bound showing the combined algorithm has similar convergence issues as the time-average approximation.

### 3.5 Frequency-domain filtering

The number of resolvable multipaths in the time domain,  $L$ , is approximately inversely proportional to the transmission bandwidth, assuming the center frequency is kept fixed

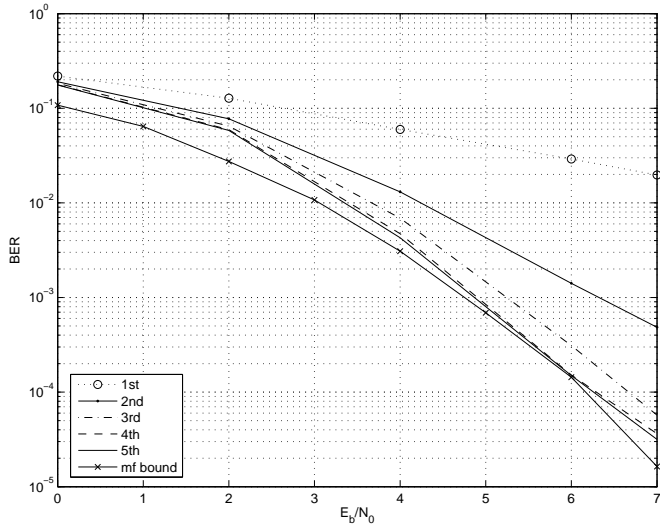


**Fig. 10. 2-by-2 system BER with time-average and MF approximation.**

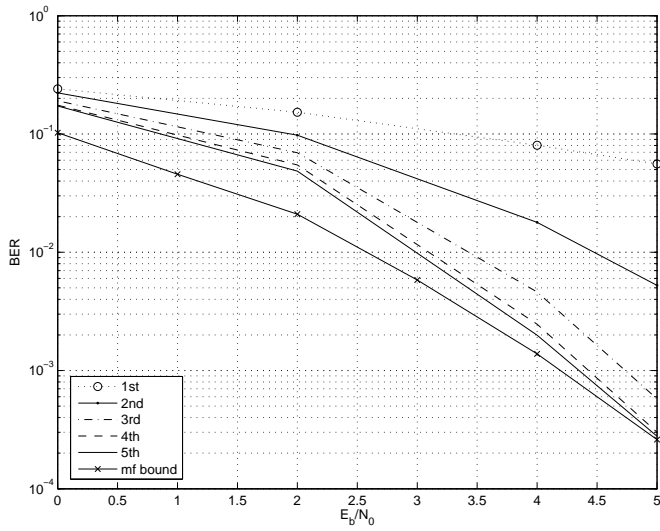


**Fig. 11. 4-by-4 system BER with time-average and MF approximation.**

and the channel is rich in multipaths. For very wideband transmissions, the number of multipaths can vary significantly depending on the channel delay spread, and can be very large in extreme propagation conditions. In such cases it is beneficial to utilize a receiver whose complexity is robust against delay spread variations. Channel shortening pre-filters can be used to restrict the effective channel length [113, 114] so that the complexity required by either time-domain MMSE or MAP equalization reduces to some desired level. Alternatively, low-complexity equalization can be implemented in the frequency-domain [115, 116]. In this section, an algorithm for frequency-domain MMSE turbo equalization is derived. Earlier work on such algorithms has been reported in [38, 117, 118] for single-antenna systems, in [46] for spatially multiplexed MIMO systems and in [119] for space-time coded systems.

The algorithm presented in Section 3.1 is converted into a block-wise frequency-domain form. A block-cyclic transmission according to (20) is assumed. A similar approach in the spirit of [69] is provided in [46]. The output of the time-domain equalizer for transmit antenna  $k$ , given by (55), can be stacked into a vector giving the MMSE estimates of the transmitted symbols within the frame as

$$\mathbf{x}_k = (\mathbf{I} + \mathbf{D}_k \mathbf{B}_k)^{-1} [\mathbf{D}_k \hat{\mathbf{s}}_k + \mathbf{H}_c^H \boldsymbol{\Sigma}_{\tilde{\mathbf{r}}}^{-1} \tilde{\mathbf{r}}], \quad (94)$$

where the diagonal matrices

$$\mathbf{D}_k = \text{diag} \left\{ \mathbf{H}_{c,k}^H (\mathbf{H}_c \boldsymbol{\Lambda} \mathbf{H}_c^H + \sigma_0^2 \mathbf{I})^{-1} \mathbf{H}_{c,k} \right\} \quad (95)$$

$$\mathbf{B}_k = \text{diag} \left\{ |\hat{\mathbf{s}}_k|^2 \right\}, \quad (96)$$

have been defined. Eq. (95) effectively contains the values of  $\beta_k(n)$  over  $n = 1 \dots N$  on the main diagonal. The filter output consists of two components: a weighted prior soft estimate and a correction term. The correction term can be computed for the frame with a single filter per transmit antenna, a fact that will be exploited in the definition of an approximate block-wise equalizer filter. By expressing the channel matrix by its frequency-domain equivalent (22), the block-wise filter output (94) for transmit antenna  $k$  can be expressed as

$$\mathbf{x}_k = (\mathbf{I} + \mathbf{D}_k \mathbf{B}_k)^{-1} \left[ \mathbf{D}_k \hat{\mathbf{s}}_k + \mathbf{F}^H \boldsymbol{\Xi}_k^H (\boldsymbol{\Xi} \mathbf{F}_K \boldsymbol{\Lambda} \mathbf{F}_K^H \boldsymbol{\Xi}^H + \sigma_0^2 \mathbf{I})^{-1} \mathbf{F}_J \tilde{\mathbf{r}} \right], \quad (97)$$

where (95) now becomes

$$\mathbf{D}_k = \text{diag} \left\{ \mathbf{F}^H \boldsymbol{\Xi}_k^H (\boldsymbol{\Xi} \mathbf{F}_K \boldsymbol{\Lambda} \mathbf{F}_K^H \boldsymbol{\Xi}^H + \sigma_0^2 \mathbf{I})^{-1} \boldsymbol{\Xi}_k \mathbf{F} \right\}. \quad (98)$$

Eq. (97) gives the filtering equation in the frequency domain. The elements of the diagonal matrix  $\boldsymbol{\Lambda}$  are i.i.d. and the frequency-domain covariance matrix of the feedback soft estimates

$$\boldsymbol{\Delta} = \mathbf{F}_K \boldsymbol{\Lambda} \mathbf{F}_K^H \quad (99)$$

$$= \text{diag} \{ \text{circ} \{ \mathbf{F} \boldsymbol{\lambda}_k \} \} \quad (100)$$

is a  $KN \times KN$  block-diagonal Hermitean matrix with  $N \times N$  circulant blocks with the columns of the  $k$ th block defined by the Fourier transformation of the  $k$ th transmit antenna

symbol residual covariance matrix given by

$$\mathbf{\Delta}_k = \mathbf{F} \left( \mathbb{E} \{ \mathbf{s}_k \mathbf{s}_k^H \} - \hat{\mathbf{s}}_k \hat{\mathbf{s}}_k^H \right) \mathbf{F}^H. \quad (101)$$

The operator  $\text{circ}(\cdot)$  denotes a circulant matrix with the argument vector on the first column. From (100) it can be noted that the time-variant time-domain MMSE filter translates into a frequency-domain filter with cross-frequency interference terms. Naive use of (97) requires the inversion of a  $NJ \times NJ$  matrix, and even more optimized approaches utilizing the structure of the matrix require significant computational effort [120]. The diagonal elements of each diagonal block in  $\mathbf{\Delta}_k$  are defined by the constant

$$\bar{\lambda}_k = \frac{1}{N} \text{tr} \mathbf{\Delta}_k, \quad (102)$$

expressing the average residual interference energy after cancellation. When the diagonal elements are large compared to the off-diagonal elements, each diagonal block can be approximated with a diagonal matrix, so that an approximate frequency-domain symbol residual interference matrix can be expressed by

$$\mathbf{\Delta} \approx \text{diag} \{ \bar{\lambda}_1 \mathbf{I}^N, \dots, \bar{\lambda}_k \mathbf{I}^N, \dots, \bar{\lambda}_K \mathbf{I}^N \} = \mathbf{\Delta}_a. \quad (103)$$

By neglecting the inter-frequency interference with the above approach, the filtering defined by (94) can be approximated by filtering whose output  $\mathbf{z}_{k,a}$  is given by

$$\mathbf{x}_{k,a} = (1 + \bar{\gamma}_k \delta_k)^{-1} [\bar{\gamma}_k \hat{\mathbf{s}}_k + \mathbf{F}^H \mathbf{\Psi}_k \mathbf{F}_J \tilde{\mathbf{r}}], \quad (104)$$

where the following definitions have been used

$$\bar{\gamma}_k = \frac{1}{N} \text{tr} \left\{ \mathbf{\Xi}_k^H (\mathbf{\Xi} \mathbf{\Delta}_a \mathbf{\Xi}^H + \sigma_0^2 \mathbf{I})^{-1} \mathbf{\Xi}_k \right\} \quad (105)$$

$$\delta_k = \frac{1}{N} \sum_{n=1}^N |\hat{s}_k(n)|^2 = 1 - \bar{\lambda}_k \quad (106)$$

$$\mathbf{\Psi}_k^H = \mathbf{\Xi}_k^H (\mathbf{\Xi} \mathbf{\Delta}_a \mathbf{\Xi}^H + \sigma_0^2 \mathbf{I})^{-1}. \quad (107)$$

Eq. (107) defines the frequency-domain filter, consisting of a single coefficient per frequency bin, using the residual signal  $\tilde{\mathbf{r}}$  as input. Eq. (105) can be considered to represent the average ratio of effective SNRs of the prior symbol estimate and the output of the filter given by (107). Eq. (106) represents the average energy of the prior symbol estimates. A block diagram of the algorithm is depicted in Fig. 12.

The above filter optimization is performed with the mean squared error of a single symbol cost function. An identical result can be obtained by considering the sum of square errors as the cost function [121]. The filter output distribution can be approximated by the normal distribution  $N(\mu_{k,a} \mathbf{s}_k, \mu_{k,a} (1 - \mu_{k,a}))$ , where

$$\mu_{k,a} = \bar{\gamma}_k (1 + \bar{\gamma}_k \delta_k)^{-1}. \quad (108)$$

It is instructive to note that due to the averaging in (102), the resulting equalizer is effectively the frequency-domain counterpart to the time-average approximation filter, with the

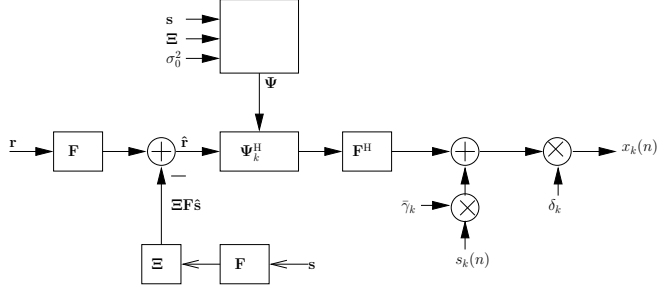


**Fig. 12. A block diagram of the frequency-domain MMSE turbo equalizer for antenna  $k$ .**

main difference being the effective filter length. By extending the above derivation, it is also straightforward to derive a frequency-domain version of the matched filter approximation provided in Section 3.4. If the frequency-domain residual covariance matrix is approximated by

$$\Xi \Delta_a \Xi^H + \sigma_0^2 \mathbf{I} \approx \frac{1}{JN} \text{tr} \{ \Xi \Delta_a \Xi^H + \sigma_0^2 \mathbf{I} \} \mathbf{I} \quad (109)$$

$$\approx \frac{1}{JN} \text{tr} \{ \tilde{\mathbf{r}} \tilde{\mathbf{r}}^H \} \mathbf{I} \quad (110)$$

$$= \frac{1}{JN} \|\tilde{\mathbf{r}}\|_2^2 \mathbf{I}. \quad (111)$$

Now, the frequency-domain matched filter approximation is given by the modification of (105) and (107) into

$$\tilde{\gamma}_k^{[\text{MF}]} = J \|\Xi_k\| \|\tilde{\mathbf{r}}\|_2^{-2} \quad (112)$$

$$\left( \Psi_k^{[\text{MF}]} \right)^H = JN \|\tilde{\mathbf{r}}\|_2^{-2} \Xi_k^H. \quad (113)$$

Eq. (112) indicates the frequency-domain channel matched filter (113) computes the output reliability using the ratio between the average squared channel response and the average squared interference whereas the MMSE filter utilizes the average of the frequency-wise ratios.

The frequency-domain turbo equalizer (104) is evaluated with numerical simulations. First, a comparison to the time-domain equalizer results in the previous sections is performed. The two systems in a 10-path Rayleigh fading channel are simulated with the results reported in Figs. 13 and 14. Also the frequency-domain algorithm can reach the matched filter bound, but with less iterations than the time-domain algorithms. The second iteration is already close to the bound and the third one is practically indistinguishable from it.

A further evaluation is performed in a single-antenna scenario with a number of different coding and modulation combinations to evaluate the behavior of the link with regard

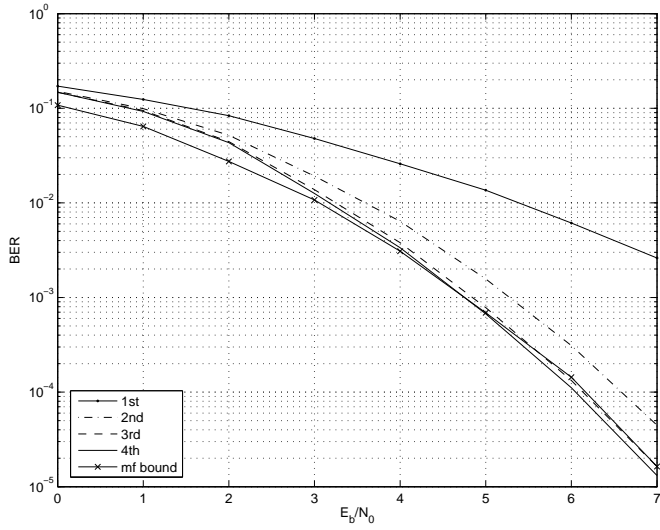


**Fig. 13. 2-by-2 system BER with the frequency-domain algorithm.**

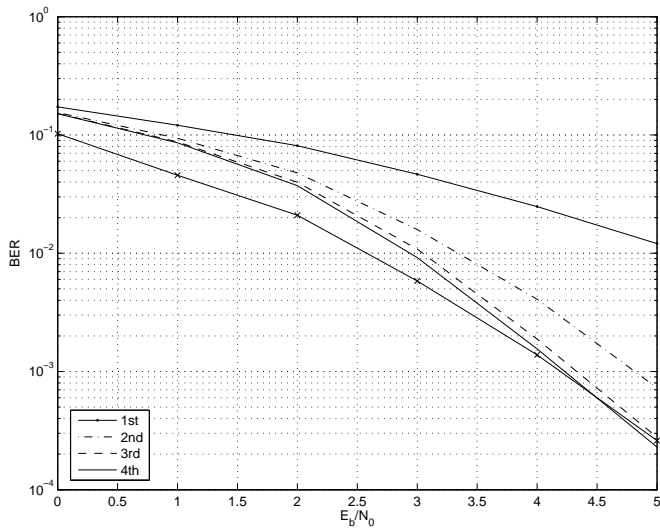


**Fig. 14. 4-by-4 system BER with the frequency-domain algorithm.**

Table 1. Transmission parameters.

Parameter	Value
Bandwidth	20MHz
Symbol rate	16.25Msps
Symbols per block	832
Prefix symbols	80
Pulse shaping	Root-raised cosine
Roll-off	0.23
Pulse filter length	8 symbols
Receiver sampling	16.25Msps

to a potential combination with adaptive modulation and coding (AMC). Punctured convolutional codes are chosen as the channel code for their straightforward application to such scenarios.

The coding and modulation combinations used are BPSK, QPSK and 16-QAM modulation combined with the convolutional  $(133, 171)_8$  mother code punctured to rates  $1/2$ ,  $2/3$ ,  $3/4$  and  $5/6$  according to the puncturing patterns given in [122]. The parameters of the transmission are listed in Table 1. The propagation channel for an urban macro environment with a maximum propagation delay of  $4.625\mu\text{s}$  is considered. The average power delay profile of the channel is given in Table 2. For comparison, the performance of a linear MMSE equalizer is evaluated. The linear equalizer algorithm is identical to the first pass of the turbo equalizer with no prior information. The performance results of the linear equalizer are listed in Fig. 15 until the FER of  $10^{-2}$ . Assuming that the link, if considered as a part of a realistic wireless system, would utilize automatic repeat request techniques in addition to the applied error correction coding, the evaluated range of operation in terms

Table 2. 5GHz urban macro channel power delay profile with 18 coefficients.

Coeffs. 1-6		Coeffs. 7-12		Coeffs. 13-18	
Delay [ $\mu\text{s}$ ]	Power [dB]	Delay [ $\mu\text{s}$ ]	Power [dB]	Delay [ $\mu\text{s}$ ]	Power [dB]
0,000	-3,0000	0,360	-5,2204	2,730	-12,0516
0,010	-5,2200	0,370	-7,4404	2,740	-14,2716
0,030	-6,9800	0,385	-9,2004	2,760	-16,0316
0,250	-4,7184	1,040	-8,1896	4,600	-15,5013
0,260	-6,9384	1,045	-10,4096	4,610	-17,7213
0,280	-8,6984	1,065	-12,1696	4,625	-19,4813

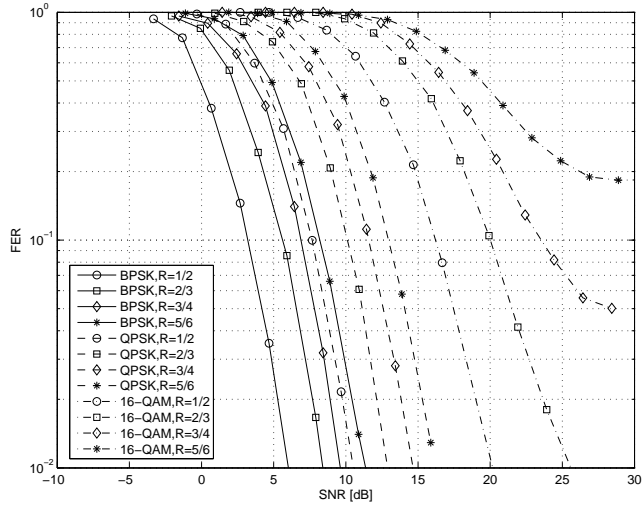


Fig. 15. Linear MMSE FDE FER with different coding and modulation combinations.

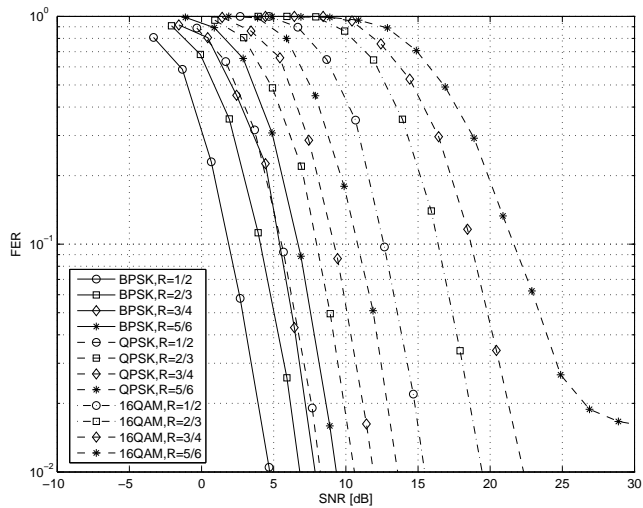


Fig. 16. Turbo MMSE FDE FER with different coding and modulation combinations.

Table 3. Mapping from complex to real operations.

Complex operation	Real operations
Mul	$4M + 2A$
Add	$2A$
Div	$6M + 3A + 2D$
M: Multiplication, A: Addition, D: Division	

of FER can be considered adequate. The linear FDE is seen to capture the channel diversity well and to operate consistently with different modes all the way up to 2/3-rate 16-QAM. The two highest modes experience a FER saturation limiting the usefulness of these modes. The mode using BPSK and rate 5/6 coding also performs worse than QPSK with rate 1/2, and is essentially useless for link adaptation. It must be noted, that if *widely linear* processing [123, 124, 125] were to be applied for BPSK, the performance would be improved.

When the results above are compared to the performance of the FDTE reported in Fig. 16, two essential results are imminent. Firstly, the turbo equalizer exhibits an overall gain wrt. the linear equalizer. With the aid of modulation selection, the gain can be exploited either as higher spectral efficiency, or as higher link reliability. Secondly, the turbo equalizer also makes possible the use of the two highest modes, thereby enabling higher maximum spectral efficiency.

### 3.6 Computational complexity comparison

The computational complexity of the algorithms is one of the first issues to be studied in an implementation feasibility study. Increasing the complexity of an algorithm imposes either an increased processing delay or the requirement for additional hardware for parallel operation, if the latter is possible. In battery-operated devices additional complexity also influences battery life through increased power required by the processing. Therefore, it is worthwhile to assess the computational complexity of algorithms, even if the assessment is approximate. In this section such an evaluation on the computational complexity of the algorithms presented in this section is made based on the mathematical expressions given in the previous sections. Complex operations are mapped into real operations using Table 3. If the algorithm contains a matrix inverse, it is always executed on a hermitian symmetric matrix, which in the current context is also always positive definite and has a Cholesky factorization. The matrix inverse is assumed to be computed through the inverse of the Cholesky factorization of the argument matrix and to have the computational complexity listed in Table 4. In some cases computational complexity and the memory requirements of an algorithm can be exchanged, but the memory requirements of the algorithms are not considered here.

Table 4. Complexity of Cholesky factorization with matrix dimension  $JL$ .

Operation	Complexity
Mul	$2/3J^3L^3 + 5J^2L^2 + 1/3JL + 4$
Add	$1/2J^3L^3 + 3J^2L^2 + 2/3JL + 4$
Div	$1/2J^2L^2 - 1/3JL - 1$
Sqrt	$JL$

All algorithms exclude the operations computing the expected value and variance of the soft estimates in (44) and (45), which are identical for all algorithms as well as the effect of other receiver algorithms including channel estimation, which are an essential part of the receiver but external to the equalizer. The channel estimates, however, are assumed to be available in time-domain form and need to be converted to the frequency-domain. The time-domain equalizers are assumed to have length  $JL$ , which is the minimum filter length covering the receiver ISI window and consistent with the simulation configuration used for the results reported in the previous sections.

An approximate operation count of the original recursive algorithm [36], the proposed square root recursion, the time-average approximation, the frequency-domain equalizer, and the frequency-domain matched filter approximation are tabulated in Table 5 for a single equalization iteration. An approximate total flop count as a function of the number of separable channel multipaths for a  $4 \times 4$  MIMO setup is also depicted in Fig. 17, where all operations have been assumed to require a single flop. This assumption favours algorithms having square-roots and divisions, which in practice need more operations than multiplications and additions, but does not have an effect on the conclusions in this case. The receiver is using an FFT size of 2048. All time domain algorithms have essentially  $O(JK^2L^2)$  complexity, and the recursive algorithm of [36] has only double the complexity of the time-average version. This is partly due to the fact that the time-average algorithm is performing the covariance computation over the whole frame. The square-root algorithm requires more operations than the original recursive version, most notably divisions and square-roots, mainly due to the utilized Givens rotations. In general, unitary rotation operations can be assumed to be implemented using the CORDIC method, which may decrease the operation count of the square-root algorithm. By making the quite realistic assumption that  $K \log N \geq J^2$ , the frequency-domain equalizer has  $O(JK \log N)$ , which is due to the conversion of the time-domain channel estimates for each transmit-receive antenna pair. It is possible to optimize the operation since the input to the FFT is heavily zero-padded, but it may be unrealistic to assume any receiver would be built with special purpose hardware only for that one purpose. Comparing the time- and frequency-domain algorithms, the latter exhibit a lower complexity in almost all channels. The time-domain matched filter approximation has the lowest complexity, but can only be used in MIMO configurations if the equalizer iterations are initiated with another algorithm [45]. The low complexity of the time-domain MF approximation makes it possible to be implemented in a different technology than all the other equalizers. Among the frequency-domain equalizers, the difference in computational complexity is surprisingly

Table 5. Computational complexity per symbol, time-domain filter length  $L$ , frequency-domain block length  $N$ .

Algorithm	Mul	Add
Recursive [36]	$(8K + 12) J^2 L^2$ $+ 6K J L + 2K + 2$	$(8K - 4) J^2 L^2 + 2K J L$ $- 2J^2 L - 2J L + J - K - 1$
Sqrt recursive	$(6K + 22) J^2 L^2 + 6K J L$ $- 32J L + 6K + 10$	$(6K + 17) J^2 L^2 - 2J^2 L$ $- (K + 26) J L - 13K + J + 7$
Time-average	$(4K + 12 \frac{1}{2}) J^2 L^2$ $+ (6K + 2 \frac{1}{2}) J L + 4K$	$(4K + 9) J^2 L^2$ $+ (4K + 1) J L - K - 1$
MF approx.	$5K J L + 5K + 4$	$(2K + 6) J L + K - 6$
Freq	$4(JK + K + J) \log N$ $+ 2/3 J^3 + 5J^2 + 4K + 5$ $+ (12K + 4 \frac{1}{3}) J$	$4(JK + K + J) \log N$ $+ 1/2 J^3 + 3J^2 + 2K + 4$ $+ (9K + 5 \frac{1}{2}) J$
Freq MF	$4(JK + K + J) \log N$ $+ 8K J + 4K + 3$	$4(JK + K + J) \log N$ $+ 7K J + K$
	Div	Sqrt
Recursive [36]	$K + 2$	2
Sqrt recursive	$2J L + K - 1$	$J L$
Time-average	$K + 1$	–
MF approx.	$2K$	–
Freq	$3/2 J^2 - 1/2 J - 1$	$J$
Freq MF	–	–

small given the heavy use of matrix inverses in the FDE, and is due to the dominating complexity of the FFT operations. If the FFT is implemented in special purpose hardware, the remaining complexity drops well below one thousand flops per symbol, which is also below the complexity of the time-domain matched filter approximation.

### 3.7 Summary and discussion

Algorithms for the MMSE turbo equalization of a single-carrier layered MIMO system were presented, with the original MMSE turbo equalization algorithm given as a starting point. A new algorithm based on a square-root recursion and a new computation technique for approximate filtering through time-average interference computation were provided. A new efficient matched filter approximation was proposed to be combined with the time-average filtering through algorithm switching. A frequency-domain MMSE

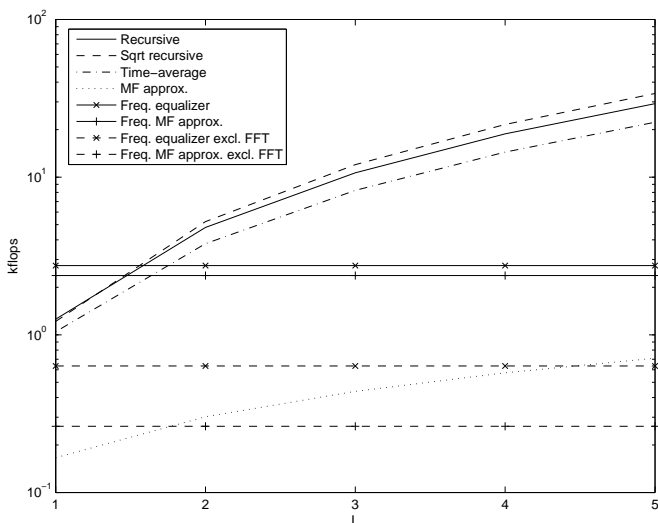


**Fig. 17. Algorithm complexity per symbol in kflops for a 4x4 MIMO case.**

turbo equalizer was derived and found to be dual to the time-domain time-average filter. A frequency-domain interpretation for the matched filter approximation was also derived. Complexity-wise, the frequency-domain turbo equalizer was found to be superior to the time-domain counterparts. Excluding FFT operations, it has a complexity comparable to the time-domain matched filter approximation, which cannot be utilized alone in MIMO scenarios, however.

The performance of the time-domain approximate time-average equalizer, alone and combined in a switching arrangement with the matched filter approximation, and the FDTE performance were compared. Both the switching configuration and the FDTE reach the matched filter bound of the code, with the FDTE requiring less iterations. The frequency-domain equalizer was found to efficiently utilize multipath diversity and to have robust performance with several punctured rates of the applied convolutional mother code. Even though the simulations of different algorithms are not directly comparable due to the sub-optimal time-domain equalizer filter length, it is straightforward to choose the frequency-domain turbo equalizer as the most promising algorithm for further studies based on the combination of performance and computational complexity. The time-domain time-average filter may have comparable performance when configured with a longer filter, but with radically increased complexity. Also, the original algorithm implemented with the matrix inversion recursion should have comparable or better performance when configured with a longer filter, but again with an even higher complexity than that reported in Table 5.

The fact that all algorithms reach the matched filter bound of the code indicates the system is not well optimized. Intuitively, more significant differences should be visible between the algorithms if the system operated close to the performance limits.

## 4 Convergence analysis

Turbo equalization, as well as any algorithm using the turbo principle, relies on the information exchange between the equalizer and the decoder. In the case of successful convergence, the information becomes more reliable as the iterations proceed, but such a generic statement of the iterative process provides little information on the requirements of successful convergence and the more detailed characteristics of the iterative process. A more rigorous approach should then be applied to the convergence analysis of the turbo equalizer. Such a framework is provided by extrinsic information transfer (EXIT) charts. This chapter begins with an overview of the properties of EXIT charts in the SISO case, and an extension to the analysis of the detection of multiple transmitters with multi-dimensional charts is made. The properties of multi-dimensional charts and their relation to system performance limits are presented. A semi-analytical method for computing the MMSE turbo equalizer EXIT chart is developed, and its accuracy verified. Analytical evaluations on the dependency of the EXIT chart and propagation channel parameters are made through further analysis of the method.

### 4.1 Mutual information and EXIT charts

The convergence of iterative algorithms can be tracked by measuring the evolution of the probability density function of the exchanged information [67]. In cases where the information consists of multiple parallel exchanges, or where some part of the system has random properties, the complexity of the tracking becomes quite severe and the visualization and interpretation of the results becomes problematic. The distribution of the outputs of a Gaussian channel fulfills a particular symmetry property [67] that make it possible to parametrize the distribution using a single variable, simplifying the task of tracking the density evolution considerably. The remaining question relates to the choice of the parameter to track. If the requirement is to be able to express the information with a single parameter and when the information exchange is tracked empirically by measuring the distribution of the exchanged likelihoods, the most reliable measure for the information flow between the equalizer and the decoder has been found to be mutual information between the exchanged values and the transmitted data [68].

EXIT charts have been successfully applied in the convergence analysis of turbo decoding of codes with parallel [67, 66] and serial concatenation [105]. Further applications have been found in the performance evaluation of turbo detection of MIMO systems [84] and turbo equalization of frequency-selective channels [126]. By customizing the behavior of one or more of the components of the concatenated system, the simplicity of the analysis lies in the modeling of the properties of each functional component of the iteration as a mutual information input-output transfer function. This has proven to be a rather accurate analysis method regardless of the nature of the overall system. Capacity approaching codes have been designed by the modification of system components (based on their EXIT charts) in [127, 128]. High accuracy has been achieved even for the prediction of the BER of turbo equalization schemes combined with a relatively weak convolutional code in [126, 83, 81]. In cases where a simplifying assumption of the distribution of mutual information is made, the accuracy of the EXIT analysis relies on the accuracy of the assumption. However, even in cases where no explicit assumption on the distribution of mutual information can be made, EXIT analysis has proven to provide reliable results. While in many cases the central limit theorem makes distribution modeling easier, the strength of EXIT analysis also appears to be related to the fact that mutual information is a measure of the distribution of soft information rather than a mere parameter of an assumed distribution.

For the turbo equalizer, the information exchange between the equalizer and the decoder, consisting of the log-likelihoods for encoded binary bits, must be tracked. In the SISO case, the mutual information between the likelihood  $\xi^d$  provided by the decoder and the transmitted data  $\mathbf{b}$  is denoted as [129] (duplicated from Section 2.5 for clarity)

$$I_d = \lim_{N \rightarrow \infty} \frac{1}{N} \mathcal{I}(\mathbf{b}; \xi^d) \in \mathbb{E}, \quad (114)$$

and the mutual information between the equalizer output likelihoods  $\xi_k^e$  and the transmitted data as

$$I_e = \lim_{N \rightarrow \infty} \frac{1}{N} \mathcal{I}(\mathbf{b}; \xi^e) \in \mathbb{E}, \quad (115)$$

where the range of mutual information is defined by the set

$$\mathbb{E} = \{I_d, I_e : 0 \leq I_d \leq 1, 0 \leq I_e \leq 1\}. \quad (116)$$

The limitation to the range  $[0, 1]$  is due to the binary channel codes assumed. In the case of higher-order modulation (than binary), the mutual information is measured at the demodulator (de-mapper) output.

In order to be able to analyze the convergence of the turbo iterations, the properties of the equalizer and the decoder concerning the transformation of the mutual information of the input information to mutual information of the extrinsic output must be evaluated. These properties are encapsulated in the two EXIT functions

$$f_d : I_d \rightarrow f_d(I_d) \in \mathbb{E} \quad (117)$$

$$f_e : I_d \rightarrow f_e(I_d) \in \mathbb{E}, \quad (118)$$

for the decoder and the equalizer, respectively. The functions are valid definitions of the input-output characteristics given infinite block length, whereas in the case of finite block

length, the input-output characteristic acquires a random variation around the asymptotic [130]. The equalizer EXIT function corresponds to the equalizer input- (extrinsic) output mutual information transfer characteristic. For convenience, the decoder EXIT function (117) is defined as the inverse of the decoder input-output mutual information transfer function so that both EXIT functions can have compatible definitions. The tracking of the turbo equalizer convergence is then possible by concatenating the input-output mutual information transfer functions. At iteration  $i$  the equalizer output mutual information can be given by the recursion

$$I_e(i) = f_e(f_d^{-1}(I_e(i-1))), \quad (119)$$

where  $I_e(i-1)$  is the equalizer output mutual information at the previous iteration.

Since the equalizer provides an extrinsic information value at its output, information of all bits except those corresponding to the output is utilized as prior information in computing the output bit. In a turbo equalizer that provides a symbol estimate at its output, the prior information used for the computation of one output consists then of symbol level soft information of all but the desired symbol. The logical conclusion of this is that equalizers for symbol-orthogonal channels (e.g. a flat fading channel) have an EXIT function given by a constant. The prior information of the bits other than the desired bit within one modulated symbol can be used as prior information at the symbol de-mapper. However, with Gray-mapped BPSK, QPSK and 16-QAM no dependency is introduced between modulated bits and prior information does not provide any gain. The gain is very small for Gray-mapped 8-PSK [131]. If no prior information is used in the de-mapping, the EXIT function of a flat fading SISO channel with multilevel modulation is constant.

Assuming the studied algorithm behaves well, i.e., increasing prior information improves performance, and the channel is always frequency-selective, all EXIT functions are monotonically increasing. The case of a flat EXIT function indicates independence between the prior information and the value being estimated. In addition, all decoder EXIT functions have the two extreme values

$$f_d(0) = 0 \quad (120)$$

$$f_d(1) = 1. \quad (121)$$

For practical computations, the task to evaluate the EXIT function of the decoder is relatively straightforward, as it is fixed. In some cases [71] it is possible to compute the EXIT function analytically, but such a method is currently known neither for the decoding of channel codes over Gaussian channels nor for the equalization of Gaussian frequency-selective channels. Thus, in this thesis, EXIT charts of channel decoders are generated through simulations.

The decoder EXIT function is specific to the decoding algorithm. For example, log-MAP and max-log-MAP decoders have different functions, whereas MAP and log-MAP algorithms have the same function due to their functional equivalence. In this thesis the log-MAP decoder is used for all simulations and the generation of decoder EXIT charts. If the decoder inputs are the output likelihoods of a binary input channel with additive Gaussian noise, the likelihoods can be modeled as

$$\xi_k^e(n) = \frac{\sigma_e^2}{2} b_k(n) + w_e, \quad (122)$$

where  $w_e \sim N(0, \sigma_e^2)$ , and whose mutual information with the bits can be computed with (the  $J$ -function in [66])

$$\mathcal{J}(\sigma_e) = 1 - \int_{-\infty}^{\infty} \frac{e^{-(\phi - \sigma_e^2/2)^2/2\sigma_e^2}}{\sqrt{2\pi}\sigma_e} \log_2(1 + e^{-\phi}) d\phi. \quad (123)$$

With (122), the EXIT function of the decoder can be empirically estimated by feeding the decoder random inputs according to Eq. (122) and measuring the mutual information between the transmitted data and the likelihoods of the encoded data provided by the decoder. As an example, the EXIT functions of convolutional codes with different constraint lengths are provided in Fig. 18. The error performance of the code is related to how it behaves when the input mutual information approaches one, since the decoder output (decoded bits) mutual information is related to the extrinsic information. Fig. 18 also shows how increasing the code memory allows the code to reach a higher output mutual information at a lower input mutual information.

The EXIT function of the equalizer provides the mapping from input to output mutual information for the equalizer. It is clear that since all characteristics of the channel depend on the channel state, also the convergence characteristic of the channel equalizer does so. For instance, in the case of a MAP equalizer, the channel state determines the trellis structure the equalizer operates with. As in the case of channel decoding, also the equalizer EXIT chart depends on the equalization algorithm used. Examples of EXIT functions of different turbo equalization algorithms can be found in e.g. [69].

Given a channel realization, the receiver noise variance and the equalizer algorithm, the EXIT function of the channel can be computed empirically. An example of channel EXIT functions for different received SNRs is depicted in Fig. 20. By combining an equalizer function and a decoder function into one EXIT chart, the convergence of the algorithm can be tracked by invoking the iteration (119). The process begins with no prior information at  $(I_e = 0, I_d = 0)$ , followed by alternating activations of the equalizer and decoder executing the convergence steps until the point where the exit functions of the equalizer and decoder cross, or the point of error-free decoding  $(I_e = 1, I_d = 1)$  is reached. A vertical line represents an equalizer activation, and a horizontal line represents a decoder activation. The process is illustrated with a hypothetical equalizer EXIT function in Fig. 21. To reach error-free decoding, there must be an opening in the EXIT chart between the equalizer function and the decoder function for the iterations to pass through. Formally, the constraint

$$f_e(I_d) - f_d(I_d) > 0, \forall I_e \in \mathbb{E} \quad (124)$$

must be fulfilled. As seen in Fig. 20, none of the equalizer EXIT functions reaches the point  $\{1, 1\}$ , which would be required for error-free decoding according to (124). In reality, all decoder EXIT functions cross the equalizer EXIT function at a fixed point, which then defines the error probability of the decoded data.

EXIT functions have an area property, which relates the area under the curve to the transmission rate. For an optimally decoded channel code, whose *a priori* inputs are generated by a binary erasure channel (BEC), the area under the EXIT function is equivalent to the code rate, as provided in Eq. 43. The property has been empirically observed to approximately hold also for *a priori* information from Gaussian channels [105]. Its effects can be observed from Figs. 18 and 19, where the EXIT functions of higher rate codes are

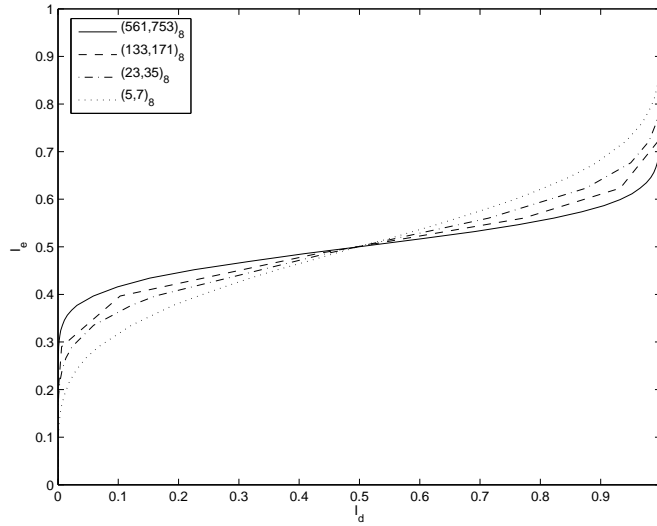


**Fig. 18. EXIT charts of convolutional codes with different memory order.**

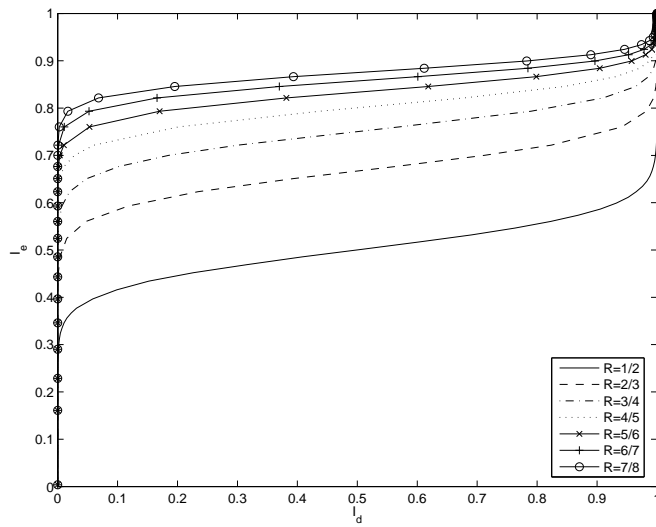


**Fig. 19. EXIT charts of codes punctured from the rate-1/2,  $(561, 753)_8$  convolutional code.**

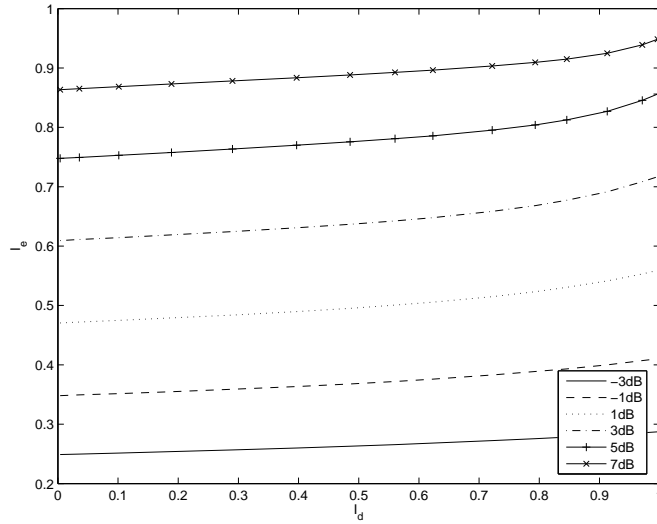


**Fig. 20. EXIT charts of the MMSE turbo equalizer at -1,1,3,5 and 7dB SNR.**

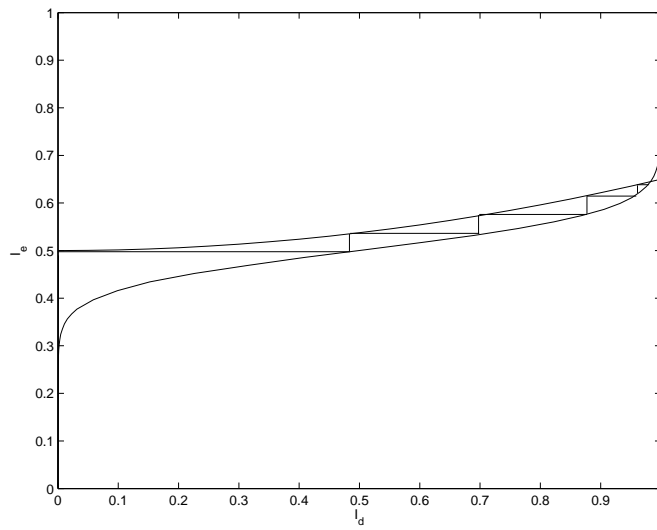


**Fig. 21. Convergence tracking with an EXIT chart.**

locate higher in the chart of Fig. 19 but the change of encoder memory in Fig. 18 results in approximately symmetrical changes around the diagonal leaving the area approximately unaltered. The area property of the channel relates the EXIT function of an optimally equalized channel, with *a priori* inputs generated by a BEC, to the uniform input capacity of the channel [71], and for higher order modulations to the capacity divided by the modulation cardinality [105]. Even though the area property has not been rigorously proved to strictly hold in the case of turbo equalization using feedback generated by a Gaussian channel, the current knowledge justifies its usage as an approximated analysis and design tool.

The area property provides the framework for understanding the limits of system optimization through EXIT function matching. With optimal algorithms as components, suitably optimized systems can approach channel capacity. In turbo equalization context this means the channel code must be capacity achieving, and must enable a design matched to the channel so that  $f_d = f_e$ . Since the equalizer EXIT function is conditioned on the channel state, this matching effectively requires channel knowledge at the transmitter. The area property also implicitly proves that any suboptimal algorithms used for equalization (which have their EXIT function below that of the optimal algorithm) have a lower achievable rate than the optimal, i.e. they cannot reach channel capacity.

## 4.2 Multi-dimensional EXIT charts

In cases where there are multiple separately encoded and transmitted parallel data sources to be detected, multiple parameters must be tracked. Such cases include multi-user transmissions, MIMO transmissions with layered schemes and multilevel coded transmissions, where the first two cases are equivalent in terms of analysis and the last is a special case of the former having fully correlated propagation channels between transmissions. For multiple separate transmissions, the prior information is defined by the vector

$$\mathbf{I}_d = [I_{d,1}, \dots, I_{d,k}, \dots, I_{d,K}]^T \in \mathbb{E}^K, \quad (125)$$

and the equalizer EXIT function is defined by

$$\mathbf{f}_e : \mathbf{I}_d \rightarrow \mathbf{f}_e(\mathbf{I}_d) \in \mathbb{E}^K. \quad (126)$$

The joint decoder EXIT function is defined for notational convenience as the vector

$$\mathbf{f}_d : \mathbf{I}_d \rightarrow \mathbf{f}_d(\mathbf{I}_d), \quad (127)$$

where

$$\mathbf{f}_d = [f_{d,1}(I_{d,1}), \dots, f_{d,k}(I_{d,k}), \dots, f_{d,K}(I_{d,K})], \quad (128)$$

with each  $f_{d,k}$  defined by (117). If the transmissions are assumed spatially non-orthogonal, and the channel experienced by each transmission is frequency-selective, the equalizer vector EXIT function (126) has non-zero partial differentials. In the general case, when the actual mechanism generating the EXIT function is not necessarily perfectly known

or understood, it is impossible to state whether the equalizer EXIT function is bijective or not. For the equalizer EXIT function to be bijective, among other requirements, the determinant of the EXIT function Jacobian should always be non-zero, i.e.,

$$\left| \frac{\partial \mathbf{f}_e}{\partial \mathbf{I}_d} \right| \neq 0 \forall \mathbf{I}_d \in \mathbb{E}^K. \quad (129)$$

On the other hand, the decoder EXIT functions (117) are monotonous (and bijective) separately and, thus, also the vector mapping of Eq. (127) is bijective. This is due to (127) being a diagonal matrix of monotonous scalar functions, and the determinant of such a vector function is always positive.

An example for two parallel transmissions illustrates the multidimensional convergence analysis. In this example the analysis is applied to tracking the convergence of the equalizer combined with a convolutional code. For the case of two transmissions, the EXIT chart is visualized in three dimensions and the vector EXIT function  $\mathbf{f}_e$  is given by two surfaces, one for each equalizer output. The equalizer convergence characteristic is fully defined by these two surfaces and two decoder surfaces. In the case where identical channel codes and decoding is used for both antennas, the decoder surfaces are a mirror image of each other across the vertical plane defined by the curve on the  $I_{d,1}, I_{d,2}$  plane defined by the parametric representation

$$g_d(t) = \bar{\mathbf{I}}_d t, \quad (130)$$

where  $t$  is the representation parameter and  $\bar{\mathbf{I}}_d$  denotes the  $K$ -dimensional vector base for the equalizer EXIT function

$$\bar{\mathbf{I}}_d = \sum_{k=1}^K \bar{I}_{d,k}. \quad (131)$$

It is useful to consider the example presented in Fig. 22, where an example of  $I_{e,1}$  is presented with the EXIT function of the 1/2-rate convolutional code (561, 753). The iterations of this equalization loop begin at the point  $\mathbf{I}_d = \{0, 0\}$  and the iteration may assume any values for the tuple  $\mathbf{I}_d$  in the sets defined by the constraints

$$\tilde{\mathcal{C}}_1 : \{ \mathbf{I}_d \in \mathbb{E}^2, f_{e,1}(\mathbf{I}_d) > f_{d,1}(\mathbf{I}_d) \} \quad (132)$$

$$\tilde{\mathcal{C}}_2 : \{ \mathbf{I}_d \in \mathbb{E}^2, f_{e,2}(\mathbf{I}_d) > f_{d,2}(\mathbf{I}_d) \} \quad (133)$$

for decoders 1 and 2, respectively. In Appendix 2 it is shown, that for successful convergence, the system convergence set must then be a connected set given by the union of the two antenna-wise convergence sets including the starting and ending points

$$\mathcal{C}^0 = \{ \mathbf{I}_d = \mathbf{0}^K \} \quad (134)$$

$$\mathcal{C}^1 = \{ \mathbf{I}_d = \mathbf{1}^K \}. \quad (135)$$

Visually this means the points where each of the equalizer EXIT surfaces is above the corresponding decoder EXIT surface define two regions which must connect with each other and their union must connect with the convergence starting and ending points. In the general case of  $K$  transmit antennas, the convergence requirement can be used with the generic inequality expression

$$\tilde{\mathcal{C}}_k = \{ \mathbf{I}_d \in \mathbb{E}^2, f_{e,k}(\mathbf{I}_d) > f_{d,k}(I_{d,k}) \} \subset \mathbb{E}^K, \quad (136)$$

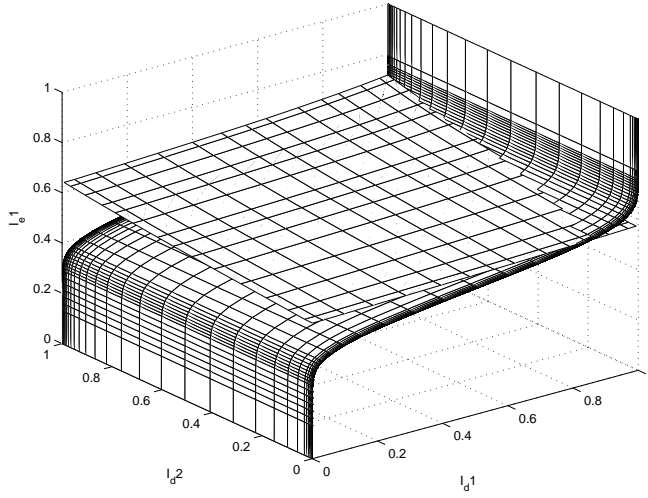


**Fig. 22.** Equalizer EXIT function  $f_{e,1}$  example in three dimensions for a two-transmission case.

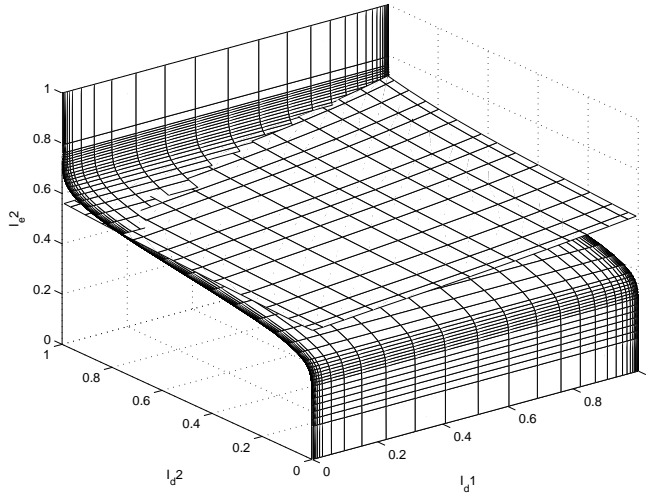


**Fig. 23.** Equalizer EXIT function  $f_{e,2}$  example in three dimensions for a two-transmission case.

where the inequality is taken component-wise. The generic  $K$ -dimensional convergence requirement now becomes

$$\mathcal{C}^0 \cup \mathcal{C}^1 \bigcup_{k=1}^K \tilde{\mathcal{C}}_k. \quad (137)$$

Note, that applying the analysis with different codes results in different convergence constraints.

### 4.2.1 Approximate rate interpretations from EXIT functions

Apart from applications to convergence tracking, EXIT functions can provide indications of system performance without explicit consideration to the applied channel codes. The approximate area property of channel codes and its application to the case of multidimensional EXIT functions can provide a valuable technique to understanding the limits of the considered system. The two transmission case can be analysed for further insights by assuming channel knowledge at the transmitter side. The channel state knowledge is used for the sole purpose of matching the channel code to the equalizer EXIT function. It is assumed, that by using the channel state knowledge, the equalizer EXIT function can be acquired, and the two channel code EXIT functions can be jointly matched *arbitrarily closely* to the equalizer EXIT function for the channel realization, given a usable design target and method. The actual choice of the code family is not considered or assumed explicitly, other than the family must have the degree of freedom in their design to allow the required EXIT function shaping, excluding for instance simple convolutional and turbo codes. In practice, code families having the required degree of freedom include at least irregular LDPC [80] and irregular repeat accumulate (RA) codes [132] and turbo codes with multiple parallel concatenated component codes [131]. Since these are all iteratively decoded codes, the effects of detector scheduling due to loops in the joint detector graph [25] must be considered in the case of finite block lengths. However, the EXIT analysis assumes infinite block length, and in such a case for many multiuser systems [25, 80, 133] finite loops can be proven to disappear from the system graph while a message-passing algorithm converges within finite iterations.

The EXIT function describes the convergence property of a single channel realization, with some arbitrary but fixed transmitted power, modulation method and iterative detector. As stated in Section 2.5, the capacity region of such a fixed two-transmission case is given by a pentagon. The rate interpretations made using the EXIT function will be interesting especially when compared to the shape of the capacity region, but it will not be possible to claim any absolute rates, let alone capacity-achievability of the system, without further knowledge on an actual equalizer EXIT function and the values it takes. It should be further noted, that in most cases the EXIT function is an approximation and cannot provide exact results.

In the generic case the approach should be extendable to the case of transmitter side processing using the channel knowledge, e.g. spectrum shaping or Tomlinson-Harashima pre-coding, but such extensions are beyond the scope of this thesis. Such methods would also effectively change the equivalent channel experienced by the transmitted data, and

would require a new EXIT function to be computed by taking their use into consideration.

Considering the two equalizer EXIT surfaces in the three-dimensional chart, the code design becomes a question of choosing the path

$$g_p(t) = g_{p,1}(t)\bar{I}_{d,1} + g_{p,2}(t)\bar{I}_{d,2} \quad (138)$$

through the  $\mathbf{I}_d$ -plane. To minimize rate loss due to the gap between the code and equalizer EXIT functions any design should be optimized to have the convergence set of the system reduced to a curve. Such a convergence set implies infinite complexity due to the increasing number of equalizer iterations as the convergence set becomes narrower. The area property of the channel code to be designed extends to the two transmission case so that

$$R_1 < \int_0^1 f_{g_p,1}(I_{d,1}) dI_{d,1} \quad (139)$$

$$R_2 < \int_0^1 f_{g_p,2}(I_{d,2}) dI_{d,2}, \quad (140)$$

where  $f_{g_p,k}(I_{d,k})$  denotes the projection of the equalizer EXIT function  $f_{e,k}$  values on the path  $g_p$  onto the dimension of  $I_{d,k}$  as depicted in Fig. 24 and formally expressed using the vector inner product (dot product) as

$$f_{g_p,k}(I_{d,k}) = f_{e,k}(g_p) \bullet \bar{I}_{d,k}. \quad (141)$$

The rate inequality (140) extends to the  $K$ -dimensional case so that the curve  $g_K$  through the  $K$ -dimensional space defines the rates of each transmission  $k$  as

$$R_k < \int_0^1 f_{g_p,k}(I_{d,k}) dI_{d,k}. \quad (142)$$

The application of the area property in the two transmission case is illustrated in Fig. 24, where the decoding path due to code design is shown with the two corresponding space curves at the intersection of the equalizer EXIT functions and the vertical plane defined by  $g_p$ . The areas defining the achievable rates  $R_1$  and  $R_2$  are shown as the space curves are projected to the corresponding sides of the cube-shaped EXIT chart.

Fig. 25 presents the two opposite extremes of the design: allocating maximum rate to one transmission and minimum rate to the other, i.e., either  $(R_1^{min}, R_2^{max})$  or  $(R_2^{min}, R_1^{max})$ . The smaller allocation is referred to as the minimum, even though it is actually the maximum rate given the other rate allocation. With suitable code design the rate allocation can be made to favor either transmission, within the constraints of the equalizer EXIT function. It is notable, that if an extreme rate allocation is made, it also corresponds to strict detection ordering, where one transmission is detected first through turbo equalization iterations, followed by the turbo detection of the other transmission, since the decoding path follows the sides of the EXIT chart.

Having an understanding of the maximum and minimum individual rates supportable by the system given a particular realization of EXIT functions, an important remaining

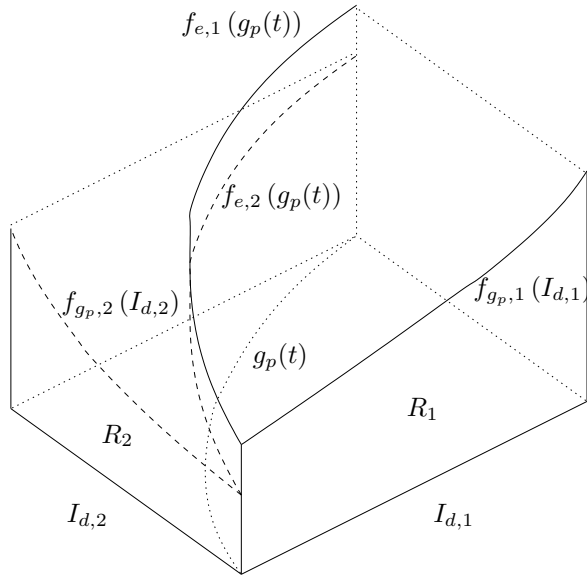


Fig. 24. Area property applied in the two transmission case.

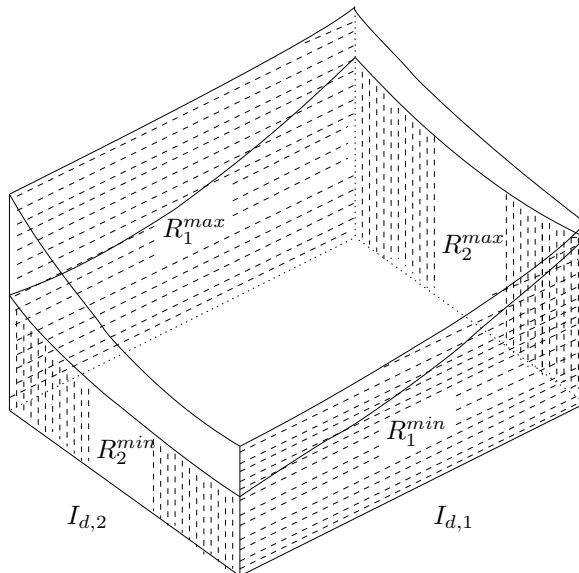
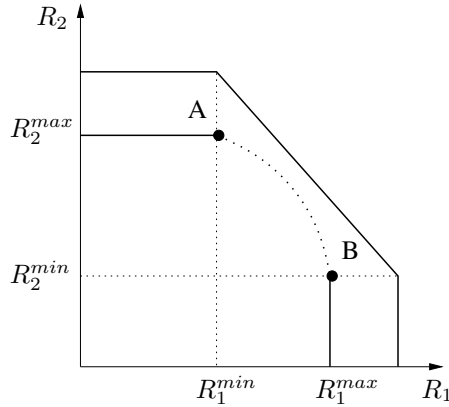


Fig. 25. Minimum and maximum achievable rates for the two transmissions due to the area property.



**Fig. 26. Multiple-access channel capacity region.**

question concerns the interpretation of the maximum sum rate and how the corresponding design is found on the EXIT chart. In Appendix 4 it is shown, that the sum rate design follows the eigenvector corresponding to the maximum Jacobian eigenvalue at each point of the curve starting from  $C^0$  and ending at  $C^1$ . The sum rate maximization also indicates that unless transmissions are orthogonal, i.e.,  $\partial f_{e,k}/\partial I_{d,k'}, k \neq k' = 0$ , or one of the transmissions has been totally removed, the optimal path is never parallel to any of the chart sides. Thus, strict serial detection ordering is sub-optimal in the sum rate sense. It is interesting to compare the three previous designs with the achievable rate region of a multiple access channel with two transmitters. The capacity region of a two transmission system is defined by the rate inequalities describing the mutual information between the received signal  $\mathbf{r}$  and the transmitted bits

$$R_1 < I(b_1; \mathbf{r}|b_2) \quad (143)$$

$$R_2 < I(b_2; \mathbf{r}|b_1) \quad (144)$$

$$R_1 + R_2 < I(b_1, b_2; \mathbf{r}), \quad (145)$$

which can be visualized as a pentagon as shown in Fig. 26. The rate region of the turbo equalizer system lies somewhere within the capacity region. Examining Fig. 25 it can be seen that the design with  $(R_1^{\min}, R_2^{\max})$  corresponds to point A and the design with  $(R_1^{\max}, R_2^{\min})$  to point B, which reside somewhere inside the capacity region. These extreme code rates also correspond to the case of decoding with perfect knowledge of the other transmission.

Beyond establishing the connection between the points A and B and the EXIT chart sides, it is interesting to examine what the EXIT function predicts of the rate region between them. Without explicit consideration of the EXIT function shape it is impossible to prove the shape of the predicted achievable rate region beyond the following. If the predicted achievable rate region between the points A and B were illustrated by a line segment, either one or both of the points A and B would be optimal in the sum rate sense. However, earlier it was indicated that such a rate combination corresponds to the code

design where the decoding path proceeds along the sides of the EXIT chart. But such decoding is only sum rate optimal if the Jacobian (A4.269) is diagonal, which can happen only if the transmissions do not interfere (i.e. they are orthogonal). Thus, unless the transmissions are orthogonal, there must be a sum rate exceeding that described by a line segment between the points A and B. This rate region is illustrated with the arc drawn between the points A and B in Fig. 26.

Another result concerning the rate region between points A and B can be produced using the methods of differential geometry. The area integrals  $R_k$  for each  $k$  can be combined to express the sum rate as [134]

$$\sum_{k=1}^K R_k < \int_0^1 \sum_{k=1}^K f_{g_p,k}(I_{d,k}) dI_{d,k} \quad (146)$$

$$= \int_0^1 \sum_{k=1}^K f_{e,k}(g_p(t)) \frac{dI_{d,k}}{dt} dt \quad (147)$$

$$= \int_{g_p} \mathbf{f}_e(\bar{\mathbf{I}}_d) \bullet d\bar{\mathbf{I}}_d, \quad (148)$$

where  $\bar{\mathbf{I}}_d$  denotes the  $K$ -dimensional vector base for the equalizer EXIT function. Now, in the special case that the sum rate is constant and, thus, independent of the design, the region between the points A and B is given by a straight line with a decay of  $-1$ . In such a case the integral (148) is independent of the integration path  $g_p$ . This indicates that the curl of the vector EXIT function (vector field) is zero, i.e.,

$$\nabla \times \mathbf{f}_e = 0. \quad (149)$$

This would then in the two transmission case require, that

$$\frac{\partial f_{e,1}}{\partial I_{d,2}} = \frac{\partial f_{e,2}}{\partial I_{d,1}} \quad \forall \mathbf{I}_d \in \mathbb{E}^2, \quad (150)$$

so that the EXIT function Jacobian is symmetric throughout the function domain. This would require, however, that increasing prior information would have a symmetric effect between any two transmissions. A simple counter-example is the case of discrete modulation, for instance, where the slope of equalizer output extrinsic information depends on the absolute extrinsic information value. Thus, any point where the absolute extrinsic mutual information of the two outputs differ significantly will have a non-symmetric EXIT function Jacobian.

### 4.2.2 Symmetric design

The generic design in Section 4.2.1 assumes that the transmissions, or channel codes of each transmission, can be jointly optimized and results in transmission-specific channel codes. In cases where only channel statistics are known rather than the instantaneous

state is known, this is not desirable and a symmetric design resulting in the same channel code for all the transmissions is a reasonable approach. When the principle of designing a symmetric code for one channel realization, represented by its EXIT function, is known, such a design principle can be used as the starting point for developing codes for arbitrary channel statistics. Since the same code is used for all transmissions, the code will not be optimal in the maximum rate sense as given in Section 4.2.1. This rate loss will be visible in the more rapid convergence of the detector, however, due to the wider opening between the equalizer and decoder functions. Note that if further system optimization is desired, the design can be combined with either power or rate control [26, 132]. Both of these techniques, however, require some amount of channel knowledge at the transmitter when the system is operating.

The symmetry constraint provides a convenient starting point for the design. Since all transmissions use the same channel code, to maximise the total transmission rate, the area below the EXIT function  $f_{e,\text{opt}}$  of that code should be maximized. Furthermore, since all transmissions should successfully converge, the code EXIT function should be below the equalizer EXIT function of all transmissions when taking the decoding path of the design. More formally, the definition of the convergence set (A2.257), as given in Appendix 2, should be fulfilled. It is the simplest approach for the code optimization by considering the upper limits of the projected functions for each  $k$  and how they relate to the optimum code.

The two transmission case depicted in Fig. 25 serves as a good illustration. The maximum rate of each transmission is limited by the EXIT function value given full prior knowledge of the other transmission. For example, for transmission 2, this function then reduces into the maximum projected function  $f_{e,2}(I_{d,2}, I_{d,1} = 1)$ , and the convergence constraint set  $C_2$  is now by the top-right edge of the EXIT chart marked by  $R_2^{\text{max}}$ . Since the convergence set must be connected,  $C_1$  must have an intersection with  $C_2$ , while having a tunnel open for convergence. The constraint for the code of transmission 2 is then given by the projected function  $f_{e,1}(I_{d,1}, I_{d,2} = 0)$ . Since the optimal code design should have its EXIT function below the projected EXIT functions of *both* transmissions, the optimal code EXIT function is bounded above by the point-wise minimum of these two equalizer EXIT functions. To be precise, the design converges successfully if the code EXIT function fulfills

$$f_{d,\text{opt}}(I_d) < \min \{f_{e,1}(I_{d,1}|I_{d,2} = 0), f_{e,2}(I_{d,2}|I_{d,1} = 1)\}, \quad (151)$$

which guarantees that both parallel iterations converge successfully. The point-wise minimum is necessary since the projected EXIT functions can cross. In this example it is relatively easy to see how to find the optimal design. In the more generic it may be not as obvious which extreme projected functions to choose. Even in this example, there is another potential pair of extreme functions, at the chart sides denoted by  $R_2^{\text{min}}$  and  $R_1^{\text{max}}$ , but this design is an inferior choice due to the visible limiting effect of the projected function  $f_{e,2}(I_{d,2}, I_{d,1} = 0)$ . However, the choice of extreme functions can be considered a form of ordering that is performed to minimize the limitation to maximum rate due to the projected EXIT functions.

From the above, the principles to perform the code optimization with the EXIT function can be drawn. Firstly, to reach maximum rate, consider projected EXIT functions. Secondly, detection must be implicitly ordered to fulfill the connected union requirement

of Eq. (A2.260) of the convergence set. In the  $K$ -dimensional case, there are  $K!$  possible orderings and  $K$  projected EXIT functions for each ordering. Find the ordering that limits the maximum rate the least. Thirdly, find the optimum design function for the code by considering the point-wise minimum of the projected EXIT functions within the ordering to guarantee convergence in all dimensions.

Formalizing the above in the case of  $K$  parallel transmissions, an ordering vector for the transmissions  $\bar{o} = [o_1, \dots, o_k, \dots, o_K]$  can be defined so that  $\bar{o}_k = [o_1, \dots, o_k]$  holds the first  $k$  indexes of the ordering. The following shorthand is introduced for any variables computed with prior information. For transmission  $k$ , a variable  ${}^b_a C_k(I_d)$  denotes the value of variable  $C_k$  computed with prior information  $a \in \{0, 1\}$  on transmissions  $1 \dots k-1$  and with prior information  $b \in \{0, 1\}$  on transmissions  $k+1 \dots K$ . If ordering is applied, the absolute indexes can be replaced by relative indexes given by the ordering so that  $k \rightarrow o_k$ . Now, the optimal code EXIT function is given by the constraint

$$f_{d,\text{opt}}(I_d) < \arg \max_{\bar{o}} \int_0^1 \min \{ {}^0_1 f_{e,k}(I_d) \} dI_d, \quad (152)$$

which finds the ordering that maximizes the area below the point-wise minimum of all maximal projected EXIT functions within the ordering so that each maximal projected EXIT function assumes full prior information of transmissions preceding it in the ordering. Since the maximal projected EXIT function corresponds to the ordering principle, it is denoted as “order-projected” in the remainder of the thesis.

In practice, any channel code whose EXIT function fulfills

$$f_d < f_{d,\text{opt}} \forall I_d \quad (153)$$

can be successfully detected and the opening between the code and equalizer EXIT functions is largest at the chart sides. Actually, since convergence is guaranteed by the minimum order-projected EXIT function, some order-projected functions within the ordering may be well below the equalizer EXIT function. In such a case using strict ordering at the detector will result in slower convergence than simultaneously detecting all transmission and letting the detector take whatever path it may within the convergence set. A gap between the order-projected EXIT function and the optimal code EXIT function indicates the convergence set extends to the area next to the chart side.

The optimal ordering finds the largest point-wise minimum over all order-projected EXIT functions on the chart edges. A related sub-optimal ordering finds the largest minimum starting point,  $f_{g_p,k}(0)$ , of the order-projected EXIT functions within the ordering. Then, given the ordering, the point-wise minimum of the order-projected EXIT functions is found to guarantee convergence of all transmissions. If the channel is flat, the order-projected EXIT functions along each chart side are constant, and the transmission to be decoded can be optimally chosen based on the EXIT function value at each chart corner. Conceptually, the ordering at the detector chooses the optimal convergence path and provides receiver diversity through equalizer convergence.

Finally, the number of possible orderings and the number of order-projected EXIT functions in each ordering, whose point-wise minimum function must be found in order to identify the optimal ordering, makes it obvious that further knowledge of the behavior of the equalizer EXIT functions in question would simplify the optimization considerably.

### 4.3 Semianalytical EXIT charts

Based on the previous section, it is obvious the knowledge of the equalizer EXIT function can provide much information on the behavior and the achievable limits of the system even without knowledge of the utilized channel codes. On the other hand, such knowledge, if available, can be used to evaluate the convergence behavior of real systems. In multi-dimensional cases, however, acquiring knowledge of system behavior by resorting to simulation based EXIT analysis quickly becomes prohibitively complex. Furthermore, the dependence of the equalizer EXIT function on the channel state makes any simulation based approach inadequate.

In this section, a method to compute an approximate EXIT function of a frequency-domain MMSE turbo equalizer will be derived assuming Gray-mapped BICM modulation. Frequency-domain equalization is considered due to its superiority in performance and complexity over other methods considered in Chapter 3. The choice of coded modulation is a pragmatic one: BICM has a simple design that makes the use of adaptive modulation and coding straightforward. However, a price is paid by using a single channel code only in that the coded modulation cannot reach the modulation capacity [135].

A Gaussian approximation is made for both the equalizer output likelihoods and the decoder feedback likelihoods so that for a transmitted encoded bit  $b_k$ ,

$$\xi_k^e \sim N(\sigma_{e,k}^2/2, \sigma_{e,k}^2) \quad (154)$$

$$\xi_k^d \sim N(\sigma_{d,k}^2/2, \sigma_{d,k}^2), \quad (155)$$

where the subscript  $m$  has been dropped since the same distribution applies to all bits within a symbol. The former distribution is supported by the central limit theorem and the fact that the output is generated by a linear filter. The latter has been widely applied in the analysis of turbo algorithms [41, 69], though in some cases more accurate results may be achievable through more detailed distribution modeling [78].

The method to compute the equalizer EXIT function can be roughly divided into three phases. The first one describes how *a priori* knowledge is used in the equalizer for interference cancelling and, thus, how the equalizer behaves with different levels of mutual information of *a priori* information. The second phase describes how the extrinsic filter output equivalent channel SNR is computed using the *a priori* mutual information. Last, the filter output SNR is converted into average mutual information at the symbol de-mapper output.

In the first phase, decoder feedback likelihood is transformed into soft symbol estimates for interference cancellation, and the feedback mutual information is embodied in the variance of the residual symbol interference given by (102). As the EXIT function is defined for infinite block length assuming i.i.d. likelihoods, (102) can be replaced by its expectation given by the  $M$ -fold integral

$$\begin{aligned} E\{\bar{\lambda}_k\} &= 1 - M^{-1} \sum_{m=1}^M \sum_{s_i \in S} |s_i|^2. \\ &\int_{-\infty}^{\infty} \prod_{m=1}^M P_a(s_k = s_i) \prod_{m=1}^M P(\xi_k^d | b_k) \prod d\xi_k^d, \quad (156) \end{aligned}$$

where  $P(\xi_k^d|b)$  is the conditional distribution of the likelihood  $\xi_k^d$  given the transmitted encoded data bit defined in (155). In a corresponding manner, the ensemble variance of the soft symbol estimates (106) can be replaced by the respective expected value. The distribution of the likelihood is defined by the feedback mutual information using (123) so that

$$\sigma_{d,k} = \mathcal{J}^{-1}(I_{e,k}). \quad (157)$$

In practice the value of (156) can be computed by Monte-Carlo integration and since the dependence of  $\bar{\lambda}_k$  and  $\delta_k$  on the prior information is modulation-specific, the computation needs to be performed once for each studied modulation. A look-up table or a suitable functional approximation can be used in the numerical convergence analysis studies.

The expected values of the symbol residual interference  $E\{\bar{\lambda}\}$  and the soft symbol estimate variance can now be used in the computation of the SNR of the equivalent Gaussian channel at the output of the equalizer. Using (108), the instantaneous SNR of the equalizer output conditioned on the channel state and the receiver noise variance can be expressed as

$$\mathcal{L}_{k,a} = \frac{\mu_{k,a}}{1 - \mu_{k,a}}, \quad (158)$$

The mutual information between transmitted bits and the de-mapper output is then computed as the average bitwise mutual information of the equivalent Gaussian channel output as [136]

$$I_{e,k} = C_B(\mu_{k,a}, B) - \frac{1}{2M} \sum_{j=1}^M \sum_{k=0}^1 C_{B_k^j}(\mu_{k,a}, B), \quad (159)$$

where  $C_{B_k^j}$  is the constellation constrained capacity (CCC) of the  $j$ th sub-constellation consisting of the points where the bit  $j$  takes the value  $k$ . The CCC of a constellation in an AWGN channel with variance  $\mu_{k,a}(1 - \mu_{k,a})/2$  per dimension is defined as

$$C_B(\mu_{k,a}, B) = M - 2^{-M} \sum_{i=1}^M \mathbb{E} \left\{ \log_2 \sum_{j=1}^M \exp \left( - \frac{|\mu_{k,a}(b_i - b_j) + v|^2 - |v|^2}{\mu_{k,a}(1 - \mu_{k,a})/p} \right) \right\}, \quad (160)$$

where  $p = 1$  for complex and  $p = 2$  for real modulations. The sub-constellations are defined by the mapping rule assumed and the value of  $C_{B_k^j}$  can be computed with (160) by setting  $M \rightarrow M - 1$  and defining  $b_i$  and  $b_j$  for the sub-constellation. The expectation in (160) is taken over the two-dimensional Gaussian distribution of the zero-mean complex noise variable  $v$ . In the case of real valued binary signaling (160) specializes into (123).

For practical numerical computations, the functions (159) for the desired mapping can be precomputed, and approximated by (c.f. [131])

$$I_{e,k}(\sigma_{e,k}) \approx \left( 1 - 2^{-H_1 \sigma_{e,k}^{2H_2}} \right)^{H_3}, \quad (161)$$

where the parameter  $\sigma_{e,k}$  is defined as

$$\sigma_{e,k} = \begin{cases} 2\sqrt{2\mathcal{L}_{k,a}} & \text{real modulation} \\ 2\sqrt{\mathcal{L}_{k,a}} & \text{complex modulation,} \end{cases} \quad (162)$$

$$(163)$$

Table 6. Approximation parameters for Eqs. (161), Gray mapping.

Modulation	$H_1$	$H_2$	$H_3$
BPSK [131]	0.3073	0.8935	1.1064
QPSK	0.3073	0.8935	1.1064
8PSK	0.2516	0.7274	1.2392
16QAM	0.2224	0.6783	1.3617

and the mapping-specific parameters  $H_1$ ,  $H_2$  and  $H_3$  can be obtained by least-squared curve fitting. The parameter values for BPSK and Gray-mapped QPSK, 8PSK and 16QAM are listed in Table 6.

In summary, the average mutual information at the equalizer (de-mapper) output for a given mutual information of the channel decoder feedback extrinsic information  $I_{d,k}$ , conditioned on the channel state and receiver noise variance can be evaluated by:

- A: computing  $E\{\bar{\lambda}_k\}$  and  $E\{\delta_k\}$  using  $I_{d,k}$  for all  $k$ ,
- B: computing  $E\{\bar{\gamma}_k\}$  and  $E\{\mu_{k,a}\}$  for all  $k$ ,
- C: evaluating the average mutual information using (161).
- D: Look-up the decoder output extrinsic information corresponding to the input information.

If the method is to be used for tracking the equalizer convergence through the turbo iterations, the initial condition of  $I_{d,k} = 0$  is applied for all  $k$ , and the iterations are tracked through repeating steps A-D above until a fixed point is reached. A fixed point can be detected with a suitable stopping condition, e.g. that the change of  $I_{a,k}$  between two consecutive iterations is below a suitable threshold, here chosen to be  $10^{-6}$ . In the numerical evaluations, based on the fact that in simulations with fading channels most gain of turbo equalizers is experienced within 3-4 iterations, the maximum allowed number of iterations was limited to 30. The channel decoder *a posteriori* information corresponding to the fixed point is then obtained from a simulated lookup table. It must be noted, that the combination of a maximum number of iterations and the used stopping condition can provide pessimistic results, if the convergence tunnel is very small and the code and the equalizer are well matched.

### 4.3.1 Accuracy verification

The accuracy of the proposed method for computing the approximate EXIT function for the frequency-domain equalizer is tested by comparing the analytical results with EXIT functions obtained empirically through numerical simulations using histograms [66]. Two scenarios were considered, the first of which is a single-input-single-output case using BPSK modulation, with the absolute value of the channel coefficients given by  $\mathbf{h} = \mathbf{1}_2^T \otimes [1.1, 2.26, 3.47, 2.33, 1.1]$ , where  $\mathbf{1}_n \in 1^{n \times 1}$  is an all-ones vector. The absolute

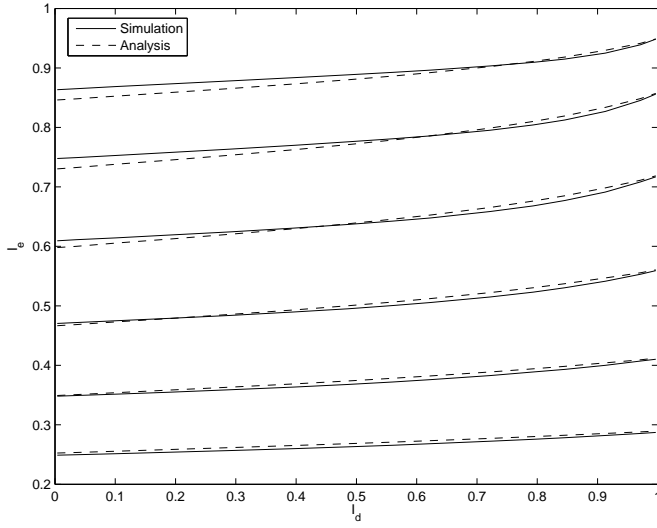


**Fig. 27. Analytical and simulated EXIT functions, and the analysis error at (bottom to top)  $-3, -1, 1, 3, 5, 7$ dB SNR.**

value of each coefficient is rotated with a randomly generated phase drawn from a uniform distribution over  $[0, 2\pi]$ . The equalizer is simulated with a block length of 16384 coded symbols over 10 blocks per each EXIT function point. The measured mutual information at the equalizer output is compared to the value computed using the  $J$ -function approximation (161). The analytical EXIT function is computed with an FFT length of 256. The result indicates that in an SISO case the analysis is very accurate when  $\mathbf{I}_{d,k} \rightarrow 1$ , regardless of the SNR. The analysis is less accurate when prior information is low. A closer examination of the test simulation results reported in Fig. 27 confirm the relative error of the analysis compared to the simulation is less than 2.5% in the tested case. The second verification case is a two-by-two spatially uncorrelated MIMO scenario, and the utilized channel is randomly generated assuming 20 channel coefficients with equal average energy. In Fig. 28, the EXIT function surface is shown for both the simulated system and an analytically computed equivalent at -3dB SNR. In this case, the relative error can be as high as 11% at low SNR, but reduces quickly at higher SNRs. In general, the accuracy of the method can be considered sufficient for generic evaluations of convergence and the behavior of the equalizer. If accurate absolute performance evaluations are required, the accuracy should be further evaluated.

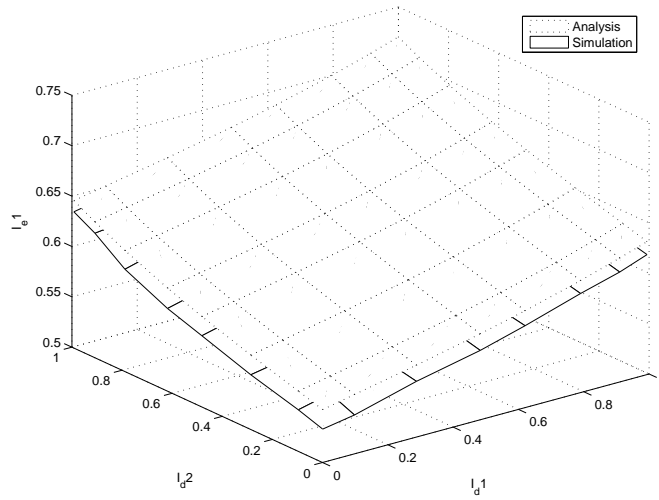


**Fig. 28. Analytical and simulated EXIT functions for  $-3\text{dB}$  SNR.**

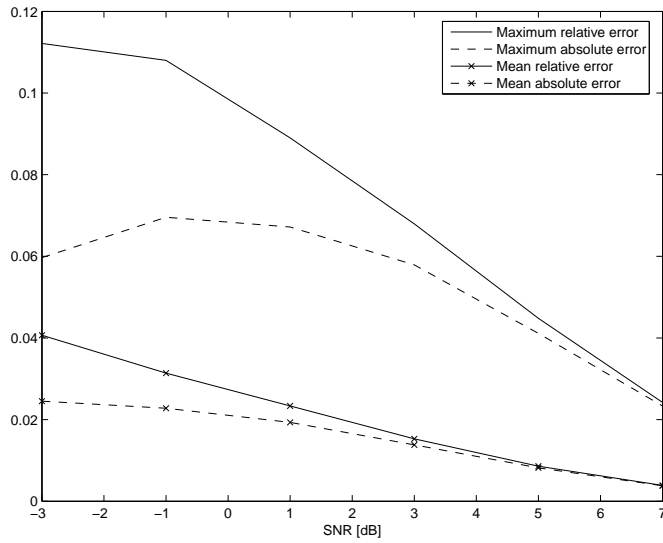


**Fig. 29. Error between the analysis and simulated EXIT surfaces.**

#### 4.4 EXIT function characteristics

It is worthwhile considering the characteristics of equalizer EXIT functions. The expression (159) due to the discrete constellation makes direct evaluations of mutual information difficult. However, the mutual information is monotonic in  $\mathcal{L}_{k,a}$ , which in turn is monotonic in  $\mu_{k,a}$ . Therefore, the behavior of  $\mu_{k,a}$  in extremes of the EXIT function can be analyzed to gain a level of understanding of EXIT function behavior.

The eigenvalue decompositions of the matrices  $\Xi_k \Xi_k^H$  and  $\Xi \Xi^H$  are given by

$$\Xi_k \Xi_k^H = \Phi_k \Upsilon_k \Phi_k^H \quad (164)$$

$$\Xi \Xi^H = \Phi \Upsilon \Phi^H, \quad (165)$$

where  $\Phi_k$  and  $\Phi$  represent the left eigenvectors of the desired and the total received composite signal, respectively. The  $(J(f-1)+j)$ th column of  $\Phi_k$ , denoted as  $\phi_k(J(f-1)+j)$  ( $\Phi$  and  $\phi(J(f-1)+j)$  have a corresponding relation), expresses the  $j$ th left spatial eigenvector of the desired signal's channel at frequency bin  $f$ , and has  $J$  non-zero elements  $(f, f+J, f+2J, \dots)$ , with the corresponding diagonal entry of  $\Upsilon_k$ , denoted as  $s_k(f+j)$ , being the  $j$ th spatial eigenvalue at frequency bin  $f$ . The covariance matrix of the interference-canceled signal can be expressed by the sum

$$\Xi \Delta_a \Xi^H + \sigma_0^2 \mathbf{I} = \sum_{k=1}^K \bar{\lambda}_k \Phi_k \Upsilon_k \Phi_k^H \quad (166)$$

$$= \mathbf{V} \bar{\Upsilon} \mathbf{V}^H. \quad (167)$$

Now (105) can be expressed by

$$\bar{\gamma}_k = N^{-1} \text{tr} \left\{ \Upsilon_k^{H/2} \left( \bar{\lambda}_k \Upsilon_k + \sum_{\substack{k'=1 \\ k' \neq k}} \bar{\lambda}_{k'} \mathbf{P}_{kk'} \Upsilon_{k'} \mathbf{P}_{kk'}^H + \sigma_0^2 \mathbf{I} \right)^{-1} \Upsilon_k^{1/2} \right\} \quad (168)$$

$$= N^{-1} \text{tr} \left\{ \Upsilon_k^{H/2} \Phi_k^H \mathbf{V} (\bar{\Upsilon} + \sigma_0^2 \mathbf{I})^{-1} \mathbf{V}^H \Phi_k \Upsilon_k^{1/2} \right\}, \quad (169)$$

where  $\mathbf{P}_{kk'} = \Phi_k^H \Phi_{k'}$  expresses the overlap between the eigenbases of the signals of different transmit antennas.

##### 4.4.1 Single transmit and single receive antenna

Using (105)–(106) and (168), the minimum and maximum values of (108) that define the corresponding extreme values of the equalizer EXIT function can be obtained. The difference between these values represents the generic orientation of the function. In practical terms, the difference demonstrates the usefulness of prior information in equalization, i.e., “turbo gain”. In a system with one transmit and one receive antenna, Eq. (168) can be computed with  $\Xi_k = \Xi$ ,  $v_f = h(f)$ , and  $\mu_{k,a}$  is given by

$$\mu_a(I_d = 0) = N^{-1} \sum_{f=1}^N \frac{|h(f)|^2}{|h(f)|^2 + \sigma_0^2}, \quad (170)$$

and

$$\mu_a(I_d = 1) = \frac{N^{-1} \sum_{f=1}^N |h(f)|^2}{N^{-1} \sum_{f=1}^N |h(f)|^2 + \sigma_0^2}, \quad (171)$$

for the cases of no and full prior information, respectively. The mean squared channel response and the receiver noise level  $\sigma_0^2$  in (171) fully determine the instantaneous equalizer output SNR with perfect prior information. Also, it can be noted, that  $\mu_a(I_d = 1) \rightarrow 1$  as  $\sigma_0^2 \rightarrow 0$  if the channel response is non-zero.

By simple arithmetic the difference of (170) and (171) can be expressed by

$$\begin{aligned} \mu_a(I_d = 1) - \mu_a(I_d = 0) = N^{-1} & \left( 1 + \frac{\sigma_0^2}{N^{-1} \sum_{f=1}^N |h(f)|^2} \right)^{-1} \times \\ & \sum_{f=1}^N \left( 1 + \frac{|h(f)|^2}{\sigma_0^2} \right)^{-1} \left( 1 - \frac{|h(f)|^2}{N^{-1} \sum_{f=1}^N |h(f)|^2} \right). \end{aligned} \quad (172)$$

In (172), the first term inside the summation is a factor inversely proportional to the instantaneous frequency-wise SNR taking values in the range of  $(0, 1)$ . The second term is the difference of the squared channel frequency response within each frequency bin to the mean squared response. The product of the two terms has an effect of emphasizing deep spectral nulls. If the squared channel frequency response is expressed by the sum of its mean and a zero-mean random component as

$$|h(f)|^2 = \overline{|h|^2} + |\widetilde{h(f)}|^2, \quad (173)$$

Eq. (172) can be expressed as

$$\begin{aligned} \mu_a(I_d = 1) - \mu_a(I_d = 0) = \\ -N^{-1} \left( \overline{|h|^2} + \sigma_0^2 \right)^{-1} \sum_{f=1}^N \left( 1 + \frac{\overline{|h|^2}}{\sigma_0^2} + \frac{|\widetilde{h(f)}|^2}{\sigma_0^2} \right)^{-1} |\widetilde{h(f)}|^2. \end{aligned} \quad (174)$$

By noting that the frequency-varying squared component  $|\widetilde{h(f)}|^2$  corresponds to the energy of the separable multipath components with a non-zero relative delay to the first received path, (174) represents a *measure of channel delay dispersion*. The result is intuitively satisfying and consistent with earlier results in [82] linking the frequency-selectivity of the channel to turbo equalizer convergence.

#### 4.4.2 EXIT function slope with single transmit and single receive antenna

The EXIT function shape can be studied in more detail by considering the 1st derivative (slope) of the function. Only the case of BPSK modulation is considered explicitly, but the analysis is applicable and easily extendable to higher order modulations.

The 1st derivative of  $I_e$  can be expressed as

$$\frac{dI_e}{dI_d} = \frac{dI_e}{d\sigma_e} \frac{d\sigma_e}{d\delta} \frac{d\delta}{dI_d}, \quad (175)$$

where the first term is simply the 1st derivative of the *CCC*-function at the given point  $\sigma_e$ , the second term expresses the change of  $\sigma_e$  with the prior information embodied in  $\delta$ , and the last term expresses the dependence of  $\delta$  on the prior information. These represent the characteristics of the de-mapper, the equalizer, and the soft symbol estimator, respectively. An example of the contribution of these three components is depicted in Fig. 30 together with the error between the computed and the 1st derivative of the EXIT function computed with the method in Section 4.3.

When  $I_d \rightarrow 1$  the 1st derivative approaches zero indicating a flattening of the EXIT function close to the point of perfect prior information. This implies the equalizer operates very close to the GAD bound even if the feedback is not perfect and is the result of the third term of (175) approaching zero when  $I_d \rightarrow 1$ . The behavior is related to the soft symbol estimator and is, thus, modulation dependent. Incidentally, a similar discovery of the EXIT function shape was made in [73] for the MAP equalizer.

The 1st derivative component due to the de-mapper is almost constant, which results from the relatively small output range of the EXIT functions, as demonstrated by Fig. 27. This indicates the function values are the result of a relatively small range of inputs (for each function) to the de-mapper function (159), which is locally well-approximated as linear.

Fig. 31 shows a plot of the 1st and 2nd components of Equation (175) as functions of prior information and instantaneous SNR (ranging from  $-10$  to  $10$ dB). The third term is omitted since it depends only on prior information and the characteristic is shown in Fig. 30. The plot is computed directly from the analytical EXIT charts for the channel also used in Fig. 27. The 1st term decreases at high and low values of  $\sigma_e$  but remains almost constant over the range of  $I_d$  for a particular SNR. The 1st term compensates for the large values of the 2nd term (filter term) at high SNR. The first and the third terms in (175) are dependent on the utilized symbol mapping. In the following, an analytical expression is developed for the second term, which depends on the channel realization, and a look-up table aided interpolation. A functional approximation for the first and third terms, respectively, are used to produce the numerical results.

With the definition of

$$\varsigma(\delta) = \frac{|h(f)|^2}{(1-\delta)|h(f)|^2 + \sigma_0^2}, \quad (176)$$

the second term due to the linear filter in (175) can be expressed, using (108), (158) and

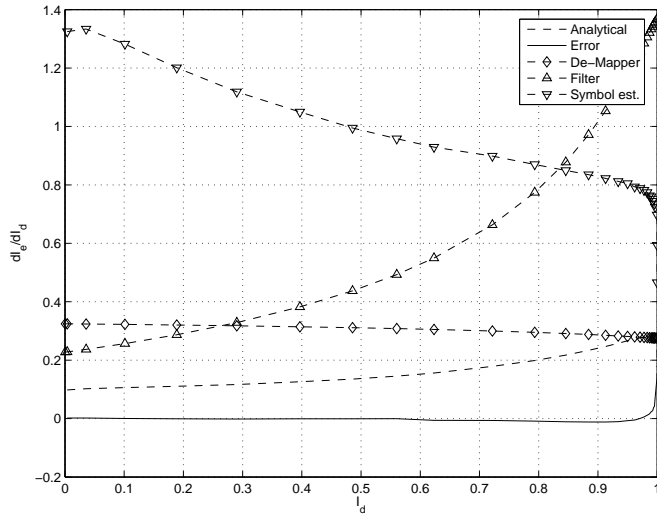


Fig. 30. Components and error of the EXIT function slope.

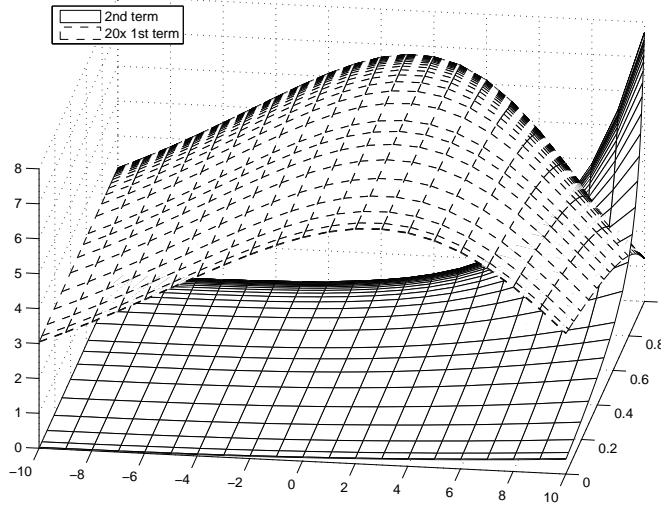


Fig. 31. 1st and 3rd components of the EXIT function slope at different SNRs.

(163), by

$$\frac{\partial \sigma_c}{\partial \delta} = \sqrt{2} \gamma^{-\frac{1}{2}} (1 + \gamma(\delta - 1))^{-\frac{3}{2}} N^{-1} \sum_{f=1}^N (\zeta(\delta) - \bar{\zeta}(\delta))^2, \quad (177)$$

where

$$\bar{\zeta}(\delta) = N^{-1} \sum_{f=1}^N \zeta(\delta). \quad (178)$$

It can be noted from (177) and (178), that the EXIT function slope is dependent on the second central moment of the per-frequency SINR. As in (174), this measure is proportional to the channel frequency-selectivity.

#### 4.4.3 Spatial separation of multiple antennas

Consider a MIMO case ( $J > 1, K > 1$ ), where (168) for no prior information results in

$${}^0\mu_{k,a}(0) = N^{-1} \text{tr} \left\{ \mathbf{\Upsilon}_k^{\text{H}/2} \left( \mathbf{\Upsilon}_k + \sigma_0^2 \mathbf{I} + \sum_{\substack{k'=1 \\ k' \neq k}}^K \mathbf{P}_{kk'} \mathbf{\Upsilon}_{k'} \mathbf{P}_{kk'}^{\text{H}} \right)^{-1} \mathbf{\Upsilon}_k^{1/2} \right\} \quad (179)$$

Eq. (179) indicates the effect of spatial eigenvectors and gets its minimum and maximum values

$$\min_{\mathbf{P}_{kk'} \forall k'} \{ {}^0\mu_{k,a}(0) \} = N^{-1} \text{tr} \left\{ \mathbf{\Upsilon}_k^{\text{H}/2} (\mathbf{\Upsilon} + \sigma_0^2 \mathbf{I})^{-1} \mathbf{\Upsilon}_k^{1/2} \right\} \quad (180)$$

$$\max_{\mathbf{\Phi}_k, \mathbf{V}} \{ {}^0\mu_{k,a}(0) \} = N^{-1} \text{tr} \left\{ \mathbf{\Upsilon}_k^{\text{H}/2} (\mathbf{\Upsilon}_k + \sigma_0^2 \mathbf{I})^{-1} \mathbf{\Upsilon}_k^{1/2} \right\}, \quad (181)$$

with  $\mathbf{\Phi}_k^{\text{H}} \mathbf{V} = \mathbf{I}$  in the case of fully correlated channels, and  $\mathbf{P}_{kk'} = \mathbf{0} \forall k, k'$  in the case of orthogonal channels. The overlap of the signal eigenbases then defines the effective SNR with no prior information.

In the case of full prior information, the EXIT function value depends purely on the eigenvalues of the channel matrix so that

$$\mathcal{L}_{k,a} = N^{-1} \sigma_0^{-2} \text{tr} \{ \mathbf{\Upsilon}_k \}. \quad (182)$$

Since no interference is present, spatial separation plays no role in (182), but the distribution of eigenvalues is influenced by spatial correlation. Increasing correlation reduces the number of significant spatial eigenvalues [94] and reduces the values assumed by (182) on average.

#### 4.4.4 EXIT function orientation

In Figures 22 and 23 it appears that the equalizer EXIT surface slope towards the co-channel interference direction is larger. This would indicate co-channel interference cancellation brings more gain than self-interference cancellation. This effect can be analyzed by considering an arbitrary point of a three-dimensional EXIT chart, for which  $\bar{\gamma}_k$  can be expressed by

$$\bar{\gamma}_k = N^{-1} \text{tr} \left\{ \mathbf{R}_k (\sigma_0^2 \mathbf{I} + (1 - \delta_k) \mathbf{R}_k + (1 - \delta_{k'}) \mathbf{P}_{kk'} \mathbf{R}_{k'})^{-1} \right\}, \quad (183)$$

where  $\{k, k'\} = \{1, 2\}$  or  $\{k, k'\} = \{2, 1\}$  depending on which transmission is considered. Self-interference cancellation gain can be illustrated by the partial derivative of the mean equalizer output

$$\frac{\partial \mu_{k,a}}{\partial \delta_k} = \frac{\partial}{\partial \delta_k} \frac{\bar{\gamma}_k}{1 + \delta_k \bar{\gamma}_k} \quad (184)$$

$$= \frac{\partial \bar{\gamma}_k / \partial \delta_k - \bar{\gamma}_k^2}{(1 + \delta_k \bar{\gamma}_k)^2}, \quad (185)$$

and the co-channel interference cancellation gain correspondingly by

$$\frac{\partial \mu_{k,a}}{\partial \delta_{k'}} = \frac{\partial}{\partial \delta_{k'}} \frac{\bar{\gamma}_k}{1 + \delta_k \bar{\gamma}_k} \quad (186)$$

$$= \frac{\partial \bar{\gamma}_k / \partial \delta_{k'}}{(1 + \delta_k \bar{\gamma}_k)^2} \quad (187)$$

$$= \frac{\partial \mu_{k,a}}{\partial \delta_k} + \frac{\bar{\gamma}_k^2 + \partial \bar{\gamma}_k / \partial \delta_{k'} - \partial \bar{\gamma}_k / \partial \delta_k}{(1 + \delta_k \bar{\gamma}_k)^2}. \quad (188)$$

The above indicates that the EXIT function increase is always larger towards co-channel interference suppression if

$$\partial \bar{\gamma}_k / \partial \delta_k - \partial \bar{\gamma}_k / \partial \delta_{k'} < \bar{\gamma}_k^2. \quad (189)$$

The partial derivative of  $\bar{\gamma}_k$  with respect to  $\delta_{k'}$  can be expressed, after converting the quadratic form (183) into a sum, by

$$\frac{\partial \bar{\gamma}_k}{\partial \delta_{k'}} = -N^{-1} \sum_{i=1}^N (v_{k,i})^2 \sum_{j=1}^N \frac{|\mathbf{P}_{kk'}, [j, i]|^2}{\bar{v}_j^2} \frac{\partial \bar{v}_j}{\partial \delta_{k'}} \quad (190)$$

and bounded from below and above, as shown in Appendix 3, by

$$\begin{aligned} N^{-1} \sum_{i=1}^N (v_{k,i})^2 \sum_{j=1}^N \frac{|\mathbf{P}_{kk'}, [j, i]|^2}{\bar{v}_j^2} \min(v_{k'}) &\leq \frac{\partial \bar{\gamma}_k}{\partial \delta_{k'}} \\ &\leq N^{-1} \sum_{i=1}^N (v_{k,i})^2 \sum_{j=1}^N \frac{|\mathbf{P}_{kk'}, [j, i]|^2}{\bar{v}_j^2} \max(v_{k'}), \end{aligned} \quad (191)$$

where  $v_{k,i}$  is the  $i$ th eigenvalue of  $\mathbf{\Upsilon}_k$ ,  $\bar{v}_i$  is the  $i$ th eigenvalue of  $\bar{\mathbf{\Upsilon}}$  and  $\mathbf{P}_{kk'}^{[i,j]}$  denotes the  $j$ th component on the  $i$ th row of  $\mathbf{P}_{kk'}$ . Unfortunately the bounds depend on the maximum and minimum eigenvalues of the channel matrix, and are quite loose. The slope depends heavily on the overlap between the signal spaces of the transmissions given by the matrix product  $\mathbf{P}_{k'}$ . For spatially orthogonal signals,  $\mathbf{P}_{kk'} = 0$ , and the slope towards co-channel interference is zero. For fully correlated signals  $\mathbf{P}_{kk'} = \mathbf{I}$  and the slope gets its maximum value

$$\frac{\partial \bar{\gamma}_k}{\partial \delta_{k'}} = N^{-1} \sum_{i=1}^N (v_{k,i})^2 \frac{v_{k',i}}{\bar{v}_i^2}, \quad (192)$$

as given in Appendix 3. Since

$$\frac{\partial \bar{\gamma}_k}{\partial \delta_k} = N^{-1} \sum_{i=1}^N (v_{k,i})^2 \frac{v_{k,i}}{\bar{v}_i^2}, \quad (193)$$

the constraint (189) can now be expressed as

$$N^{-1} \sum_{i=1}^N \left( \frac{v_{k,i}}{\bar{v}_i} \right)^2 (v_{k,i} - v_{k',i}) < \left( N^{-1} \sum_{i=1}^N \frac{v_{k,i}}{\bar{v}_i} \right)^2, \quad (194)$$

which can be given in a more compact form as

$$N^{-1} \text{tr} \{ \mathbf{\Upsilon}_k^2 \bar{\mathbf{\Upsilon}}^{-2} (\mathbf{\Upsilon}_k - \mathbf{\Upsilon}_{k'}) \} < (N^{-1} \text{tr} \{ \mathbf{\Upsilon}_k \bar{\mathbf{\Upsilon}}^{-1} \})^2. \quad (195)$$

By taking the upper bound

$$N^{-1} \text{tr} \{ \mathbf{\Upsilon}_k^2 \bar{\mathbf{\Upsilon}}^{-2} (\mathbf{\Upsilon}_k - \mathbf{\Upsilon}_{k'}) \} < N^{-1} \text{tr} \{ \mathbf{\Upsilon}_k \bar{\mathbf{\Upsilon}}^{-1} \}^2 (\text{tr} \{ \mathbf{\Upsilon}_k \} - \text{tr} \{ \mathbf{\Upsilon}_{k'} \}), \quad (196)$$

the constraint becomes

$$\text{tr} \{ \mathbf{\Upsilon}_k \} - \text{tr} \{ \mathbf{\Upsilon}_{k'} \} < N^{-1}. \quad (197)$$

The above indicates, that unless the channel of the transmission  $k'$  is weaker compared to the desired transmission, suppressing co-channel interference is more beneficial than self-interference suppression in the correlated case. In the partially correlated case, the amount of spatial overlap of signal eigenbases determines the EXIT function 1st differential towards co-channel interference.

#### 4.4.5 EXIT function slope with multiple transmit antennas

When multiple transmit antennas are used, the shape of the EXIT functions along the chart sides, i.e., when a number of interfering antennas have been totally suppressed, becomes relevant. It relates to the shapes of order-projected EXIT functions when different orderings are assumed. The expressions for the mean equalizer output at the endpoints of the order-projected EXIT functions  ${}^0_1 f_{e,ok} (I_{d,ok})$  corresponding to an arbitrary ordering  $\bar{o}$  can

be defined by

$${}^0_1\mu_{o_k,a}(0) = N^{-1}\text{tr} \left\{ \mathbf{\Upsilon}_{o_k}^{\text{H}/2} \left( \mathbf{\Upsilon}_{o_k} + \sigma_0^2 \mathbf{I} + \sum_{k'=o_k+1}^K \mathbf{P}_{kk'} \mathbf{\Upsilon}_{k'} \right)^{-1} \mathbf{\Upsilon}_{o_k}^{1/2} \right\}, \quad (198)$$

and

$${}^0_1\mu_{o_k,a}(1) = \frac{{}^0_1\tilde{\gamma}_{o_k}(1)}{1 + {}^0_1\tilde{\gamma}_{o_k}(1)} \quad (199)$$

$${}^0_1\tilde{\gamma}_{o_k}(1) = N^{-1}\text{tr} \left\{ \mathbf{\Upsilon}_{o_k}^{\text{H}/2} \left( \sigma_0^2 \mathbf{I} + \sum_{k'=o_k+1}^K \mathbf{P}_{kk'} \mathbf{\Upsilon}_{k'} \right)^{-1} \mathbf{\Upsilon}_{o_k}^{1/2} \right\}. \quad (200)$$

The difference between (198) and (199) is smaller when the difference between  ${}^0_1\tilde{\gamma}_{o_k}(0)$  and  ${}^0_1\tilde{\gamma}_{o_k}(1)$  is small, and they both have small values. It can be shown, that the eigenvalues of the covariance matrix for interference and noise for a given point in the ordering  $\bar{o}$ , ordered on the diagonal of  $\mathbf{\Upsilon}_{\bar{o}_k}$  in

$$\sum_{k'=o_k}^K \mathbf{P}_{o_k k'} \mathbf{\Upsilon}_{k'} \mathbf{P}_{o_k k'}^{\text{H}} + \sigma_0^2 \mathbf{I} = \mathbf{V}_{\bar{o}_k} \tilde{\mathbf{\Upsilon}}_{\bar{o}_k} \mathbf{V}_{\bar{o}_k}^{\text{H}} \quad (201)$$

have the property that [137]

$$\mathbf{\Upsilon}_{o_1} \geq \mathbf{\Upsilon}_{o_2} \geq \dots \geq \mathbf{\Upsilon}_{o_{K-1}} \geq \mathbf{\Upsilon}_{o_K}, \quad (202)$$

where the inequality denotes semidefinite ordering, but can be considered component-wise due to the matrices being diagonal. The property is the result of each matrix being the sum of the subsequent matrix and a positive definite matrix. This property has a decreasing effect on the values of (198) and (199) with increasing order index. Thus, the slope of the order-projected EXIT function of transmission  $k$  is smaller the earlier the transmission is placed in the ordering. Also, the vertical placement of the order-projected EXIT function on the chart is dependent on the ordering, highlighting the importance of optimal ordering in the successful detection of transmissions with several antennas. A simple example of this is the optimal ordering in the two-transmission case of Fig. 25 where the optimal ordering selects the transmission with the larger EXIT function value at the initial point  $\mathbf{I}_d = \{0, 0\}$ .

## 4.5 Summary and discussion

The tracking of extrinsic likelihood mutual information provides a suitable framework for the convergence analysis of turbo equalizers. With a few simple assumptions of the behavior of equalizer EXIT functions and utilizing the area property of channel codes, the principles for analyzing achievable rates using the functions can be developed. Some simple interpretations of the approximate shape of the rate region were shown, whereas a

more detailed analysis requires concrete knowledge of the EXIT functions. In the case of symmetric code design for transmit antennas, the achievable rate was found to be bounded by the point-wise minimum of the order-projected EXIT functions in an ordering giving the maximum EXIT function area among all detector orderings. A simpler design principle selects the ordering based on the largest minimum starting point of the order-projected EXIT functions. The achievable rate is then bounded above by the point-wise minimum of the order-projected EXIT functions within that ordering.

The properties of the frequency-domain MMSE turbo equalizer were analyzed by introducing a semi-analytical method for computing the equalizer EXIT chart. The method uses the expressions for the equalizer output SNR given the channel state, receiver noise level and prior information accuracy, and computes the de-mapper output average mutual information. The method was found to be accurate enough for analyzing equalizer behavior. Increased frequency-selectivity was found to increase the slope of the EXIT function. Spatial channel correlation properties influence the co-channel interference severity and, thus, the EXIT function slope towards co-channel interference directions. Increased spatial correlation increases the EXIT function slope and decreases the EXIT function value with no prior information and with full prior information. In the case of multiple transmit antennas, the order-projection of the EXIT function of a transmission was found to be closer to horizontal the earlier in the ordering the transmission is placed.

It is well known that Gray mapping is the worst mapping choice in terms of iterative de-mapping [138, 65]. However, if any other than Gray mapping was used, iterative de-mapping should be modeled in the de-mapping, effectively making the de-mapper a function of the equalizer output SNR and the prior information. Such two-dimensional modeling of the de-mapping is possible [131], but makes the procedure obviously more complex. On the other hand, if the modulation is considered as a form of inner coding, a suitable choice or design of outer coding should enable any modulation choice to reach achievable rate limits. In the case of multilevel modulation, this may mean the utilization of multilevel codes as outer codes to correctly match modulation and coding.

## 5 Fading channels

The radio propagation in the channel largely defines the performance limits of wireless transmission systems. The state of a multipath propagation channel is dependent on the physical positions of the transmitter, the scattering objects, and the receiver. If either changes, the channel state changes. If physically distant locations are considered, the statistical behavior of the channel can be very different. Locally, however, the static channel characteristics can be considered to be constant. From the wireless system's point of view, then, it becomes relevant how the statistical properties influence the system performance.

In the previous chapters, it has been shown how various instantaneous channel properties and the convergence of the MMSE turbo equalizer are coupled. In this chapter, the channel is considered to be a random process, and its parameters influence the performance statistics of the MMSE turbo equalizer. The convergence statistics of the equalizer are evaluated with channel codes whose implementations are widely available, i.e., can be considered off-the-shelf. Furthermore, a code design principle is developed for reaching a convergence outage with the MMSE turbo equalizer in quasi-static fading channels. The principle is applied to the case of an SIMO channel, and an extension to MIMO transmission is provided.

### 5.1 Convergence in fading channels

The method used in the sequel for interpreting the computed EXIT chart of the channel decoder is demonstrated in Fig. 32, which illustrates the enlarged rightmost part of a regular two-dimensional EXIT chart. First, the fixed point of detector iterations is found through the repetition of the convergence tracking iteration steps as listed in Section 4.3. The extrinsic and *a posteriori* information at the decoder output corresponding to the fixed point of detector iteration are given by  $I'_{e,k}$  and  $I'_{a,k}$ , respectively. The latter is the point in the *a posteriori* information function  $I_{a,k}$  corresponding to the fixed point as indicated in Fig. 32. The mutual information reached by genie-aided detection is found by computing the equalizer output mutual information with perfect prior knowledge and finding the corresponding value of  $I_{a,k}$ , shown in Fig. 32 as  $I'_{a,k,GAD}$ . The resulting GAD mutual information then represents the attainable mutual information given the selected channel

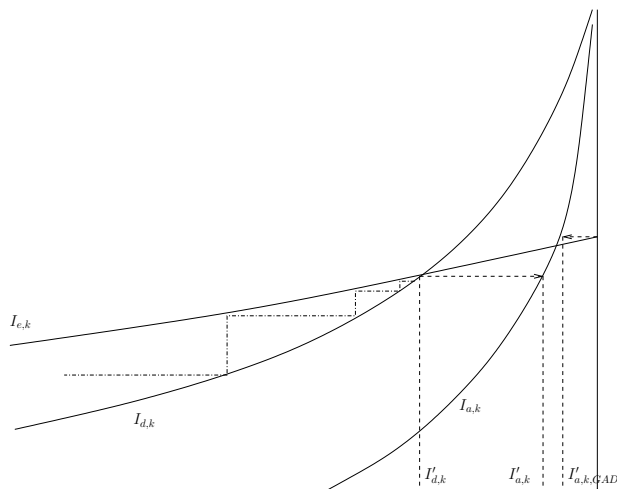


**Fig. 32. Measures recorded from the EXIT chart for each channel state.**

code, and can be utilized as the reference to equalizer convergence.

Each random realization of the quasi-static fading channel, which remains constant over the transmitted frame, but varies independently from frame to frame, is used to generate an EXIT function of the equalizer. The joint distribution of the channel results in an empirical distribution of EXIT functions, which can be evaluated. The convergence tracking and mutual information analysis are performed for a sample set of channel realizations and average SNR values. When combined with a channel code, the resulting cumulative distribution functions (cdf) of *a posteriori* mutual information corresponding to the reached fixed point and for the GAD bound are computed. An outage mutual information  $I_{\text{th}}$  for which  $P(I'_{a,k} \geq I_{\text{th}}) = P_{\text{out}}$  is fulfilled for the outage probability  $P_{\text{out}}$  is computed. In the sequel, mutual information in the context of convergence implies extrinsic information, and at the fixed point *a posteriori* information.

### 5.1.1 Considered channel codes

Two channel codes are considered in the evaluations: a rate-1/2 convolutional code (CC) with polynomials  $(561, 753)_8$  and a rate-1/2 turbo code (TuC) which is obtained from the rate-1/3 turbo code with polynomials  $(1, 13/15)_8$  by puncturing even bits from the first and odd bits from the second constituent encoder. The simulated EXIT functions of these codes are presented in Fig. 33. Both of the codes can be considered off-the-shelf, due to their being included in the Third Generation Partnership Project (3GPP) standards [139]. The evaluations in this section will, thus, represent an example of what can be achieved with codes used in current standards. For improving upon this, irregular LDPC codes are

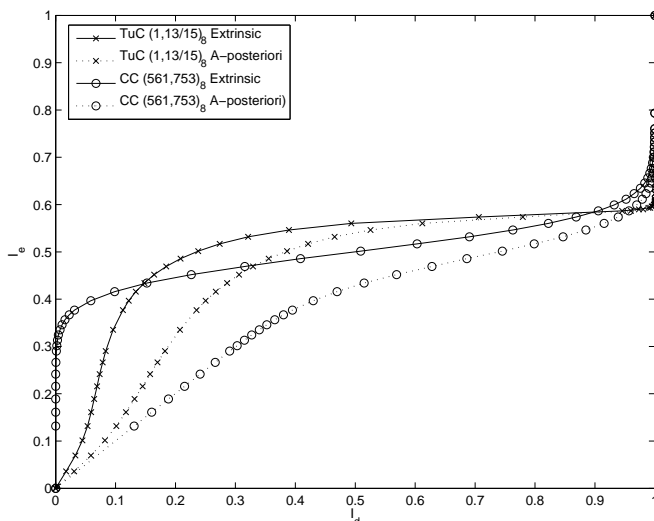


**Fig. 33. 3GPP channel code EXIT and *a posteriori* functions.**

considered in Section 5.2 for EXIT function based code design, but their characteristics are not considered here any further. The EXIT functions of the considered convolutional and turbo codes have two significant differences. Firstly, the turbo code function is larger in the middle of the range, indicating a higher SNR threshold for convergence. Secondly, the turbo code function is very flat in the high range of the input, indicating a good error performance if that part of the chart is reached by the iterations. The convolutional code has a rounder shape in the high range, indicating this range may limit the final error performance in some cases. The EXIT functions of both codes were generated by simulating 10 blocks of length 30000 coded bits, and measuring the mutual information of the extrinsic outputs with histograms. In the case of the turbo code, the decoder performs 6 iterations. In [140], it is approximated that the probability of loops of length  $c \geq 4$  in the turbo code graph is given by  $\exp(-(2^{c-1} - 4)/RN)$  when  $N$  is large. This would mean there is a probability of 0.19% for loops of length 6, and as a result, the information provided by the turbo decoder can be considered independent.

### 5.1.2 Interleaving

Interleaving is an important randomization technique in almost all wireless communication systems. In the case of multi-access systems over frequency-selective channels, interleaving has two tasks. Firstly, to randomize the correlated (due to channel memory) equalizer outputs for the decoder so that the decoder input appears independent. This randomization operates in a similar manner on the decoder feedback so that the equalizer

can assume independent feedback. Secondly, to better separate multiple transmissions by breaking channel memory due to multiple access by using different interleaving for different transmissions as demonstrated e.g. in [19, 27].

More fundamentally, iterative detection can be seen as an instance of belief propagation algorithms on the dependency graph of the system. Their convergence to the correct decision is affected, among other things, by the presence of loops in the dependency graph. The optimal belief-propagation algorithm converges to the correct solution only in tree-like graphs. If the graph has a loop of length  $c$ , the iterative algorithm is denoted as *locally optimal* and can perform a maximum of  $c$  iterations before the effect of the loop is experienced. After  $c$  iterations the algorithm begins to amplify its own results and optimality is lost. Loops can be made longer by using interleavers, and the length of the interleaver is related to the minimum loop length. When the interleaver length  $N$  is increased, the probability of finite loops in the graph decreases linearly with  $N$  [25, 26]. The graphs of multi-access systems have loops with small  $N$ , but at the limit of infinite block length their graphs can become loop-free [80] if the used channel code is loop-free.

In systems with finite block lengths, the existence of loops in the system graph is inevitable and must be accounted for. In such cases the expected lengths of the loops must be estimated, and the detection organized taking the estimate into account. If a part of the system, e.g. the turbo code, contains loops, it limits the number how many times that part can be activated during the operation of the detector without sacrificing optimality.

### 5.1.3 Channel delay spread

As indicated in Chapter 4, frequency-selectivity has a direct effect on the slope of the EXIT function. Since also the instantaneous received SNR has an effect on the function values, frequency selectivity should also make the distribution of EXIT functions more concentrated due to the added diversity. This effect is visualized in Figs. 34 and 35, where the point-wise cdf of function values of EXIT functions for randomly generated 4- and 32-path channels are presented. Each cdf is plotted for the range of *a priori* function input parameter values. The average received SNR is 0dB and the channel coefficients have an i.i.d. Rayleigh distributed envelope and random phase. To be precise, the point-wise cdf is defined as

$$\mathcal{F}_{cdf}(I_d, I) = P(f_e(I_d) < I). \quad (203)$$

It must be noted that since the cdf is over the outputs of the random functions for a given prior input mutual information, the properties of the individual functions are lost. The shape of the cdf illustrates how the random ensemble behaves, however. An interesting asymptotic result can be observed from Fig. 36, where the corresponding EXIT functions are plotted for the hypothetical case of 16384 i.i.d. multipaths. All the EXIT functions are effectively identical due to the very large diversity order. A similar result should then asymptotically be the result in the case of a finite number of multipaths, if the number of receive antennas is increased, or a diversity transmission method like cyclic delay diversity [141, 142] (CDD), which can increase the number of independent multipaths, is used to increase the diversity order.

To study the statistical convergence behavior of the equalizer in a channel with varying

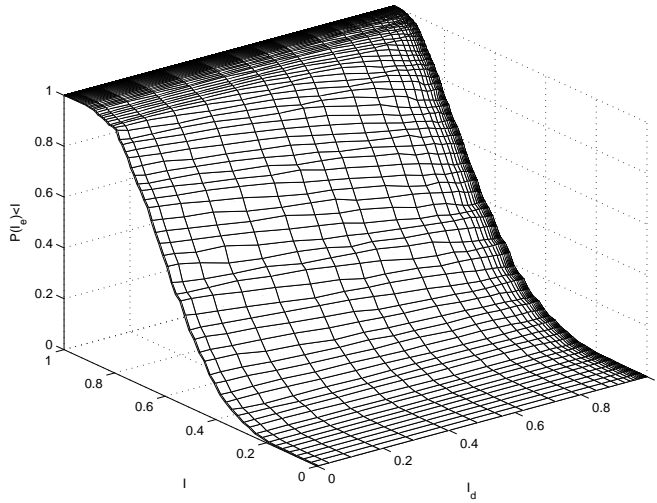


**Fig. 34.** Point-wise cdf of 500 randomly generated EXIT functions at SNR 0dB with a 4-path i.i.d. Rayleigh fading channel.

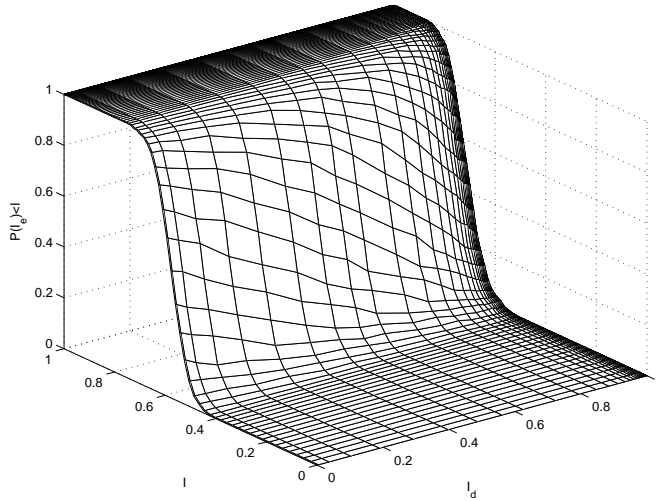


**Fig. 35.** Point-wise cdf of 500 randomly generated EXIT functions at SNR 0dB with a 32-path i.i.d. Rayleigh fading channel.

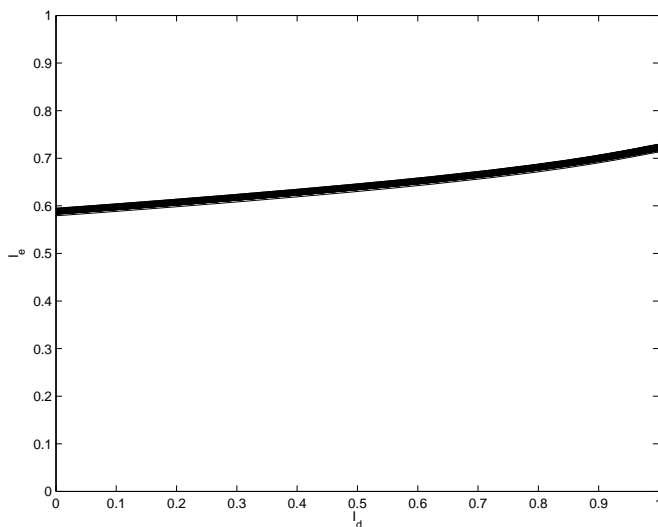


**Fig. 36. 500 Randomly generated EXIT functions at SNR 0dB with a 16384-path i.i.d. Rayleigh fading channel.**

frequency-selectivity, a channel with a varying power delay profile is considered. The exponential decay of the channel power delay profile is expressed as the average energy difference between consecutive paths (in dB). The analysis is performed for a set of 2000 random channel realizations. Figs. 37 and 38 show the 1% outage mutual information as a function of the average channel SNR for the 3GPP convolutional and turbo codes, respectively. Successful convergence over the ensemble of fading channel realizations is indicated by the small distance of the equalizer mutual information to that of the GAD, meaning the equalizer and the channel code are well matched. Having the equalizer mutual information cdf and the GAD cdf far separated indicates a poor match, which is manifested as an increase in required SNR to reach a target mutual information.

Due to the behavior of the EXIT function of the CC in Fig. 33 at high mutual information, the CC requires an increased SNR to reach good performance over what is needed for equalizer convergence only. The outage behavior can be considered to be code-dominated. Fig. 38 shows the behavior of the turbo code combined with the equalizer. The equalizer shows low mutual information up to a certain SNR point, after which the mutual information rises quickly close to the maximum. The difference to the CC is due to the shape of the code's EXIT function in the middle of the range of  $I_{d,k}$ . While the TuC has good properties over the range of high prior mutual information, the code properties limit the convergence of the equalizer, and the outage behavior can be considered convergence-dominated. A conclusion can be drawn that a good channel code for turbo equalization should have both good final performance near the GAD bound and suitable convergence properties so as not to limit the equalizer convergence. This indicates the channel code should somehow be matched to the statistics of the equalizer EXIT functions.

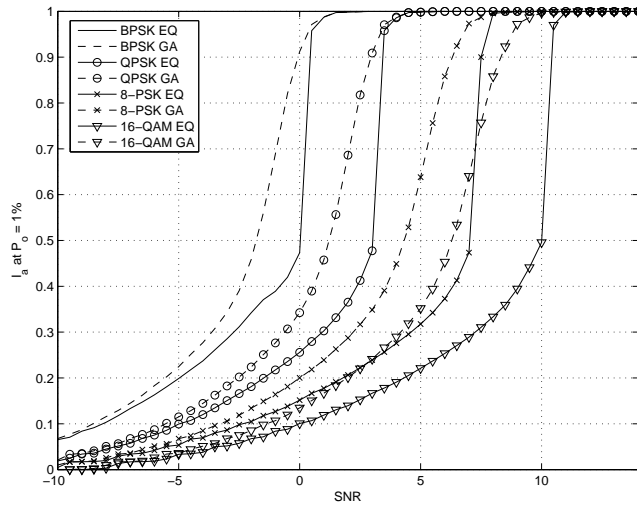


**Fig. 37.** Mutual information reached with 1% outage in an SISO channel with high delay spread, convolutional code.

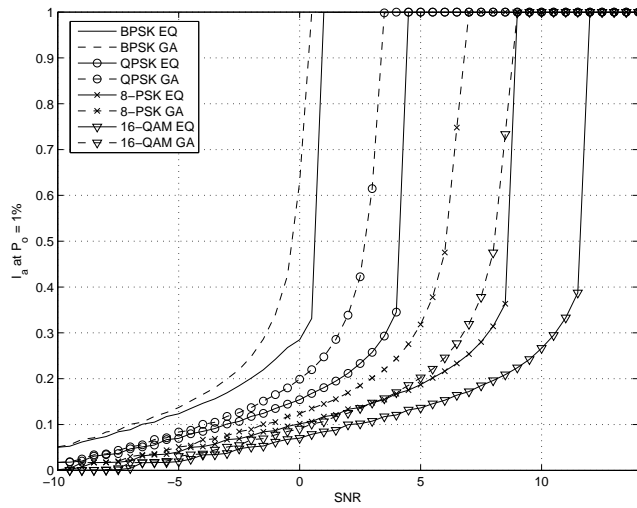


**Fig. 38.** Mutual information reached with 1% outage in an SISO channel with high delay spread, turbo code.

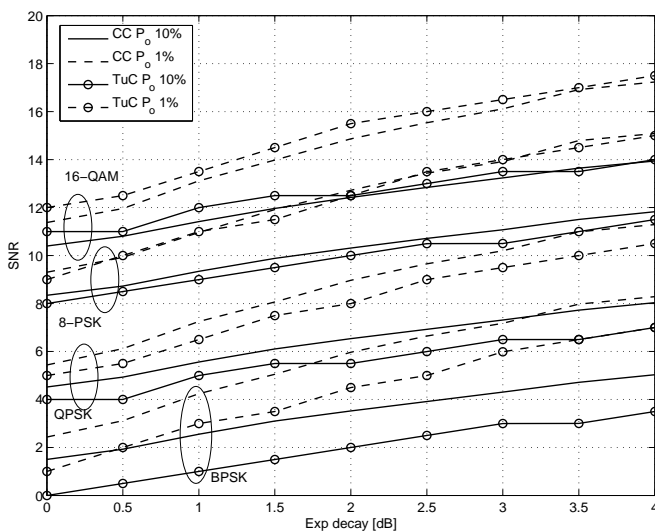


Fig. 39. Required SNR to reach target ( $I_{a,k} = 0.999$ ), SISO channel.

Next, the average SNR required to reach a target mutual information (set to 0.999) with outage 1% and 10% when the channel delay spread changes are evaluated. The exponential decay factor of the channel PDP is varied from 0dB to 4dB, so that the channel changes from a highly frequency-selective channel at one end to a channel with relatively mild delay spread at the other. From Fig. 39 it can be seen how the reduced frequency-selectivity is translated into a higher required SNR to achieve the desired outage. For a lower outage target the required SNR increase is more rapid with the increasing channel decay factor, a normal effect when the diversity order is decreased. For the considered target link reliability it can be seen that the turbo code performs better for low-order modulations, and the convolutional code for high-order modulations.

### 5.1.4 Spatial correlation in MIMO channels

A spatially correlated 32-tap Rayleigh fading channel with two different exponential decays (1 and 3dB) between consecutive paths is considered. These slightly arbitrary exponential decays are chosen to represent the cases of extreme and mild multipath and multipath diversity, with the motivation of highlighting the differences due to different multipath interference and diversity effects. The effect of spatial channel correlation and channel frequency-selectivity to the achieved *a posteriori* mutual information is evaluated. A real-valued transmit and receive-side path cross-correlation matrix with exponentially decaying off-diagonals is assumed for the Kronecker spatial channel model, so that

$$\rho_{i,j} = \tilde{\rho}^{|i-j|} \quad (204)$$

and

$$\varrho_{i,j} = \tilde{\varrho}^{|i-j|} \quad (205)$$

define the cross-correlation matrices according to (16) on the receive and (18) on the transmit side, respectively. The path cross-correlation is assumed to be the same for all channel multipaths. In the considered cases, both  $\tilde{\rho}$  and  $\tilde{\varrho}$  are varied between 0.1 and 0.9. Since the cross-correlation matrix is the dual of the power-azimuth spectrum, a receive-side cross-correlation matrix identical to all transmissions forces the same mean angle-of-arrival for all transmissions and implements the worst-case scenario in terms of spatial separation of transmissions.

In the case of correlation on either side of the link, the question of duality arises. It is known that since the eigenvalues of the product of two matrices are the same irrespective of the order of multiplication [137, p. 53], the mean of  $\tilde{\gamma}_k$  over  $k$  remains the same irrespective of the side where the correlation between antennas is experienced. As a result, an MMSE turbo equalizer utilizing a single channel code would obviously experience a dual channel. However, for strict duality in the considered case of separate transmissions the same is required for each  $\tilde{\gamma}_k$ . This requirement is equivalent to the requirement that  $\Phi_k^H \mathbf{V}$  in (169) remains invariant between the cases of transmit and receive side correlation, the analysis of which becomes quite involved. Since the simple case suggests some duality is present in the system, an evaluation can be performed by simulation to learn about duality in the separate transmission case. Figures 40 and 41 report how increasing channel correlation on the transmit and receive side results in higher required average SNR to reach the mutual information target. The result suggests channel duality holds at least approximately in the separate transmission case, but small differences exist.

Transmit side correlation seems not to influence CC transmission with BPSK and QPSK at all, while a small influence is visible due to receive side correlation. Convolutional codes have a performance advantage at high correlation and with 8-PSK and 16-QAM modulations in both transmit and receive side correlation. The higher the modulation order, the more influence spatial correlation has on the performance. Fig. 42 depicts the same multipath case with spatial correlation on both sides of the link. Most notable is the increased sensitivity to spatial correlation, but the performance characteristic is very similar to the cases with correlation on either side of the link. Figures 43 and 44 depict the evaluation for the channel with the power-delay profile decay set to 3dB and considering receive- and transmit- and receive-side correlation, respectively. The figures have been obtained by simulation of 1000 channel realizations. The reduced multipath (frequency) diversity is demonstrated by the higher overall required SNR compared to the 1dB decay channel. Also, the lower outage now requires relatively more received SNR. However, the loss due to spatial correlation is very similar to the 1dB channel. For low spatial correlation, the difference between CC and TuC is smaller than in the 1dB decay channel.

## 5.2 Coding for fading channels

In Chapter 4 it was emphasized how the channel code and the equalizer EXIT functions should be matched to enable maximum throughput or minimum required received SNR in

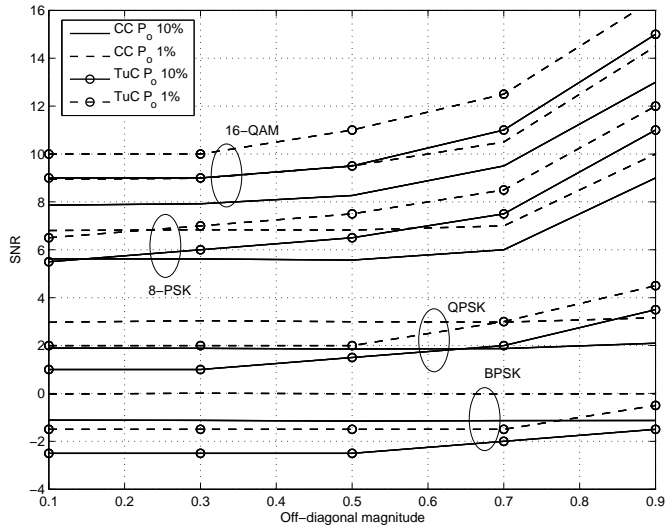


Fig. 40. Required SNR to reach target, transmit side correlation, 1dB PDP decay.

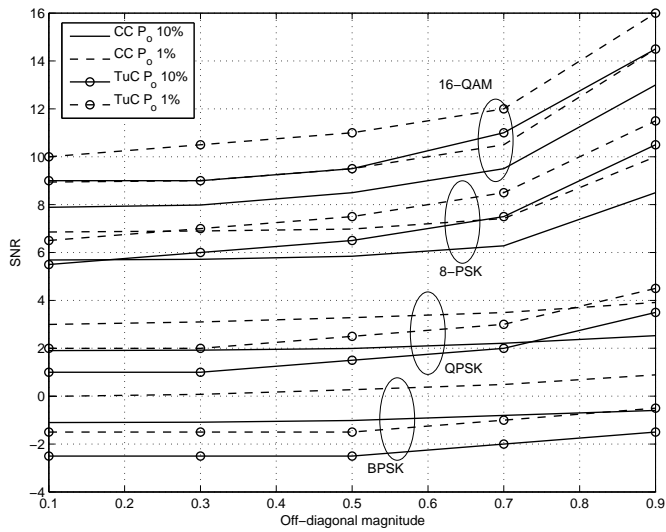


Fig. 41. Required SNR to reach target, receive side correlation, 1dB PDP decay.

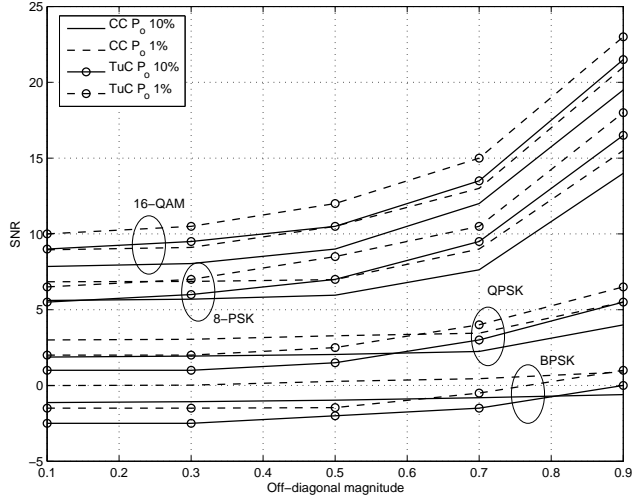


Fig. 42. Required SNR to reach target, transmit and receive side correlation, 1dB PDP decay.

a given channel. In Section 5.1 it was shown how the equalizer EXIT function behaves in a quasi-static fading channel and how off-the shelf codes perform with the random channel. Further code optimization is possible if the equalizer EXIT function statistics, i.e., the channel statistics, are assumed to be known. In the following, an SISO or SIMO transmission is assumed.

Any design based on EXIT functions is effectively defined as the relation between the designed code EXIT function and the distribution of the equalizer EXIT functions given the channel statistics. The EXIT function of the designed code is denoted as a “designed function” in the sequel. If only the knowledge of channel statistics is assumed at the transmitter, the design should be based on the concept of outage, where a certain design rate is guaranteed at a certain outage probability. In the case of turbo equalization, an outage happens when the equalizer EXIT function is below the designed function at any point within the function range. Thus, the design should enable successful convergence with the probability  $1 - P_{out}$ , or alternatively put, unsuccessful convergence with the probability  $P_{out}$ .

The case of unsuccessful convergence indicates as case where the designed function is below or crosses the equalizer EXIT function. With the outage approach, this event must have the probability  $P_{out}$ . This, however, requires that properties of all possible equalizer EXIT functions, given the channel statistics, must be taken into account in the design. Then, a suitable EXIT function design to reach the desired outage can be found. An approximative but simpler approach is to treat the equalizer EXIT functions as an ensemble, and to assume all the functions are (approximately) parallel so that they do not cross each other. The area property of the code can then be extended to random equalizer EXIT function ensembles. The design function should maximize the area below the

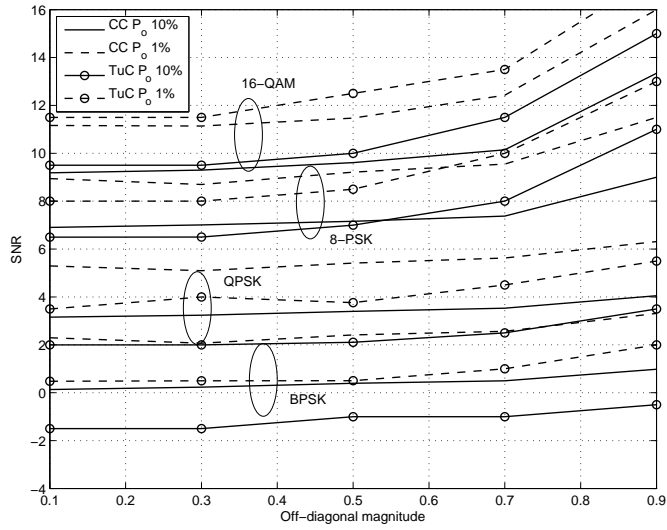


Fig. 43. Required SNR to reach target, receive side correlation, 3dB PDP decay.

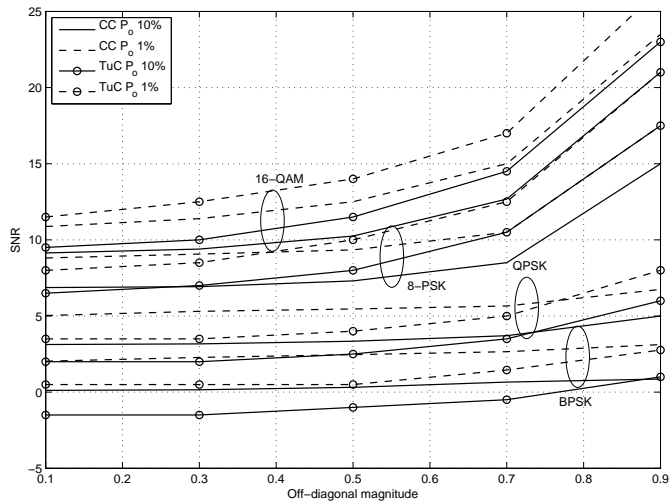


Fig. 44. Required SNR to reach target, transmit and receive side correlation, 3dB PDP decay.

designed function while minimizing the volume of the ensemble cdf below the designed function. If the designed function follows a constant value curve of the equalizer EXIT function ensemble cdf, the assumption of function parallelism guarantees any equalizer EXIT function is either above or below the designed function, and the requirement for maximum area with minimum volume is fulfilled. An example of the approach is depicted in Fig. 45. The designed function producing the desired outage is then defined by

$$\mathcal{F}_{cdf}(I_d, f_d(I_d)) = P_{out}. \quad (206)$$

showing the optimal outage design follows the constant value curve of the equalizer EXIT function cdf defined by the desired outage. In reality the equalizer EXIT functions are not strictly parallel and the designed function results in a higher outage probability than desired.

If closed-form EXIT functions are not available for the equalizer, the EXIT function cdfs can be generated for a set of average received SNRs and the resulting SNR-wise designed functions used to find a designed function giving the desired code rate. To avoid extensive generation of EXIT function sets in different SNRs, small changes in SNR can be approximated by interpolation between designed functions for SNRs that are close enough.

### 5.2.1 Code design using the combined EXIT function

Irregular LDPC codes are a good choice for outer codes due to the flexibility offered by their design and the fact that they can be made to approach channel capacity. A block diagram depicting a simple example of the code structure is given in Fig. 46. The variable nodes represent encoded data and the check nodes their dependencies, as further explained by e.g. [133]. In the EXIT analysis, the variable nodes (marked by  $v$  in Fig. 46) are modeled as encoders repeating the message corresponding to the channel input of the node. Check nodes (marked by  $c$  in Fig. 46) are modeled as single parity check decoders, computing a single parity check for each edge connected to the node. The log-likelihood ratios passed on the edges of the decoder graph during the decoding process are assumed to be Gaussian distributed. The approximation results in a small loss of accuracy with a significant simplification of the optimization process [143]. Check-regular codes with a fixed check node degree are chosen. By properly choosing the degree distribution (i.e. distribution of the number of edges connected to each node) of variable node connections, the EXIT function of the code can be controlled. The code design is not presented here in detail, but further information can be found in [71, 143, 91]. The design is based on combining the equalizer EXIT function with the EXIT function of the variable nodes, so that the extrinsic information at the output of the variable node decoders is given by

$$I_V = f_{V,e}(I_C) \quad (207)$$

$$= f_V \left( \mathcal{J} \left( \sqrt{(\mathcal{J}^{-1}(I_e))^2 + (\mathcal{J}^{-1}(I_C))^2} \right) \right), \quad (208)$$

with

$$I_e = f_e(f_V(I_C)), \quad (209)$$

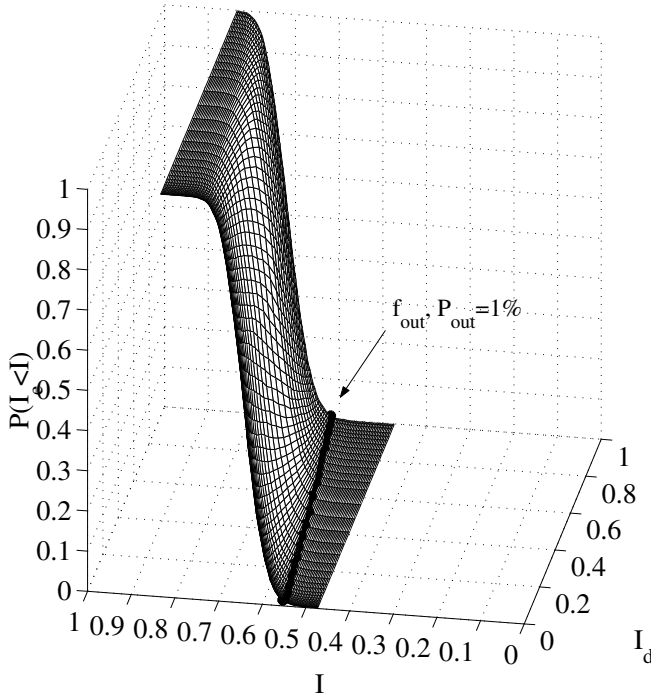


**Fig. 45. Cdf of equalizer EXIT function values  $f_e(I_d)$  and outage based designed code function  $f_{out}$ , SNR = -3dB.**

where  $I_C$  is the extrinsic information at the output of the check node decoders (CND),  $f_V$  is the EXIT function of the variable node decoders (VND) and  $\mathcal{J}$  denotes the  $J$ -function of [66] given in (123). Now, (208) effectively assumes one decoder iteration is followed by one equalizer iteration.

In decoding a serial concatenated system with a finite block length, like the one consisting of the multipath channel, the variable nodes and the check nodes, the question of optimal decoder scheduling arises. However, the detector scheduling is not considered here any further but a simple scheduling is used for simulations. Regarding the code design using EXIT charts, however, assuming the EXIT properties of the system components are independent of scheduling, in the limiting case of an infinite number of iterations the fixed point of iterations is the same regardless of scheduling [144]. This can also be supported by the vanishing probability of loops from the system graph as the block length approaches infinity, as assumed by the design.

The LDPC code design then consists of matching the combined  $f_{V,e}()$  curve to the check node curve  $f_C$  without any intersection for the lowest possible SNR by optimizing the degree distribution of the variable nodes as in [71]. The percentage of variable nodes with degree  $d_{V(i)}$  is denoted by  $a_{V(i)}$ .

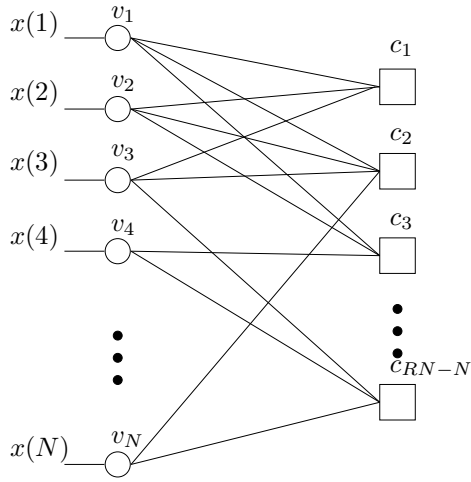


Fig. 46. LDPC code structure illustrated as a factor graph ( $v$ : variable node,  $c$ : check node).

### 5.2.2 Numerical evaluation

A channel with 32 i.i.d. channel coefficients and two uncorrelated receive antennas is considered. The LDPC design is performed for a code rate of  $1/2$  with BPSK modulation, and the corresponding degree distribution table is given in Table 7. For comparison, the parameters of the regular  $(3, 6)$  standard LDPC code and an irregular LDPC code optimized to the AWGN channel are given. The table also lists an estimate of the required  $E_b/N_0$ , denoted by  $E_b/N_0^*$ , to reach the designed outage for the equalizer optimized code and the regular code.

In Fig. 47, the FER performance of the codes of Tab. 7 are given with a block length of 992 information bits. The LDPC decoder uses the optimal message passing (or sum-product) algorithm [145], and is allowed to fully converge between each equalizer iteration.

Table 7. Node perspective degree distribution of codes.

Code	$P_{OUT}$	$R$	$d_C$	$d_{V(1)}$	$d_{V(2)}$	$d_{V(3)}$	$a_{V(1)}$	$a_{V(2)}$	$a_{V(3)}$	$\frac{E_b}{N_0}^*$ (dB)
opt	0.01	0.50	8	20	3	2	0.07	0.74	0.19	2.00
(3,6)	0.01	0.50	6	3	-	-	1.00	-	-	2.75
awgn	-	0.50	8	16	15	3	0.02	0.06	0.92	-

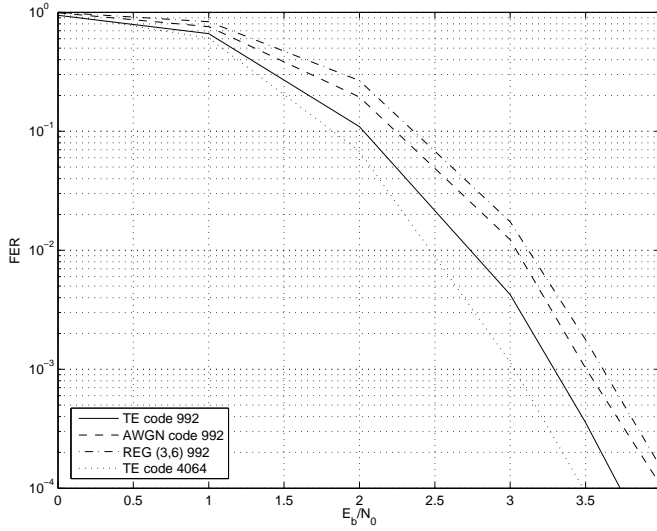


**Fig. 47. Frame error rates (FER) of optimized LDPC codes.**

tion. According to the outage based design approach it is expected that the codes perform at a frame error rate equaling  $P_{out}$  at the estimated threshold value  $\frac{E_b}{N_0}^*$ . For the optimized code the simulated threshold value equals 2.65 dB instead of 2.00 dB, and for the regular code 3.00 dB instead of 2.75 dB. The true outage probability provided by the design is then slightly above the target. One of the reasons for not achieving the estimated threshold is the finite block length. For comparison, a simulation result for the designed code with a block length of 4064 information bits is also depicted in Fig. 47, showing a threshold of approximately 2.45dB. The approximations made in the design process, most notably the approximations in the convergence analysis and the parallelism approximation in the code design also contribute to the slight inaccuracy. However, the design obviously provides a gain over both the unoptimized regular code and the AWGN optimized code. Considering the general shape of the equalizer EXIT functions, which are relatively flat, even a gain of this magnitude can be considered significant.

### 5.2.3 Code design for layered MIMO transmission

Having demonstrated in Sections 5.2.1 and 5.2.2 that a code design can be made to match a designed function and the resulting system will outperform systems using unoptimized codes, the extension of the design principle to more generic cases becomes interesting. In this section, an extension of the design principle to layered MIMO systems is outlined.

The design principle relies on the symmetry, or exchangeability, of the joint channel

statistics of the MIMO system guaranteeing the joint statistics remain invariant under any permutation of the transmit antenna index. The exchangeability also guarantees that the joint statistics of the order-projected functions of the multidimensional equalizer EXIT function are exchangeable, as well. The logical conclusion is that any outage-optimal code should be exchangeable, i.e., the same code should be used for all transmit antennas.

In Section 4.2 a method to design a symmetric maximal rate code  $f_{d,\text{opt}}(I_d)$  for a layered MIMO system given the channel state was presented. Essentially, this optimal design given the channel state can be considered equivalent to the equalizer EXIT function in the SISO case is that is the optimum code *given the channel state*. Any code design below  $f_{d,\text{opt}}(I_d)$  will converge, and any design above it will not.

The design approach is now clear. First, generate the (empirical) distribution of  $f_{d,\text{opt}}(I_d)$  for a set of channel realizations using the optimality criterion given by (152). Second, find the designed function using the constant value curve of the function value cdf with the desired outage defined by 206. Third, design the outer code for the designed function. As in Section 4.2.2, the point-wise optimality of the ordering can be replaced by ordering based on the starting point (minimum) of the order-projected EXIT function to simplify the computations while removing the optimality of the design.

### 5.3 Summary and discussion

In fading channels, the channel randomness results in channel dependent random EXIT functions of the equalizer. The statistical properties of the channel influence the properties of the EXIT function ensemble. The ensemble moves vertically in the EXIT chart with SNR, becomes vertically less spread with increasing diversity due to frequency-selectivity or multi-antenna diversity reception, and in MIMO cases, moves down with increasing spatial correlation. Correspondingly, an increased received SNR is required to compensate for any propagation channel phenomena that move the EXIT function downwards.

The semi-analytical convergence analysis method presented earlier was used to evaluate the statistical convergence properties of the equalizer in the case of BICM transmission using Gray mapped BPSK, QPSK, 8-PSK and 16-QAM modulations. The effects of frequency-selectivity and spatial correlation were studied with an outage based approach for two off-the-shelf channel codes. An LDPC code design principle based on the concept of convergence outage was presented and its effectiveness demonstrated for BPSK modulation in an SIMO channel. A performance gain was demonstrated over the reference codes, an unoptimized regular LDPC code and an irregular code optimized for the AWGN channel. An extension to layered MIMO transmission was outlined.

The main drawback of the presented methods is the semi-analytical nature of the approach, which requires simulated ensembles. While visually enlightening, it would be preferable to avoid such computations. For the code design, a deeper understanding of the behavior of the EXIT function ensembles might provide for a more elaborate model for the ordering of functions within the ensemble, thus enabling a more accurate design principle to be developed.

## 6 Multilevel coding and modulation

An essential technique for achieving high bandwidth efficiency in any wireless system is the use of a bandwidth efficient modulation method. It is of much interest to consider how the modulation interacts with the equalizer and the channel decoder and how it should be constructed to optimize performance. In this final chapter, multilevel coded modulation is studied as a part of a turbo equalizer based transmission system. The main focus is on 16-QAM modulation, but many of the results are applicable to higher order QAM modulations, as well.

The chapter begins with the introduction of multilevel coded QAM, a special case of multilevel bit-interleaved coded modulation (MLBICM), and a corresponding efficient MMSE turbo equalizer receiver. The behavior of the coded modulation is tested with channel measurement data based simulations, and its superiority over regular BICM is observed. Convergence analysis from Chapter 4 is extended to multilevel coding to study the convergence phenomena leading to the observed results. A new approach to designing multilevel coded modulations for turbo equalization based on the results of Chapter 5 is proposed.

### 6.1 Multilevel coded QAM

The symbol mapping principle utilized for the multilevel modulation is hierarchical block-partitioning (BP) with a square quadrature amplitude modulation (QAM) constellation. The mapping uses identical bit-to-position allocation throughout all hierarchy levels, while in related mapping methods – studied e.g. in [135] and [146] – the allocation changes between hierarchy levels. An illustration of the construction of a BP 16-QAM constellation is shown in Fig. 48. The minimum distance of the constellation points is different at each hierarchy level, resulting in an unequal error protection characteristic when a single channel code is utilized commonly for all hierarchy levels.

The transmitted MLBICM symbols are constructed as illustrated in Fig. 49 in the following manner. The bits to be transmitted over the  $k$ th antenna are further de-multiplexed into  $Q = M$  parallel levels, which are channel encoded and interleaved in parallel with different random interleavers. The resulting  $M$  parallel sequences are segmented into

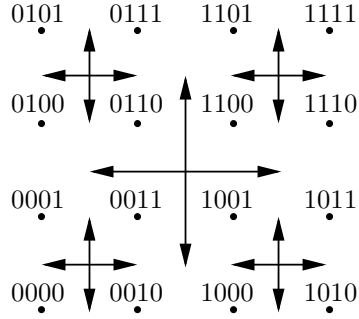


Fig. 48. Block-partitioned 16-QAM mapping. Bit value “-1” marked “0” for readability.

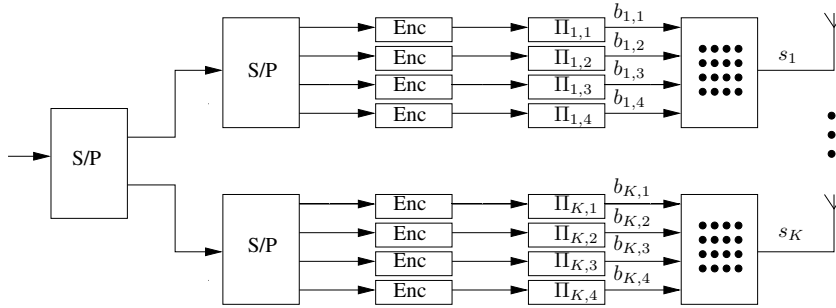


Fig. 49. Multilevel BICM encoder and modulator.

groups of  $M$  bits so that each interleaved level defines a single bit in each group. In an identical manner to the BICM scheme, the segmented bits for each frame of length  $N$  can be expressed by the vectors (1)–(3), the only difference being the construction of the modulation through the use of parallel encoders and interleavers. The definitions (1)–(3) are used also for MLBICM for convenience.

The BP mapper can be seen as a linear combination of the  $M$  BPSK-modulated symbols, where the segment of encoded bits is multiplied with a complex weight vector  $\mathbf{z}^T$  and, thus, superpositioned into QAM symbols. The weight vector consists of elements  $z_m$ , that are real for  $m$  being odd, and  $z_m = iz_{m-1}$  for  $m$  being even. In case there are multiple levels with identical  $|z_m|$ , these are treated as one “layer” when considering performance. If the  $M$ -level linear BP mapper with its levels being ordered by decreasing amplitude is given as

$$\mathbf{z} = [z_1, \dots, z_m, \dots, z_M]^T \in \mathbb{C}^M, \quad (210)$$

constrained to  $\mathbf{z}^H \mathbf{z} = 1$ , the mapped symbols within a frame can be expressed as the vector

$$\underline{\mathbf{s}} = [\underline{\mathbf{s}}_1^T, \dots, \underline{\mathbf{s}}_k^T, \dots, \underline{\mathbf{s}}_K^T]^T \in \mathbb{C}^{KN}, \quad (211)$$

where the transmitted symbols of each of the  $K$  antennas given by

$$\underline{\mathbf{s}}_k = [\underline{\mathbf{s}}_k(1), \dots, \underline{\mathbf{s}}_k(n), \dots, \underline{\mathbf{s}}_k(N)]^T \in \mathbb{C}^N, \quad (212)$$

and each symbol can be expressed by

$$\underline{\mathbf{s}}_k(n) = \mathbf{z}^T \mathbf{b}_k(n). \quad (213)$$

The symbol sequence for the whole frame can also be expressed as

$$\begin{aligned} \underline{\mathbf{s}} &= (\mathbf{I}^{KN} \otimes \mathbf{z}^T) \mathbf{b} \\ &= \mathbf{Zb}. \end{aligned} \quad (214)$$

## 6.2 MMSE turbo equalization of block-partitioned QAM

The equalizer algorithm described in Section 3.1 can be directly utilized in the detection of MLBICM by using a suitable symbol de-mapper. However, if the hierarchical structure of the mapping is exploited, a new equalizer structure with lower complexity can be derived.

As indicated by (213) the block-partitioned symbol constellation is treated as a linear combination of binary sub-constellations, where each coding level of the multilevel encoder is utilized as the input to one binary (BPSK) sub-constellation. The linear mapping is considered to be a part of an equivalent channel excited by BPSK modulated symbols. A turbo equalizer is then defined, where most of the processing for equalization and decoding of each sub-constellation can be performed in parallel [85]. The MMSE filter computation in the algorithm considers a single level as the desired signal. A block diagram of the equalizer and decoder (for one transmit antenna) is depicted in Fig. 50.

Equalization and decoding of levels is ordered. Code levels with the largest absolute weight  $z_m$  are decoded first, levels with the second largest weight from the second iteration onwards, and so on. For a 16-QAM square constellation, levels 1-2 (having equal weights) are equalized and decoded in the first iteration, and all levels 1-4 equalized and decoded in the second iteration onwards. The equalizer algorithm is illustrated in more detail with a block diagram in Fig. 51. The figure also indicates which computation results can be re-used for all detected bits, which are specific to one transmit antenna, and which are computed for each coding level. One common filter is used in the computation of the equalizer output of all sub-constellations during one turbo iteration. The algorithm to obtain the estimate of the transmitted signal of one level is obtained by applying the algorithm in Section 3.1 for BPSK modulation. First, corresponding to (44), the expected value of the soft symbol estimates is computed as

$$\hat{b}_{k,m}(n) = \tanh\left(\frac{\xi_{\underline{\mathbf{s}}_{k,m}}^d(n)}{2}\right) \quad (216)$$

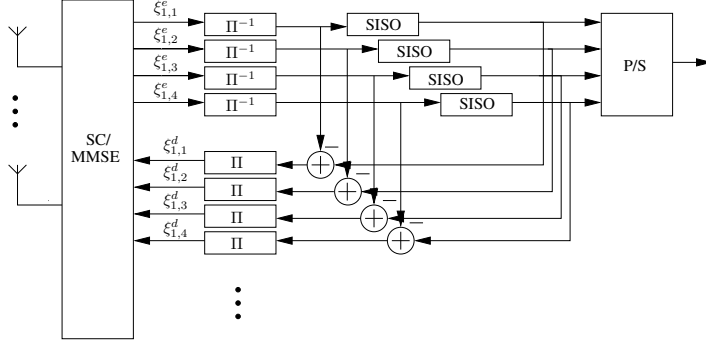


**Fig. 50. MLBICM Turbo Equalizer (16-QAM).**

where  $\xi_{k,m}^d(n)$  is the log-likelihood ratio provided by the  $k$ th user's decoder for bit  $b_{k,m}(n)$ . The residual is then computed as

$$\tilde{\mathbf{r}} = \mathbf{r} - \mathbf{H}\mathbf{Z}\hat{\mathbf{b}}. \quad (217)$$

The covariance matrix of the soft symbol estimates is then obtained similarly to (50) as

$$\underline{\mathbf{\Lambda}} = \mathbf{I} - \text{diag} \left\{ \hat{\mathbf{b}}^2 \right\}, \quad (218)$$

where the squaring is element-wise, to form the residual covariance matrix as

$$\underline{\Sigma}_{\tilde{\mathbf{r}}} = \mathbf{H}\mathbf{Z}\underline{\mathbf{\Lambda}}\mathbf{Z}^H\mathbf{H}^H + \sigma_0^2\mathbf{I}. \quad (219)$$

Both the computation results of the residual in (217) and the covariance matrix in (219) are common to all  $k$  and  $m$ . The filtering equations (52) and (53) are modified to take advantage of the linear model of the multilevel coded signal. The common filter for all levels of antenna  $k$  is given by

$$\underline{\mathbf{u}}_k^H(n) = \mathbf{h}_k^H(n)\underline{\Sigma}^{-1}(n), \quad (220)$$

which is utilized in the computation of the intermediate variables as

$$\begin{aligned} \underline{\alpha}_k(n) &= \underline{\mathbf{u}}_k^H(n)\mathbf{h}_k(n) \\ &= \mathbf{h}_k^H(n)\underline{\Sigma}^{-1}(n)\mathbf{h}_k(n) \end{aligned} \quad (221)$$

$$\underline{\beta}_{k,m}(n) = \frac{1}{1 + |z_m|^2 \underline{\alpha}_k(n) \left| \hat{b}_{k,m}(n) \right|^2}, \quad (222)$$

only the second of which is computed for each level. Finally, the prior soft symbol estimate of level  $m$  is utilized in the filter output computation for level  $m$  as

$$\underline{x}_{k,m}(n) = \underline{\beta}_{k,m}(n) \left( |z_m|^2 \underline{\alpha}_k(n) \hat{b}_{k,m}(n) + z_m^* \underline{\mathbf{u}}_k^H(n) \tilde{\mathbf{r}}(n) \right). \quad (223)$$

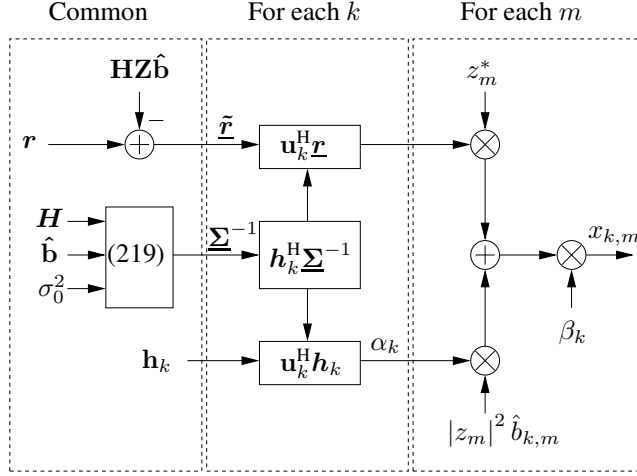


**Fig. 51. Equalizer block diagram. The dotted line encloses post-processing for one transmit antenna  $k$ .**

The  $M$  parallel channel decoders are then provided with the binary likelihood information computed as

$$\xi_{k,m}^e(n) = 4 \frac{\Re \{ \underline{x}_{k,m}(n) \}}{1 - |z_m|^2 \underline{\alpha}_k(n) \underline{\beta}_{k,m}(n)}. \quad (224)$$

Note that (224) is the result of expressing (60) for BPSK modulation. The parallel channel decoders operate independently without the need to exchange information as in multistage decoding [147]. Instead, *a priori* information exchange is carried out through the equalizer in the process of soft interference cancellation.

### 6.2.1 Numerical evaluations

Simulations were performed to test the performance of the scheme. A 10-path Rayleigh fading channel with a uniform average tap profile and two receive antennas was used. The channel taps were assumed to be uncorrelated and static over the transmission period, but changing frame-by-frame. The channel state is assumed to be known at the receiver. The channel code is the rate-1/2 convolutional code with generator polynomials  $(5, 7)_8$ . The receiver performs one processing iteration for each layer before including the next layer into processing.

To test the receiver algorithm a 16-QAM system containing two layers is simulated. The resulting bit-error-rate performance, averaged over the I/Q branches of a layer, is presented in Fig. 52 as a function of the average  $E_b/N_0$  per antenna. The two curves

groups, solid and dashed lines, correspond to the achieved BER for each receiver iteration of the first and second layers, respectively. The figure shows how the scheme provides a certain reliability for the layers at different  $E_b/N_0$ . If equal error protection of transmitted data is desired data is de-multiplexed into parallel streams and multiplexed at the receiver, and the provided reliability is the mean of the streams' reliabilities.

A further result with 64-QAM with another layer of encoding superpositioned is depicted in Fig. 53. Perhaps the most interesting issue brought forward by the simulation result is the difference in SNR required by the layers to reach certain performance. This difference is always smaller than the 6dB difference of energy allocation to the layers provided by the linear mapper, indicating the layers have a joint convergence behavior that determines the performance.

### 6.3 Evaluation in the real field

The results of a performance evaluation of transmission schemes are often highly dependent on the channel modeling used in the evaluation. The dependency between system performance and channel characteristics results in a situation where model selection dominates the end results. This problem has been highlighted in recent years by the introduction of high-performance multi-antenna schemes, that take advantage of the properties of the spatial propagation channel.

To some extent, the problem of model selection can be alleviated by resorting to testing with the real channel. Fortunately this can be performed by using measurement data recorded with an instrument capable of storing the state of the propagation channel accurately. When the evaluations are compared to the analysis of spatial channel parameters provided by suitable parameter estimation methods [148], valuable intuitive insights on the system behavior can be obtained. In this section, the proposed multilevel design is tested with channel measurement based simulations.

#### 6.3.1 Measurement scenario and propagation characterization

The measurements were carried out by the Electronic Measurement Research Lab of Ilmenau University of Technology in a courtyard on the campus of the Ilmenau University of Technology. The courtyard is surrounded by a 15m tall building. The measurement track is presented in the courtyard sketch in Fig. 54, and proceeds from the point marked as "TX1" to the point "TX2". A metal container is located between the points "TX1" and "RX" and blocks the line of sight (LOS) path between the transmitter and receiver on the measurement track in the position marked by "NLOS STAT" and the range marked by "NLOS DYN", denoting static and dynamic non line of sight (NLOS) propagation, respectively. In the "NLOS STAT" position, the transmitter was held stationary momentarily in the beginning of the measurement. In the last range marked "LOS" a line of sight path is present between the transmitter and receiver. From the measurements, 108 samples with even spacing were used for simulations. The total consisted of 15, 40 and 53 samples for

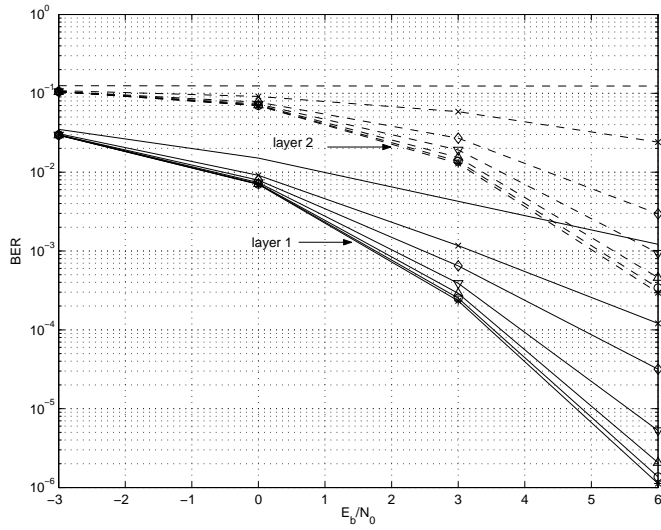


Fig. 52. 16-QAM bit-error rate. Solid line: 1st layer, dashed line: 2nd layer.

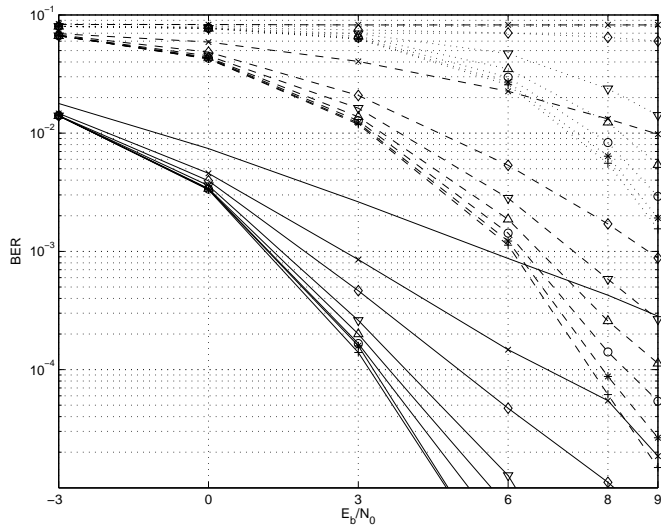


Fig. 53. 64-QAM bit-error rate. Solid line: 1st layer, dashed line: 2nd layer, dotted line: 3rd layer.



*Table 8. Measurement parameters.*

Parameter	Value
Centre frequency	5.2GHz
Bandwidth	120MHz
Tx antenna type	UCA
Tx antenna elements	16
Tx antenna height	2.1m
Rx antenna type	ULA
Rx antenna elements	8
Rx antenna height	1.67m

### ***6.3.2 Measurement data based performance results***

An MLBICM scheme with a 16-QAM symbol constellation was compared to the standard Gray-mapped 16-QAM BICM with the corresponding receivers presented in Sections 3.1 and 6.2. Random interleaving and a frame length of 512 information bits were used with the rate-1/2 convolutional code having the generator polynomials  $(5, 7)_8$  for both schemes. The frame length results in interleaver lengths of 1024 encoded bits for the BICM scheme and 256 encoded bits for each level in the MLBICM scheme. For both schemes, the receivers perform six iterations of equalization and decoding.

In measurement data based simulations, the transmitted signal is convolved with the transmitter filter, the measured CIR, and the receiver filter, whereby the two filters define the system bandwidth. Results of performance evaluations for a class of turbo-equalizers in measured MIMO channels are presented [150, 149]. The motivation was to study the throughput efficiency offered by the MLBICM scheme and to compare it with that of the standard BICM scheme. The results will enable the evaluation of the characteristics of the link as seen by the higher protocol layers when the channel conditions vary. The FERs of the two schemes were evaluated in a measured channel using a two transmit – two receive antenna configuration to examine the throughput efficiency (TPeff) [151, chap. 15] given by

$$\text{TPeff} = R(1 - \text{FER}), \quad (225)$$

where selective-repeat ARQ with infinite buffering is assumed, with  $R$  being the channel code rate. The transmitter and receiver employ root-raised cosine filters, both with a roll-off factor of 0.25, so that the simulated channel bandwidth of 25MHz translates into a symbol rate of 20Msym/s. The overall maximum throughput efficiency of 0.5 then corresponds to a data rate of 80Mbits/s in the tested two-by-two configuration using 16-QAM and rate-1/2 channel coding with 4bits/symbol total spectral efficiency. The number of frames transmitted per snapshot was 350.

Fig. 56 reports the average FER over code levels for MLBICM and the average FER of BICM, and indicates a generic trend in the performance of the studied schemes. Both MLBICM and BICM achieve excellent performance in the static NLOS multipath rich en-

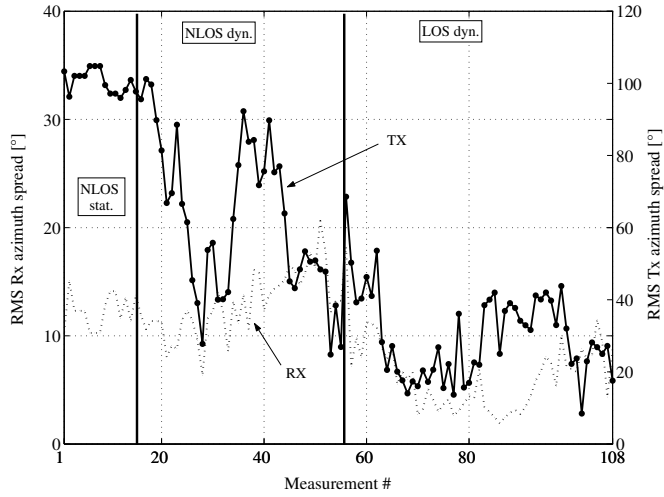


Fig. 55. Channel azimuth spread over the measurement track.

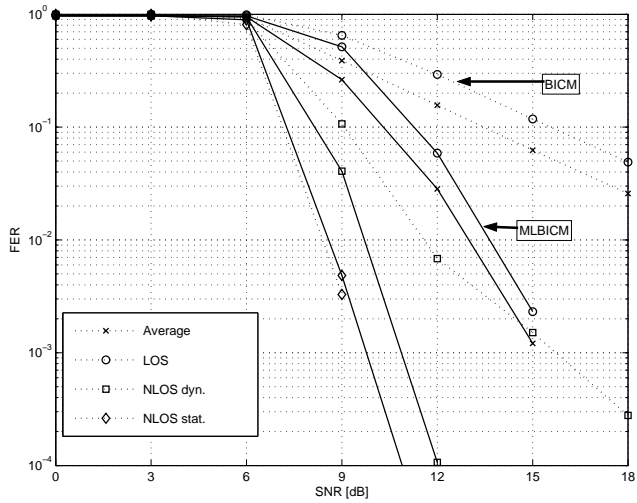


Fig. 56. FER of MLBICM and BICM on the measurement track, different channel conditions separated.

vironment, with BICM performing somewhat better. The difference between the schemes can be found in channels with less multipath richness. In those scenarios (dynamic NLOS, LOS) both schemes degrade in performance compared to the static NLOS case, but the MLBICM system performance loss is more graceful than that of the BICM system. The LOS channel condition dominates the results for both schemes when the average FER over all scenarios is considered. It should be noted that the average FER for MLBICM is computed after re-multiplexing the decoded streams, and for which errors from layer 2 dominate the result. In general the result indicates that MLBICM with turbo-equalization is less sensitive to the variation in channel conditions than the BICM counterpart. It indicates that the MLBICM scheme exhibits a minor loss compared to the BICM scheme in the best channel conditions of the static NLOS scenario, but offers significant gain in the other scenarios identified. layer 1 of the MLBICM has higher error protection than layer 2 and is able to provide reliable feedback to the equalizer in a large variation of channel conditions. Thus, the MLBICM turbo-equalizer can reach partial convergence even though all coding levels cannot be successfully decoded. The convergence of the BICM scheme, on the other hand, depends on reliable decoding and feedback of all the transmitted information bits.

The average TPeff over the measurement track shown in Fig. 57 indicates the same tendency: The BICM scheme offers a small advantage in the static NLOS channel when  $TP_{eff} < 0.1$ , but in all other cases MLBICM offers superior performance, especially when TPeff approaches its maximum ( $= 0.5$ ).

In the results reported in Fig. 57 it is assumed that a single ARQ controller process handles the re-transmission and the whole 512-bit frame is re-transmitted in case of frame errors. This approach is denoted by S-ARQ in the sequel to indicate the single ARQ controller. The total re-transmission probability and the resulting TPeff of MLBICM is dominated by errors from layer 2. If the two layers are handled by separate ARQ controllers, this can be avoided and thereby the overall TPeff can be improved. Fig. 58 shows the average TPeff for MLBICM over the measurement track with layered ARQ (L-ARQ), where each of the two ARQ controllers handle re-transmissions on a single layer. The maximum throughput efficiency of each layer is scaled to match the spectral efficiency of one layer when computing the TPeff of (225). Fig. 58 shows the difference in TPeff between the two layers and demonstrates that the total TPeff is the TPeff sum over the layers. For further analysis of the gain in different channel scenarios, the TPeffs with S-ARQ MLBICM, L-ARQ MLBICM and the standard BICM scheme in the two extreme channel conditions; static NLOS and LOS, are compared.

Fig. 59 shows the TPeffs with S-ARQ and L-ARQ MLBICM averaged over the measurement snapshots in static NLOS channel conditions. For comparison, the TPeff with the BICM scheme in the same conditions is shown. The average TPeff with BICM is better than that with MLBICM and S-ARQ, as already indicated in Fig. 57. However, since the total average TPeff of MLBICM with L-ARQ is equal to the mean of the average TPeff in the two layers, the MLBICM scheme with L-ARQ offers superior performance to both MLBICM and BICM schemes utilizing S-ARQ. It should be recognized that the comparison is not completely fair due to the larger frame length of BICM, which slightly inflates the mean FER. Shortening the frame length with BICM is problematic, however, due to convergence problems with short interleaving. Fig. 59 demonstrates how L-ARQ provides a smooth transition from low to high TPeff as the SNR is improved.

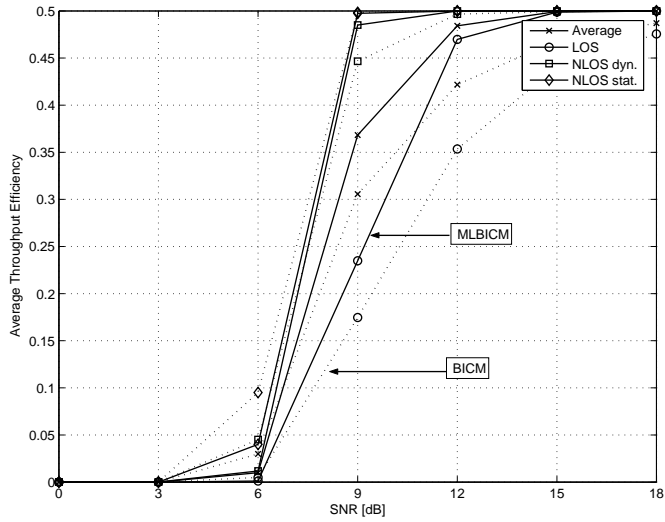


Fig. 57. TPeff of MLBICM and BICM on the measurement track, different channel conditions separated.

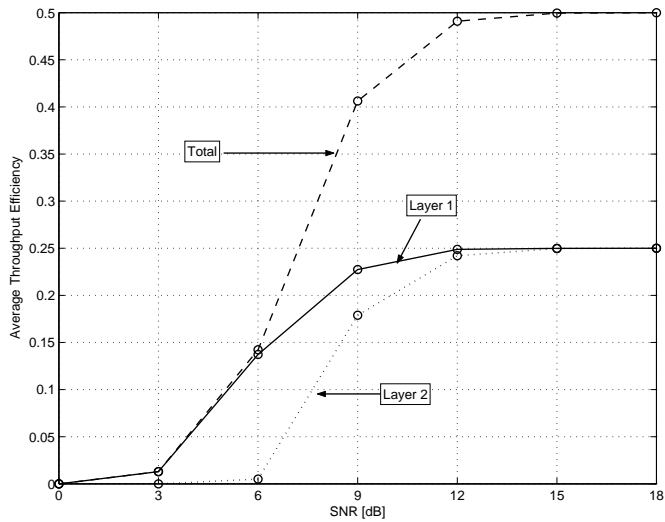


Fig. 58. Average TPeff over the measurement track when MLBICM exploits L-ARQ.

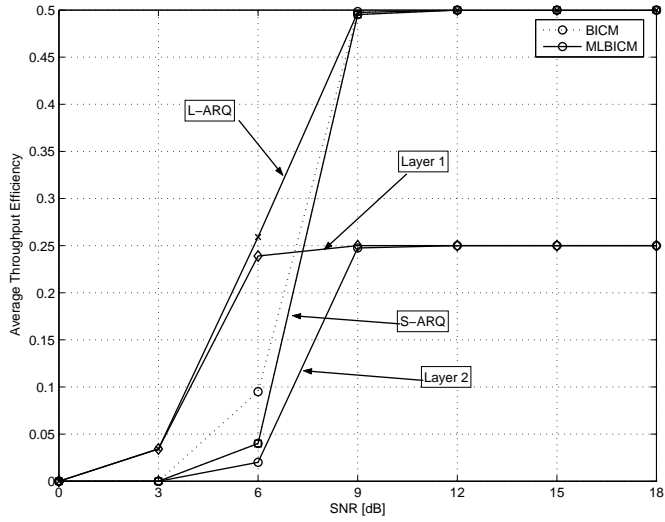


Fig. 59. Average TPeff in static NLOS with different ARQ setups.

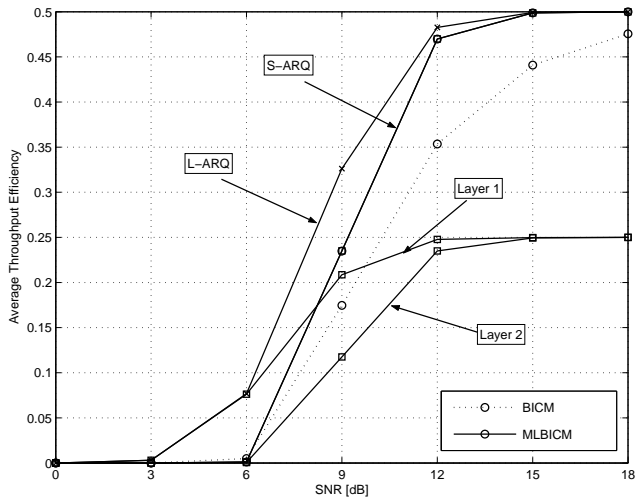


Fig. 60. Average TPeff in LOS with different ARQ setups.

The performance of L-ARQ MLBICM and BICM is emphasized in LOS channel conditions, where the FER performance of MLBICM is better than that of BICM. Fig. 60 shows the LOS results showing a superior TPeff of MLBICM with both types of ARQ. A gain of 2dB with L-ARQ MLBICM can be seen at TPeff > 0.2.

## 6.4 Convergence analysis

To enable a more informative analysis on the convergence properties of the MLBICM 16-QAM coded modulation, the convergence analysis from Chapter 4 can be extended to the MLBICM case. The extension is straightforward if the multiple coding levels are considered multiple transmit antennas with fully correlated channels.

For simplicity, a two-level coding is assumed, with each level modulating a Gray-mapped QPSK modulation. The transmission can be modeled by the linear model given in (213), since the bits in the Gray-mapped QPSK are independent on the in-phase and quadrature branches and the QPSK modulation can be thought of as consisting of two orthogonal BPSK modulations. The expected symbol variance after interference cancellation can be computed as the sum of the two levels as

$$E \{ \bar{\lambda}_k \} = \sum_{q=1}^2 E \{ \bar{\lambda}_{k,q} \}, \quad (226)$$

where  $q$  denotes the coding level and  $E \{ \bar{\lambda}_{k,q} \}$  is computed for the QPSK modulation using (156). Then, the MMSE filter output effective SNR can be computed for each  $q$  with (158) so that

$$\mathcal{L}_{k,q,a} = \frac{\mu_{k,q,a}}{1 - \mu_{k,q,a}}, \quad (227)$$

where

$$\mu_{k,q,a} = \frac{|z_q|^2 \bar{\gamma}_k}{1 + |z_q|^2 \delta_{k,q} \bar{\gamma}_k}, \quad (228)$$

with the correct level energy weighting taken into account by

$$z_q = \begin{cases} z_1 & q = 1 \\ z_3 & q = 2. \end{cases} \quad (229)$$

$$(230)$$

The de-mapper for the Gray-QPSK is equivalent to the BPSK de-mapper with an input down-scaling, and its output average mutual information can be computed by the functional approximation given by (161), so that the utilized approximation parameters are those of the QPSK modulation in Table 6. The result is then two computed level-wise mutual information values corresponding to the two coding levels.

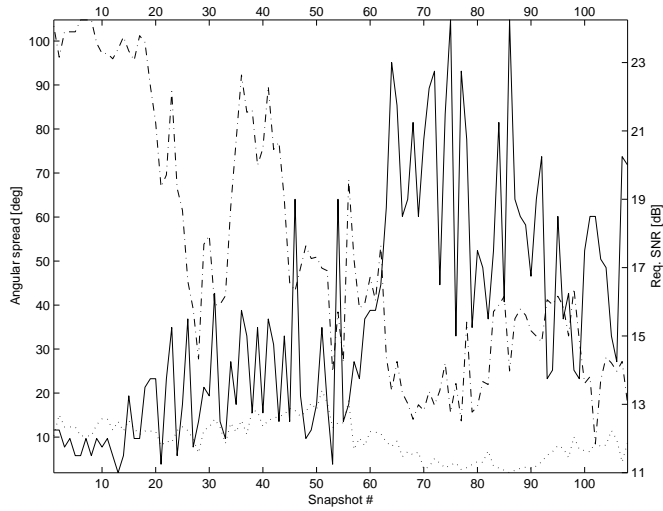


**Fig. 61. Required SNR (solid) for BICM, TX and RX azimuth spread (dash-dot, dot).**

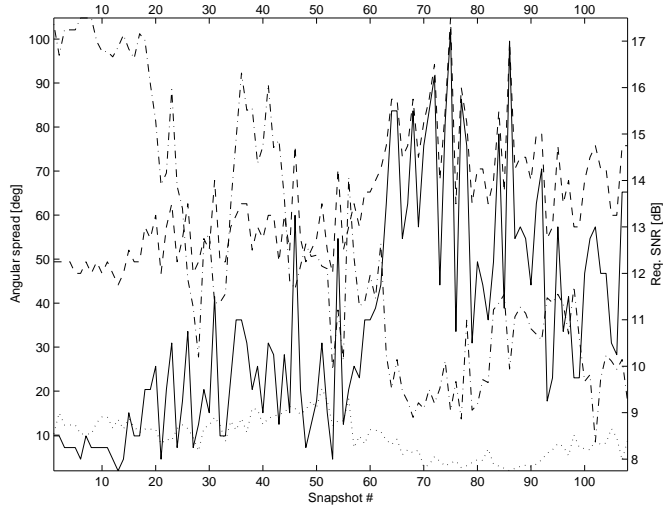


**Fig. 62. Required SNR (Layer-1: solid, Layer-2: dashed) for MLBICM, TX and RX azimuth spread (dash-dot, dot).**

## 6.5 Analytical evaluation in the real field

With the convergence analysis technique outlined in Section 6.4 the required SNR to reach a certain mutual information target at the channel decoder *a posteriori* output (here chosen to be 0.999) can be evaluated. The considered channel code is the rate-1/2 convolutional code with generators  $(561, 753)_8$ . Fig. 61 reports the required SNR for BICM in each snapshot along the measurement track. The dependence between the azimuthal spreads and the required SNR is easily verified. A comparable result for MLBICM is reported in Fig. 62, where the two levels are reported separately. Level 2 exhibits an SNR threshold (approx. 12dB) below which it does not reach the target.

It is notable that in snapshots where the SNR requirement is higher than the threshold, both levels converge at the same SNR. This result shows when it is possible to further optimize the code design or selection for MLBICM either for increased throughput or decreased required SNR. Due to the area property of the decoder EXIT functions, a decrease in the code rate will enable convergence with a lower SNR [71]. Optimally both levels should converge at the same SNR, since otherwise power is wasted improving level 2 performance to the desired operation point. Fig. 62 indicates where the level 2 code rate can be decreased and traded for the level 1 rate in high spatial spread environments and achieve a lower required SNR, while preserving the sum rate. This results does not, however, prove the optimality of the unbalanced design in low-spread environments, where the design is convergence-limited and dependent on successful level 1 decoding. Any puncturing of the level 1 code would lead to an increased required SNR for level 1 and, thus, the whole link in these cases. In these scenarios the additional SNR is required to reach the target, or alternatively the total transmission rate must be decreased.

The difference in required SNR between BICM and MLBICM can also be evaluated. Fig. 63 reports the SNR gain of MLBICM levels over BICM with the snapshots sorted according to increasing transmit side azimuthal spread. A corresponding figure sorted according to receive side azimuthal spread is presented in Fig. 64. Level 1 gain is mainly interesting if the link is used for the transmission of multiple classes of data and UEP is a desired feature of the link. In cases with a single class of data, level 2 dominates the link error performance, and is of primary interest. The gain is largest in low azimuthal spread cases and diminishes as the spread increases. MLBICM level 2 provides a gain over BICM in high-spread cases but has a small loss in the high-spread cases. This result coincides with the results in Section 6.3 indicating a small advantage for BICM in high spatial spread environments.

Finally, an evaluation of the differences of equalizer converge properties when combined with different channel codes is conducted with the measurement data. The mutual information reached in 90% of the snapshots given perfect channel decoder feedback (genie-aided detection) is plotted in Fig. 65 as a function of average received SNR for both MLBICM and BICM. The considered channel codes are the rate-1/2 convolutional codes with polynomials  $(5, 7)_8$  and  $(561, 753)_8$ , and the turbo code with constituent polynomials  $(1, 13/15)_8$ , which is punctured to rate-1/2. For MLBICM, the average mutual information over levels is reported for consistency with BICM. With all channel codes BICM reaches a higher mutual information than MLBICM with GAD. The outage mutual information based on the true convergence of the equalizer is reported in Fig. 66 and shows the BICM combined with all the considered codes has severe convergence problems in the

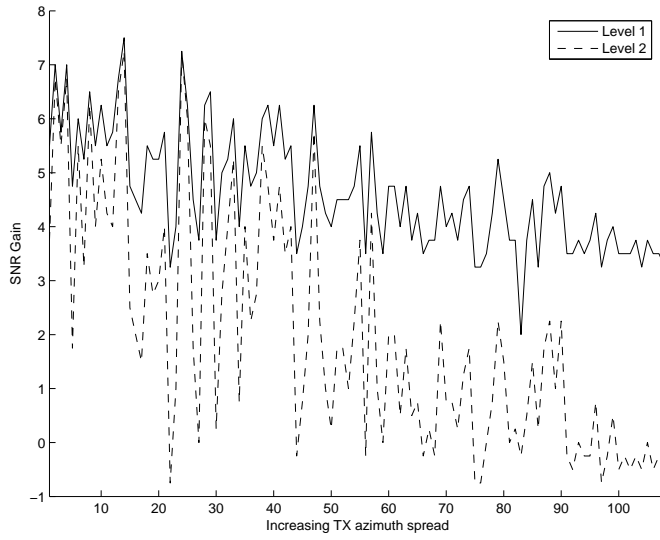


**Fig. 63. SNR gain of MLBICM levels over BICM with increasing TX azimuth spread.**

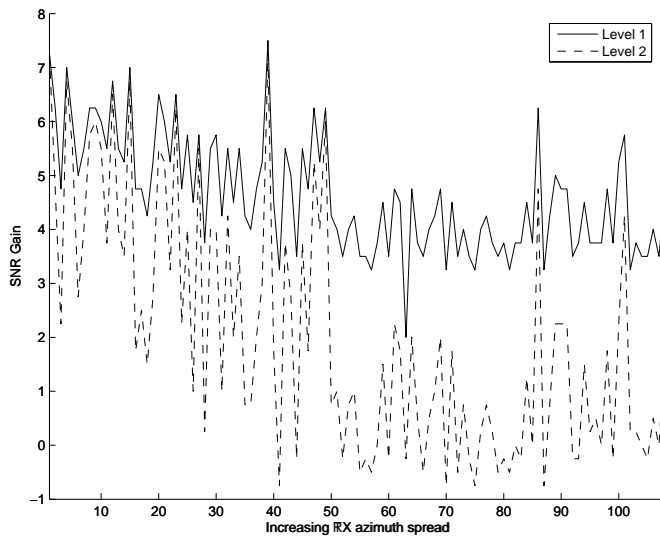


**Fig. 64. SNR gain of MLBICM levels over BICM with increasing RX azimuth spread.**

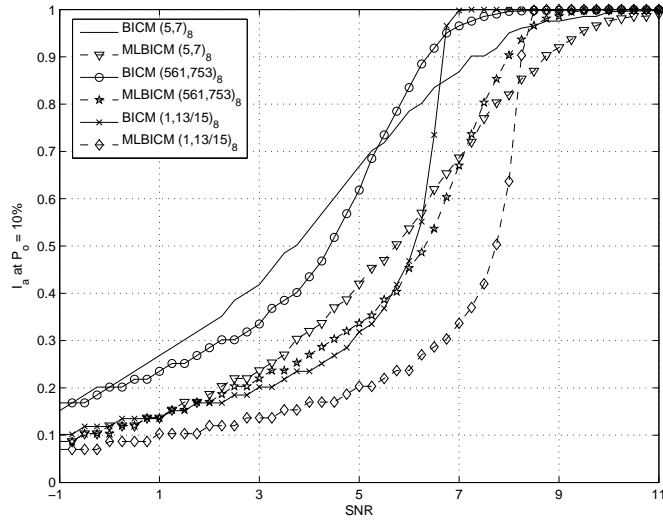


Fig. 65. 10% outage mutual information at the GAD bound with different channel codes.

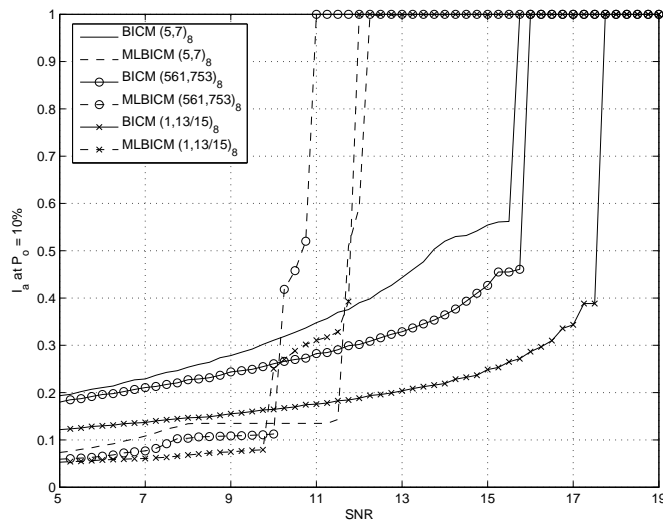
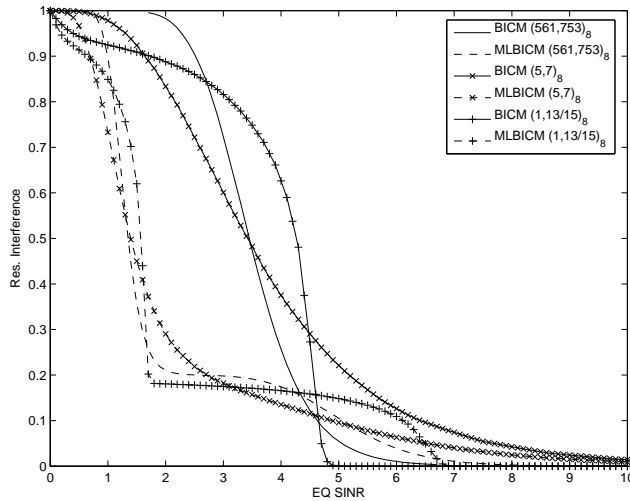


Fig. 66. 10% outage mutual information with different channel codes.



**Fig. 67. Equalizer output SNR transformed into residual interference in the second iteration.**

considered channel scenarios. With MLBICM, the outage mutual information is mainly a demonstration of the level 2 SNR threshold whose effect dominates the average mutual information between levels. Interestingly, the MLBICM modulation combines well with a high-memory outer code, while BICM does not.

A fundamental explanation of the convergence behavior difference between BICM and MLBICM is given in Fig. 67 where the residual interference power resulting from the first equalization and decoding iteration is plotted as a function of the equalizer output equivalent SNR (linear scale) in the first (linear) equalizer iteration. The early convergence of MLBICM level 1 is visibly demonstrated. The BICM characteristic for converting equalizer output SNR into low residual interference at the subsequent iteration is remarkably poorer. It is instructive to consider the differences between the two coded modulations that result in the behavior in Fig. 67. Since the mapping from decoder feedback mutual information into symbol residual variance is quite similar for Gray-mapped QPSK and 16-QAM, the reason must reside elsewhere. One reason for the behavior is the design of BICM: the de-mapper mixes all encoded bits into one stream and effectively averages the bitwise mutual information. In other words, the sub-optimal constellation constrained capacity of BICM 16-QAM limits the transformation of equalizer output SNR into mutual information entering the decoder. Since the convergence characteristic of most channel codes exhibits a threshold effect, i.e., above a certain threshold SNR convergence is greatly enhanced, the limitation due to modulation becomes dominant. To support this interpretation, in Fig. 67 it can be seen that the weakest channel code (with the lowest threshold) has the smallest difference between BICM and MLBICM convergence characteristics.

## 6.6 Outage based code design for MLBICM 16-QAM

The convergence outage based design presented in Chapter 4 can be applied to any modulation if BICM is used by concatenating the equalizer EXIT function with that of the mapper and de-mapper as is done in Section 4.3 to enable the convergence analysis. Such a design is, however, sub-optimal due to the sub-optimality of BICM wrt. channel capacity. On the other hand, it is known [135] that any modulation mapping can reach channel capacity (in the simple cases) if the outer code is suitably designed using multilevel techniques to match the multiple virtual channel capacities offered by the modulation. The example 16-QAM contains two virtual channels that require separate channel codes for optimal design. Incidentally, interleaving within the virtual channel is permissible, since it does not mix the virtual channels, as happens with BICM. The question is, how should outer codes be designed for the turbo equalizer system with multilevel coding to maximize the transmission rate, and in the fading case, achieve some design outage. A design principle to achieve that is outlined in the following.

Considering two-level 16-QAM as an example, two optimal codes should be jointly designed. First, a SISO case is considered, and an extension to layered MIMO transmission is provided through the procedure of taking the point-wise minimum of order-projected EXIT functions having found the optimal ordering. The equalizer EXIT function for the two levels can be visualized as two surfaces in a three-dimensional EXIT chart. The vector EXIT function can be defined as

$$\mathbf{f}_e : \mathbf{I}_d \rightarrow \mathbf{f}_e(\mathbf{I}_d) \in \mathbb{E}^{KQ}, \quad (231)$$

where  $K = 1$ ,  $Q = 2$  for the considered case, and

$$\mathbf{I}_d = [I_{d,1}, \dots, I_{d,q}, \dots, I_{d,Q}]^T \in \mathbb{E}^{KQ} \quad (232)$$

denotes the prior mutual information vector for all levels. The elements of  $\mathbf{I}_e$ , for a certain prior mutual information  $I'_d$ , channel state and noise variance, are in the case of the MMSE turbo equalizer, the result of monotonic functions of the same  $\bar{\gamma}_k$ . The result of this relation is, that at any arbitrary point  $\mathbf{I}'_d$ , given two arbitrary channel states  $\mathbf{H}_A$  and  $\mathbf{H}_B$ , if for any  $q \in 1 \dots Q$

$$I_{e,q}(\mathbf{I}'_d|\mathbf{H}_A) \geq I_{e,q}(\mathbf{I}'_d|\mathbf{H}_B), \quad (233)$$

then

$$\mathbf{I}_{e,q'}(\mathbf{I}'_d|\mathbf{H}_A) \geq \mathbf{I}_{e,q'}(\mathbf{I}'_d|\mathbf{H}_B) \forall q' \in 1 \dots Q, \quad (234)$$

where  $I_{e,q}(\mathbf{I}'_d|\mathbf{H}_A)$  and  $I_{e,q}(\mathbf{I}'_d|\mathbf{H}_B)$  are the equalizer EXIT function components conditioned on the two channel states  $\mathbf{H}_A$  and  $\mathbf{H}_B$ , respectively. In practice this means the EXIT functions have the same ordering within all levels at any arbitrary point in  $\mathbb{E}^{KQ}$ . For simplicity, a similar ordering rule can be assumed to hold also for other turbo equalizers in the sequel to maintain the generality of the developed approach.

Assuming the knowledge of the distribution of the EXIT function surfaces over the channel distribution, the level-wise cdf of EXIT function values can be expressed for each point in  $\mathbb{E}^2$  as

$$\mathcal{F}_{cdf}^q(\mathbf{I}_d, I) = P(\mathbf{f}_e^q(\mathbf{I}_d) < I), \mathbf{I}_d \in \mathbb{E}^Q. \quad (235)$$

Assuming parallelism of the EXIT functions within a level, a level-wise constant value surface defined by

$$\mathcal{F}_{cdf}^q(\mathbf{I}_d, f_d^q(\mathbf{I}_d)) = P_{out} \quad (236)$$

can be found, indicating the level-wise outage designed function

$$f_d^q(\mathbf{I}_d) \in [0, 1], \mathbf{I}_d \in \mathbb{E}^2. \quad (237)$$

Any outage optimal code design for the corresponding level can be found by defining the convergence path through the EXIT set. A joint maximum rate design given the outage then follows the path defined by the eigenvector corresponding to the maximum eigenvalue of the Jacobian, which is computed for the designed surfaces of the multiple levels. The path is computed at each point through the EXIT chart from the point  $\{0, 0\}$  to  $\{1, 1\}$ , as described in Appendix 4.

As noted above, the design can be extended to layered MIMO transmission as follows. If the joint channel distribution is exchangeable, the design should be symmetric, i.e., identical to all transmit antennas. For each channel realization and each detection ordering,  $KQ$  EXIT surfaces are then computed. An optimal ordering must then be found, which gives the maximum rate given the point-wise minimum of the optimal designs within that ordering. However, since rate is allocated to levels only during the convergence path selection phase, another optimality criterion must be used for choosing the optimal ordering. Without proof, but consistently with the area property, the ordering providing maximum sum-volume below the point-wise minimum EXIT surface can be selected so that the designed function for level  $q$  given the channel state is given by

$$f_d^q(\mathbf{I}_d) < \arg \max_{\sigma} \int_0^1 \int_0^1 \min \{ {}^0 f_{e, \sigma_k}(I_{e,k}) \} dI_{d,1} dI_{d,2}, \quad (238)$$

where the minimum is taken over all  $K$  surfaces  $f_{e, \sigma_k}$  within the ordering. Even though the two levels are treated as independent transmissions, a notable difference to the ordering in the simple symmetric design case in Section 4.2.2 is that the detection ordering is only between transmit antennas, and the multiple levels are always ordered from the strongest to the weakest. The resulting  $Q$  surfaces are included into the ensemble used to find the point-wise cdf of the EXIT functions. Finally,  $Q$  cdfs are computed and their constant value surfaces found to determine the designed EXIT surfaces that can be used as the basis for the Jacobian based rate maximization.

Due to the significantly different weighting of the levels, level 1 always has its EXIT function well above that of level 2. Also, the weighting difference will favor optimal designs which emphasize the cancellation of level 1, since that brings the most gain also for level 2. These designs will then be close to the (in the SISO case) EXIT chart sides, implying a sub-optimal design restricted to the order-projected EXIT function at the chart side will not incur a large loss compared to the optimal design. Such a design procedure can record only the order-projected EXIT functions of the two levels without considering the full EXIT surface, reducing the computations considerably. The outage design function can then also be found by only considering the outage surface on the chart sides.

An ordering which further simplifies the optimization process can again be found by considering only the point of no prior information of the order-projected EXIT functions,

Table 9. Multilevel code design for outage convergence.

- 
1. Generate new random realization for  $\mathbf{H}$ .
  2. Compute  ${}^0_1\bar{\gamma}_k(0)$  for all  $k$  and for all detection orderings.
  3. Choose the ordering giving the maximum smallest  ${}^0_1\bar{\gamma}_k(0)$ .
  4. Compute the  $Q$  EXIT surfaces corresponding to the maximum.
  5. Store the surfaces to the ensemble.
  6. Repeat to achieve sufficient accuracy of the EXIT ensemble distribution.
- 

defined by  $\bar{\gamma}_k(I_{d,k} = 0, I_{d,o_{k-1}} = 1)$  for the MMSE FDTE. Such a sub-optimal ordering procedure avoids the full computation of the  $K$   $Q$ -dimensional EXIT functions and the search for the largest minimum volume used in the more optimal ordering search defined by (238). In Table 9 the procedure to generate the distribution of EXIT surfaces in a  $K$  dimensional case for 16-QAM is outlined using sub-optimal ordering and assuming the MMSE turbo equalizer.

## 6.7 Summary and discussion

A pragmatic approach of applying multilevel coding was first presented, using identical codes for all levels. A sub-optimal MMSE turbo equalizer taking advantage of the linearity of the mapping was presented and tested with Monte-Carlo simulations. An evaluation with channel measurement data was carried out, showing the robustness of the coded modulation in varying spatial channel conditions. A simple re-transmission configuration (L-ARQ) with separate re-transmission control for groups of levels operating with equal error protection was introduced to compensate for and exploit the UEP property of the coded modulation. A convergence analysis was further carried out using the same channel measurement data to enable further understanding of the convergence properties. The properties of 16-QAM BICM symbol mapping was found to result in higher convergence thresholds (experienced as higher required SNR) than those of 16-QAM MLBICM in environments with low angular spread. Finally, a convergence outage based channel code design principle was outlined for layered MIMO transmissions.

Multilevel coding can be made to approach channel capacity in the simple cases [135], and provides a good starting point to apply bandwidth efficient modulation also in turbo equalizer based systems. The optimal design principle is relatively complex, while the sub-optimal approaches are quite applicable. As in the case of the previous outage based design approaches in this thesis, closed form expressions for the equalizer EXIT functions would significantly reduce the optimization complexity.

The optimization procedure, following the approach from Chapter 4, optimizes for the successful convergence of all code levels of all transmit antennas. If this requirement were to be relaxed, i.e., each antenna or code level would be handled by a separate re-

transmission controller, the code optimization would be different. In such a case all the  $Q$ -dimensional EXIT functions ( $K$  of them) within the optimum ordering (chosen with a sum-volume criterion, for instance) would be stored into the ensemble, and a joint multi-level code design would be performed on the ensemble. The requirement for taking the point-wise minimum of the EXIT functions would be relaxed since all transmissions are not required to converge successfully.

## 7 Conclusions and future work

### 7.1 Conclusions

Of the considered receiver algorithms, the frequency-domain MMSE turbo equalizer can be considered the most interesting one in terms of implementation complexity and performance. The computational complexity of a single frequency-domain iteration is low, in addition to which the equalizer converges with fewer iterations than the time-domain counterparts. Potential integration with orthogonal frequency division multiplexing (OFDM) based systems is also another option speaking in favor of frequency-domain processing. All time-domain equalizers have a higher computational complexity or, as in the case of the matched-filter approximation, require initialization by another algorithm to reach good performance.

The convergence properties of the equalizer, which depend on the channel and the receiver SNR, together with the utilized channel code, determine the receiver performance. The properties are embodied in the equalizer EXIT function, which is a multidimensional function in the case of layered MIMO transmission. By exploiting the monotonicity of EXIT functions and the area property of channel code EXIT functions, several properties of the system can be deduced. Given a channel state, the EXIT function of a maximum sum rate code can be found. Some of the limits of the system rate region can be characterized. Also, the maximum symmetric rate can be found and the detection strategy shown to correspond to detector ordering. All these characteristics are valid regardless of the equalizer algorithm and the actual equalizer EXIT function the algorithms exhibit.

Convergence analysis can further reveal the properties of different known channel codes and their suitability in combination with the equalizer. Channel parameters have a direct effect on the equalizer convergence, and the phenomena can be analyzed through the behavior of equalizer EXIT functions given the channel parameters. Decreasing frequency-selectivity and increasing spatial correlation both increase the required average SNR to reach a desired outage probability.

Suitable code design can optimize the transmission and improve the receiver performance if the channel statistics are known. In simple single-transmission cases, convergence outage based code optimization can provide a gain over non-optimized codes and codes optimized to channels with different channel statistics. In symmetric layered MIMO cases, an identical design for all transmit antennas is possible and can be optimized ac-

cording to the convergence outage criterion. If high bandwidth efficiency is desirable, multilevel coding can be utilized. The multilevel coded modulation can be used with a simple and robust configuration, where the UEP property can be compensated for and exploited with a proper ARQ configuration. The coded modulation can also be optimized with an outage criterion if the channel statistics are known *a priori*. The design is extensible to layered MIMO transmissions. If the proposed linear bit-to-symbol mapping is used, a computationally efficient MMSE turbo equalizer can be used to avoid the complexity of symbol to bit de-mapping at the detector.

## 7.2 Future work

There are several issues that must be considered before any of the receiver algorithms studied in this thesis may be applied in any real system. Most pressing are algorithms for channel estimation, preferably with iterative methods taking advantage of the turbo iterations and receiver synchronization. Also, further optimization of the equalizer algorithms themselves is necessary before an implementation may take place.

The one major obstacle in applying the convergence analysis and the related code design principles in this thesis is the lack of knowledge on EXIT function distributions of (MMSE) turbo equalizers. The current approach can be simplified by considering the EXIT function point-wise cdf in the SNR realm. This would effectively transform the outage design function search into the search of an outage SNR with a given prior information level. In some cases, random matrix-theoretic results may aid in finding SNR distributions at the output of the equalizer. Further study of the inequality between EXIT functions given a prior information level would potentially lead to a more accurate design principle. In the general case, if the assumption of parallel EXIT functions is not made, finding the outage design function appears to be a non-trivial problem. Some asymptotic results may be obtainable by assuming Gaussian signalling, in which case the constraints due to finite modulation vanish and the interference cancellation residual becomes Gaussian, as well.

An interesting path would be to apply the results of this thesis to systems with a single channel encoder combined with MIMO transmission. Such a MIMO configuration is straightforward and the code design is much simpler than the multi-dimensional approach provided in this thesis. The proposed analytical framework also supports the application of linear transmitter processing and may serve as a fruitful starting point for studies where transmit side channel information is available.

## References

1. Falconer D & Ariyavisitakul SL (2002) Broadband wireless using single carrier and frequency domain equalization. In Proc. International Symposium on Wireless Personal Multimedia Communications (WPMC), Honolulu, Hawaii, 1: 27–36.
2. Falconer D, Ariyavisitakul S, Benyamin-Seeyar A & Eidson B (2002) Frequency domain equalization for single-carrier broadband wireless systems. *IEEE Communications Magazine* 40(4): 58–66.
3. Forney GD (1972) Maximum-likelihood sequence estimation of digital sequences in the presence of intersymbol interference. *IEEE Transactions on Information Theory* 18(3).
4. Kay SM (1993) *Fundamentals of Statistical Signal Processing: Estimation Theory*. Prentice-Hall, Englewood Cliffs, NJ, USA.
5. Proakis JG (1995) *Digital Communications*. McGraw-Hill, Inc., New York, USA, 3rd ed.
6. Cioffi J, Dudaivoir G, Eyuboglu MV & Forney G (1995) MMSE decision-feedback equalizers and coding – part I: Equalization results. *IEEE Transactions on Communications* 43(10): 2582–2594.
7. Cioffi J, Dudaivoir G, Eyuboglu MV & Forney G (1995) MMSE decision-feedback equalizers and coding – part II: Coding results. *IEEE Transactions on Communications* 43(10): 2595–2604.
8. Shamai S & Laroia R (1996) The intersymbol interference channel: Lower bounds on capacity and channel precoding loss. *IEEE Transactions on Information Theory* 42(5): 1388–1404.
9. Guess T & Varanasi MK (2005) An information-theoretic framework for deriving canonical decision-feedback receivers in gaussian channels. *IEEE Transactions on Information Theory* 51(1): 173–187.
10. Berrou C, Glavieux A & Thitimajshima P (1993) Near Shannon limit error correcting coding and decoding. In Proc. IEEE International Conference on Communications (ICC), Geneva, Switzerland, 2: 1064–1070.
11. Berrou C & Glavieux A (1996) Near optimum error correcting coding and decoding: Turbo codes. *IEEE Transactions on Communications* 44(10): 1261–1271.
12. Bahl LR, Cocke J, Jelinek F & Raviv J (1974) Optimal decoding of linear codes for minimizing symbol error rate. *IEEE Transactions on Information Theory* 20(2): 284–287.
13. Moher M & Guinand P (1998) Cross-entropy and iterative decoding. *IEEE Transactions on Information Theory* 44(7): 3097–3104.
14. Benedetto S, Divsalar D, Montorsi G & Pollara F (1998) Serial concatenation of interleaved codes: Performance analysis, design, and iterative decoding. *IEEE Transactions on Information Theory* 44: 909–926.
15. Narayanan KR & Stüber GL (1999) A serial concatenation approach to iterative demodulation and decoding. *IEEE Transactions on Communications* 47(7): 956–961.
16. Verdú S (1984) Optimum multiuser signal detection. Ph.D. thesis, University of Illinois, Urbana-Champaign, IL, USA.

17. Verdú S (1986) Minimum probability of error for asynchronous Gaussian multiple-access channels. *IEEE Transactions on Information Theory* 32(1): 85–96.
18. Verdú S (1998) *Multuser Detection*. Cambridge University Press, Cambridge, UK.
19. Tarköy F (1997) Iterative multi-user decoding of asynchronous users. In *Proc. IEEE International Symposium on Information Theory (ISIT)*, Ulm, Germany, 30.
20. Moher M (1997) Turbo-based multiuser detection. In *Proc. IEEE International Symposium on Information Theory (ISIT)*, Ulm, Germany, 195.
21. Moher M & Guinand P (1998) An iterative algorithm for asynchronous coded multiuser detection. *IEEE Communications Letters* 2(8): 229–231.
22. Alexander PD, Grant AJ & Reed MC (1998) Iterative detection in code-division multiple-access with error control coding. *European Transactions on Telecommunications* 9(5): 419–525.
23. Reed MC, Schlegel CB, Alexander PD & Asenstorfer JA (1998) Iterative multiuser detection for cdma with fec: Near-single-user performance. *IEEE Transactions on Communications* 46(12): 1693–1699.
24. Alexander PD, Reed MC, Asenstorfer JA & Schlegel CB (1999) Iterative multiuser interference reduction: Turbo CDMA. *IEEE Transactions on Communications* 47(7): 1008–1014.
25. Boutros J & Caire G (2002) Iterative multiuser joint decoding: Unified framework and asymptotic analysis. *IEEE Transactions on Information Theory* 48(7): 1772–1793.
26. Caire G, Müller RR & Tanaka T (2004) Iterative multiuser joint decoding: optimal power allocation and low-complexity implementation. *IEEE Transactions on Information Theory* 50(9): 1950–1973.
27. Moher M (1998) An iterative multiuser decoder for near-capacity communications. *IEEE Transactions on Communications* 46(7): 870–880.
28. Varanasi MK & Aazhang B (1990) Multistage detection in asynchronous code-division multiple-access communications. *IEEE Transactions on Communications* 38(4): 509–519.
29. Divsalar D, Simon MK & Raphaeli D (1998) Improved parallel interference cancellation for CDMA. *IEEE Transactions on Communications* 46(2): 258–268.
30. Miyajima T, Hasegawa T & Haneishi M (1993) On the multiuser detection using a neural network in code-division multiple-access communications. *IEICE Transactions on Communications* E76-B(9): 961–968.
31. Damen MO, Gamal HE & Caire G (2003) On maximum-likelihood detection and the search for the closest lattice point. *IEEE Transactions on Information Theory* 49(10): 2389–2402.
32. Wang X & Poor HV (1999) Iterative (turbo) soft interference cancellation and decoding for coded CDMA. *IEEE Transactions on Communications* 47(7): 1046–1061.
33. Gamal HE & Geraniotis E (1989) Iterative multiuser detection for coded cdma signals in awgn and fading channels. *IEEE Journal on Selected Areas in Communications* 37(1): 30–41.
34. Douillard C, Jezequel CM, Berrou C, Picart A, Didier P & Glavieux A (1995) Iterative correction of intersymbol interference: Turbo-equalisation. *European Transactions on Telecommunications* 6(5): 507–511.
35. Raphaeli D & Zarai Y (1997) Combined turbo equalization and turbo decoding. In *Proc. of IEEE Globecom*, 639–643.
36. Tüchler M, Singer AC & Koetter R (2002) Minimum mean squared error equalisation using a priori information. *IEEE Transactions on Signal Processing* 50(3): 673–683.
37. Reynolds D & Wang X (2000) Low-complexity turbo-equalization for diversity channels. *Signal Processing*, Elsevier Science Publishers 81(5): 989–995.
38. Tüchler M & Hagenauer J (2001) Linear time and frequency domain turbo equalisation. In *Proc. IEEE Vehicular Technology Conference (VTC)*, 4: 2773–2777.
39. Dejonghe A & Vandendorpe L (2002) Turbo-equalisation for multilevel modulation: an efficient low-complexity scheme. In *Proc. IEEE International Conference on Communications (ICC)*, New York, USA, 3: 1863–1867.
40. Dejonghe A & Vandendorpe L (2004) Bit-interleaved turbo equalization over static frequency-selective channels: constellation mapping impact. *IEEE Transactions on Communications* 52(12): 2061–2065.
41. Gamal HE & Hammons AR (2001) A new approach to layered space-time coding and signal processing. *IEEE Transactions on Information Theory* 47(6): 2321–2334.

42. Abe T & Matsumoto T (2003) Space-time turbo equalization in frequency-selective MIMO channels. *IEEE Transactions on Vehicular Technology* 52(3): 469–475.
43. Otnes R & Tüchler M (2002) Low-complexity turbo equalization for time-varying channels. In *Proc. IEEE Vehicular Technology Conference (VTC)*, 1: 140–144.
44. Liu L & Ping L (2004) An extending window MMSE turbo equalization algorithm. *IEEE Signal Processing Letters* 11(11): 891–894.
45. Oomori H, Asai T & Matsumoto T (2001) A matched filter approximation for SC/MMSE turbo equalisers. *IEEE Communications Letters* 5(7): 310–312.
46. Yee M, Sandell M & Sun Y (2004) Comparison study of single-carrier and multi-carrier modulation using iterative based receiver for MIMO system. In *Proc. IEEE Vehicular Technology Conference (VTC)*, Milan, Italy, 3: 1275–1279.
47. Veselinović NR, Matsumoto T & Juntti M (2004) Iterative STTrC-coded multiuser detection and equalization with unknown interference. *EURASIP Journal on Wireless Communications and Networking* 2: 309–321.
48. Veselinovic N (2004) Iterative receivers for interference cancellation and suppression in wireless communications. Ph.D. thesis, University of Oulu.
49. Veselinovic N & Matsumoto T (2004) Iterative receivers for STTrC-coded MIMO turbo equalization. In *Proc. IEEE Vehicular Technology Conference (VTC)*, Milan, Italy, 1: 460–463.
50. Chtorou S, Visoz R & Berthet A (2004) A class of low complexity iterative equalizers for space-time BICM over MIMO block fading multipath AWGN channel. In *Proc. IEEE International Conference on Communications (ICC)*, Paris, France, 1: 618–624.
51. Lončar M, Müller R, Wehinger J, Mecklenbräuker C & Abe T (2004) Iterative channel estimation and data detection in frequency-selective fading MIMO channels. *European Transactions on Telecommunications* 15(4): 459–470.
52. Song S, Singer A & Sung KM (2004) Soft input channel estimation for turbo equalization. *IEEE Transactions on Signal Processing* 52(10): 2885–2894.
53. Berthet A, Visoz R & Chtourou S (2004) Efficient MMSE-based turbo-decoding of space-time BICM over MIMO block fading ISI channel with imperfect CSI. In *Proc. IEEE International Symposium on Personal, Indoor, and Mobile Radio Communications (PIMRC)*, Lisbon, Portugal, 4: 2621–2626.
54. Veselinović NR & Matsumoto T (2003) Iterative signal detection in frequency selective MIMO channels with unknown cochannel interference. In *2nd Workshop of COST 273*, Paris, France.
55. Abe T, Tomisato S & Matsumoto T (2003) A MIMO turbo equaliser for frequency selective channels with unknown interference. *IEEE Transactions on Vehicular Technology* 52(3): 476–482.
56. Veselinovic N, Matsumoto T & Juntti M (2004) A PDF estimation -based iterative MIMO signal detection with unknown interference. *IEEE Communications Letters* 8(7): 422–424.
57. Yeap B, Liew T, Hámorský J & Hanzo L (2002) Comparative study of turbo equalization schemes using convolutional, convolutional turbo, and block-turbo codes. *IEEE Transactions on Wireless Communications* 1(2): 266–273.
58. Polprasert C & Rajatheva R (2001) Performance of turbo codes with multilevel modulation and turbo equalization over frequency-selective fading channel. In *Proc. IEEE International Conference on Communications (ICC)*, Helsinki, Finland, 10: 3051–3055.
59. Langlais C & Hélar M (2002) Optimization of the equalization and the interleaving in turbo-equalization for a frequency-selective channel. In *Proc. IEEE International Conference on Communications (ICC)*, New York, USA, 3: 1242–1246.
60. Langlais C, Bouvet PJ, Hélar M & Laot C (2003) Which interleaver for turbo-equalization system on frequency and time-selective channels for high order modulations. In *Proc. IEEE Workshop on Signal Processing Advances in Wireless Communications (SPAWC)*, Rome, Italy.
61. Dejonghe A & Vandendorpe L (2003) A comparison of bit and symbol interleaving in MMSE turbo equalization. In *Proc. IEEE International Conference on Communications (ICC)*, Anchorage, USA, 4: 2928–2932.
62. Dejonghe A & Vandendorpe L (2004) Bounding the error-floor of turbo-equalized BICM transmission over quasi-static frequency-selective rayleigh fading channels. In *Proc. IEEE International Conference on Communications (ICC)*, Paris, France, 2: 727–731.

63. Caire G, Taricco G & Biglieri E (1998) Bit-interleaved coded modulation. *IEEE Transactions on Information Theory* 44: 927–946.
64. Langlais C & Hélarid M (2002) Mapping optimisation for turbo-equalisation by iterative demapping. *IEE Electronics Letters* 38(22): 1365–1366.
65. ten Brink S, JSpeidel & Yan RH (1998) Iterative demapping and decoding for multilevel modulation. In Proc. IEEE Global Telecommunication Conference (GLOBECOM), Sydney, Australia, 1: 579–584.
66. ten Brink S (2001) Convergence behavior of iteratively decoded parallel concatenated codes. *IEEE Transactions on Communications* 49(10): 1727–1737.
67. Divsalar D, Dolinar S & Polara F (2001) Iterative turbo decoder analysis based on density evolution. *IEEE Journal on Selected Areas in Communications* 19(5): 891–907.
68. Tüchler M, ten Brink S & Hagenauer J (2002) Measures of tracing convergence of iterative decoding algorithms. In Proc. 4th Intern. ITG Conf. on Source and Channel Coding, Berlin, Germany, 53–60.
69. Tüchler M, Koetter R & Singer AC (2002) Turbo equalisation: Principles and new results. *IEEE Transactions on Communications* 50(5): 754–767.
70. Lee SJ & Singer A (2003) Convergence analysis for linear turbo equalization. In Proc. Annual Asilomar Conference on Signals, Systems and Computers, Pacific Grove, USA, 1: 667–671.
71. Ashikhmin A, Kramer G & ten Brink S (2004) Extrinsic information transfer functions: Model and erasure channel properties. *IEEE Transactions on Information Theory* 50(11): 2657–2673.
72. Tüchler M (2004) Design of serially concatenated systems depending on the block length. *IEEE Transactions on Communications* 52(2): 209–218.
73. Peacock M & Collings I (2005) Redundancy allocation in turbo-equalizer design. *IEEE Transactions on Communications* 53(2): 263–268.
74. Ölçer S & Keskinöz M (2004) Performance of MMSE turbo equalization using outer LDPC coding for magnetic recording channels. In Proc. IEEE International Conference on Communications (ICC), Paris, France, 2: 645–650.
75. Zakoji T, Murata H & Araki K (2004) Performance of LDPC based turbo equalization for spatial multiplexing. In Proc. IEEE International Symposium on Personal, Indoor, and Mobile Radio Communications (PIMRC), Lisbon, Portugal, 2: 1404–1408.
76. Narayanan K, Wang X & Yue G (2002) LDPC code design for MMSE turbo equalization. In Proc. IEEE International Symposium on Information Theory (ISIT), Lausanne, Switzerland, 415.
77. Narayanan K, Wang X & GYue (2002) LDPC code design for turbo equalization. In Proc. of the 2002 IEEE Information Theory Workshop, Bangalore, India, 57–60.
78. Narayanan KR, Wang X & Yue G (2005) Estimating the PDF of the SIC-MMSE equalizer and its applications in designing LDPC codes with turbo equalization. *IEEE Transactions on Wireless Communications* 4(1): 278–287.
79. Wang X, Yue G & Narayanan K (2005) Optimization of LDPC-coded turbo CDMA systems. *IEEE Transactions on Signal Processing* 53(4): 1500–1510.
80. Sanderovich A, Peleg M & Shamai S (2005) LDPC coded MIMO multiple access with iterative joint decoding. *IEEE Transactions on Information Theory* 51(4): 1437–1450.
81. Li K & Wang X (2005) EXIT chart analysis of turbo multiuser detection. *IEEE Transactions on Wireless Communications* 1(1): 300–311.
82. Roumy A, Grant A, Fijalkow I, Alexander P & Pirez D (2001) Turbo equalization: Convergence analysis. In Proc. IEEE International Conference on Acoustics, Speech, and Signal Processing (ICASSP), New Jersey, USA, 4: 2645–2648.
83. Lee SJ, Singer A & Shanbhag N (2003) Analysis of linear turbo equalizer via EXIT chart. In Proc. IEEE Global Telecommunication Conference (GLOBECOM), San Fransisco, USA, 4: 2237–2242.
84. Hermosilla C & Szczecinski L (2004) Performance evaluation of linear turbo receivers using analytical EXIT functions. In Proc. IEEE International Symposium on Personal, Indoor, and Mobile Radio Communications (PIMRC), Barcelona, Spain, 2: 1307–1311.
85. Kansanen K & Matsumoto T (2003) Turbo equalisation of multilevel coded QAM. In Proc. IEEE Workshop on Signal Processing Advances in Wireless Communications (SPAWC), Rome, Italy.

86. Kansanen K & Matsumoto T (2003) A computationally efficient MIMO turbo-equaliser. In Proc. IEEE Vehicular Technology Conference (VTC), Jeju, Korea, 1: 277–281.
87. Kansanen K, Schneider C, Matsumoto T & Thomä R (2005) Multilevel coded QAM with MIMO turbo-equalization in broadband single-carrier signaling. *IEEE Transactions on Vehicular Technology* 54(3): 954–966.
88. Kansanen K & Matsumoto T (2005) Frequency-domain MMSE turbo equalization – convergence in fading channels. *IEEE Transactions on Wireless Communications*, submitted Also available at <http://www.ee.oulu.fi/%7ekmo>.
89. Kansanen K, Matsumoto T, Schneider C & Thomä R (2005) Frequency-domain MMSE turbo equalization of multilevel coded QAM – convergence in real fields. In Proc. IEEE International Symposium on Personal, Indoor, and Mobile Radio Communications (PIMRC), Berlin, Germany.
90. Kansanen K & Matsumoto T (2005) Frequency-domain MMSE turbo equalization – convergence in spatially correlated fading channels. In Proc. International Symposium on Wireless Personal Multimedia Communications (WPMC), Aalborg, Denmark.
91. Wohlgenannt R, Kansanen K, Tujkovic D & Matsumoto T (2005) Outage -based LDPC code design for SC/MMSE turbo equalization. In Proc. IEEE Vehicular Technology Conference (VTC), Stockholm, Sweden.
92. Ng B, Falconer D, Kansanen K & Veselinovic N (2005) Frequency-domain methods for detection and estimation. In 14th IST Mobile & Wireless Communications Summit, Dresden, Germany.
93. Pedersen KI, Andersen JB, Kermaol JP & Mogensen P (2000) A stochastic multiple-input-mobile-output radio channel model for evaluation of space-time coding algorithms. In Proc. IEEE Vehicular Technology Conference (VTC), Boston, USA, 893–897.
94. Kermaol JP, Schumacher L, Pedersen K, Mogensen PE & Frederiksen F (2002) A stochastic MIMO radio channel model with experimental validation. *IEEE Journal on Selected Areas in Communications* 20(6): 1211–1226.
95. Oestges C, Clerckx B, Vanhoenacker-Janvier D & Paulraj A (2005) Impact of fading correlations on mimo communication systems in geometry-based statistical channel models. *IEEE Transactions on Wireless Communications* 4(3): 1112–1120.
96. Özcelik H, Herdin M, Weichselberger W, Wallace J & Bonek E (2003) Deficiencies of "kno-neck" MIMO radio channel model. *IEEE Electronics Letters* 39(16-7): 1209–1210.
97. Biglieri E, Proakis J & Shamai S (1998) Fading channels: Information-theoretic and communications aspects. *IEEE Transactions on Information Theory* 44(6): 2619–2692.
98. Tse DNC & Hanly SV (1998) Multiaccess fading channels. I. polymatroid structure, optimal resource allocation and throughput capacities. *IEEE Transactions on Information Theory* 44(7): 2796–2815.
99. Cheng RS & Verdú S (1993) Gaussian multiaccess channels with ISI: capacity region and multiuser water-filling. *IEEE Transactions on Information Theory* 39(3): 773–785.
100. Goldsmith A (2005) *Wireless Communications*. Cambridge University Press, New York, USA.
101. Arnold D & Loeliger HA (2001) On the information rate of binary-input channels with memory. In Proc. IEEE International Conference on Communications (ICC), Helsinki, Finland, 9: 2692–2695.
102. Pfister H, Soriaga J & Siegel P (2001) On the achievable information rates of finite state ISI channels. In Proc. IEEE Global Telecommunication Conference (GLOBECOM), San Antonio, Texas, USA, 5: 2992–2996.
103. Zhang Z, Duman T & Kurtas E (2004) Achievable information rates and coding for MIMO systems over ISI channels and frequency-selective fading channels. *IEEE Transactions on Communications* 52(10): 1698–1710.
104. Foschini GJ & Gans MJ (1998) On limits of wireless communications in a fading environment when using multiple antennas. *Wireless Personal Communications*, Kluwer Academic Publishers 6: 311–335.
105. Tüchler M & Hagenauer J (2002) EXIT charts of irregular codes. In Proc. Conference on Information Sciences and Systems (CISS), Princeton, USA.

106. Hassibi B (2000) An efficient square-root algorithm for BLAST. In Proc. IEEE International Conference on Acoustics, Speech, and Signal Processing (ICASSP), Istanbul, Turkey, 2: 737–740.
107. Hassibi B (2000) An fast square-root algorithm for BLAST. In Proc. Annual Asilomar Conference on Signals, Systems and Computers, Asilomar, USA, 2: 1255–1259.
108. Benesty J, Huang Y & Chen J (2003) A fast recursive algorithm for optimum sequential signal detection in a BLAST system. *IEEE Transactions on Signal Processing* 51(7): 1722–1730.
109. Zhu H, Lei Z & Chin F (2004) An improved square-root algorithm for BLAST. *IEEE Signal Processing Letters* 11(9): 772–775.
110. Haykin S (1996) *Adaptive Filter Theory*. Prentice Hall, Upper Saddle River, NJ, USA, 3rd ed.
111. Golub GH & Loan CFV (1996) *Matrix Computations*, 3rd ed. The Johns Hopkins University Press, Baltimore.
112. Malkamäki E & Leib H (1999) Evaluating the performance of convolutional codes over block fading channels. *IEEE Transactions on Information Theory* 45(5)(5): 1643–1646.
113. Monfet F, Le-Ngoc T & Zhang Q (2004) Turbo equalization using frequency-domain shortening filter for broadband single-carrier transmission over frequency-selective fading channels. In Proc. IEEE Vehicular Technology Conference (VTC), Milan, Italy, 2: 1059–1062.
114. Bauch G & Al-Dhahir N (2002) Reduced-complexity space-time turbo equalization for frequency selective MIMO channels. *IEEE Transactions on Wireless Communications* 1(4): 819–828.
115. Walzman T & Schwartz M (1973) Automatic equalization using the discrete frequency domain. *IEEE Transactions on Information Theory* 19(1): 59–60.
116. Clark M (1998) Adaptive frequency-domain equalization and diversity combining for broadband wireless communications. *IEEE Journal on Selected Areas in Communications* 16(8): 1385–1395.
117. Pancaldi F & Vitetta GM (2005) Block channel equalization in the frequency-domain. *IEEE Transactions on Communications* 53(3): 463–471.
118. Laot C, Bidan RL & Leroux D (2005) Low-complexity MMSE turbo equalization: A possible solution for EDGE. *IEEE Transactions on Wireless Communications* 4(3): 965–974.
119. Al-Dhahir N (2001) Single-carrier frequency-domain equalization for space-time-coded transmissions over broadband wireless channels. In Proc. IEEE International Symposium on Personal, Indoor, and Mobile Radio Communications (PIMRC), 1: 143–146.
120. Schniter P & Liu H (2004) Iterative frequency-domain equalization for single-carrier systems in doubly-dispersive channels. In Proc. Annual Asilomar Conference on Signals, Systems and Computers, Pacific Grove, USA, 667–671.
121. Otnes R & Tüchler M (2001) Block SISO linear equalizers for turbo equalization in serial-tone HF modems. In Proceedings of the IEEE Nordic Signal Processing Symposium, 93–98.
122. Proakis JG (2000) *Digital Communications*. McGraw-Hill, New York, 4th ed.
123. Witzke M, Bairo S & Hagenauer J (2003) Iterative detection of generalized coded MIMO signals using a widely linear detector. In Proc. IEEE Global Telecommunication Conference (GLOBECOM), San Francisco, USA, 4: 1821–1825.
124. Gerstacker WH, Schober R & Lampe (2003) Receivers with widely linear processing for frequency-selective channels. *IEEE Transactions on Communications* 51(9): 1512–1523.
125. Tulin AM & Verdú S (2001) Asymptotic analysis of improved linear receivers for BPSK-CDMA subject to fading. *IEEE Journal on Selected Areas in Communications* 51(8): 1544–1555.
126. Ramon V & Vandendorpe L (2005) Predicting the performance and convergence behavior of a turbo-equalization scheme. In Proc. IEEE International Conference on Acoustics, Speech, and Signal Processing (ICASSP), Philadelphia, USA, 3: 709–712.
127. ten Brink S, Kramer G & Ashikhmin A (2004) Design of low-density parity-check codes for modulation and detection. *IEEE Transactions on Communications* 52(4): 670–678.
128. Brännström F, Rasmussen LK & Grant A (2004) Optimal puncturing for multiple parallel concatenated codes. In Proc. IEEE International Symposium on Information Theory (ISIT), Chicago, USA, 154.
129. Cover TM & Thomas JA (1991) *Elements of Information Theory*. John Wiley, New York, USA.

130. Lee J & Blahut R (2004) Lower bound on BER of finite-length turbo codes based on EXIT characteristics. *IEEE Communications Letters* 8(4): 238 – 240.
131. Brännström F (2004) Convergence analysis and design of multiple concatenated codes. Ph.D. thesis, Chalmers University of Technology, Gothenburg, Sweden.
132. Caire G, Guemghar S, Roumy A & Verdú S (2004) Maximizing the spectral efficiency of coded CDMA under successive decoding. *IEEE Transactions on Information Theory* 50(1): 152–164.
133. Richardson T & Urbanke R (2001) The capacity of low-density parity-check codes under message-passing decoding. *IEEE Transactions on Information Theory* 47(2): 599–618.
134. Kreyszig E (1993) *Advanced Engineering Mathematics*, 7th ed. John Wiley & Sons, New York.
135. Wachsmann U, Fischer R & Huber J (1999) Multilevel codes: theoretical concepts and practical design rules. *IEEE Transactions on Information Theory* 45(5): 1361–1391.
136. Ungerboeck G (1982) Channel coding with multilevel/phase signals. *IEEE Transactions on Information Theory* 28(1): 55–67.
137. Horn R & Johnson C (1985) *Matrix Analysis*. Cambridge University Press, Cambridge, United Kingdom.
138. Li X & Ritcey JA (1999) Trellis-coded modulation with bit interleaving and iterative decoding. *IEEE Journal on Selected Areas in Communications* 17(4): 715–724.
139. 3rd Generation Partnership Project (3GPP); Technical Specification Group Radio Access Network (2002) Multiplexing and channel coding (FDD) (3G TS 25.212 version 5.0.0). Tech. rep., 3rd Generation Partnership Project (3GPP).
140. Ge X, Eppstein D & Smyth P (2001) The distribution of loop lengths in graphical models for turbo decoding. *IEEE Transactions on Information Theory* 47(6): 2549–2553.
141. Dammann A & Kaiser S (2001) Standard conformable antenna diversity techniques for OFDM and its application to the DVB-T system. In *Proc. IEEE Global Telecommunication Conference (GLOBECOM)*, 5: 3100–3105.
142. Dammann A & Kaiser S (2002) Transmit/receive antenna diversity techniques for OFDM systems. *European Transactions on Telecommunications* 13(5): 531–538.
143. Wohlgenannt R (2003) Design of low-density parity-check codes using extrinsic information transfer charts. Master's thesis, Vienna University of Technology.
144. Brännström F, Rasmussen LK & Grant AJ (2005) Convergence analysis and optimal scheduling for multiple concatenated codes. *IEEE Transactions on Information Theory* 51(9): 3354–3364.
145. Gallager R (1963) *Low-Density Parity-Check Codes*. MIT Press, Cambridge, USA.
146. Vitthaladevuni P & Alouini MS (2003) A recursive algorithm for the exact BER computation of generalized hierarchical QAM constellations. *IEEE Transactions on Information Theory* 49(1): 297–307.
147. Imai H & Hirakawa S (1977) A new multilevel coding method using error correcting codes. *IEEE Transactions on Information Theory* 23(3): 371–377.
148. Thomä R, Hampicke D, Richter A, Sommerkorn G & Trautwein U (2001) MIMO vector channel sounder measurement for smart antenna system evaluation. *European Transactions on Telecommunications* 12(5): 427–438.
149. Schneider C, Trautwein U, Matsumoto T & Thomä R (2003) Dependency of turbo MIMO equalizer performances on spatial and temporal multipath channel structure - a measurement based evaluation. In *Proc. IEEE Vehicular Technology Conference (VTC)*, Jeju, Korea, 2: 808–812.
150. Trautwein U, Matsumoto T, Schneider C & Thomä R (2002) Exploring the performance of turbo MIMO equalizer in real field scenarios. In *Proc. International Symposium on Wireless Personal Multimedia Communications (WPMC)*, Honolulu, Hawaii, 2: 422–426.
151. Lin S & Costello D (1983) *Error Control Coding*. Prentice-Hall, Englewood Cliffs, NJ, USA.

## Square-root updating of the MMSE turbo equalizer

First, the section of the inverse matrix  $\mathbf{U}(n)$  given by (63) is expressed through its factorization as

$$\begin{pmatrix} u_p & \mathbf{u}_p^H \\ \mathbf{u}_p & \mathbf{U}_p \end{pmatrix} \quad (\text{A1.239})$$

$$= \begin{pmatrix} \omega_p & \mathbf{0}^H \\ \omega_p & \mathbf{\Omega}_p \end{pmatrix} \begin{pmatrix} \omega_p^* & \omega_p^H \\ \mathbf{0} & \mathbf{\Omega}_p^H \end{pmatrix} \quad (\text{A1.240})$$

$$= \begin{pmatrix} \omega_p \omega_p^* & \omega_p \omega_p^H \\ \omega_p \omega_p^* & \omega_p \omega_p^H + \mathbf{\Omega}_p \mathbf{\Omega}_p^H \end{pmatrix}. \quad (\text{A1.241})$$

By finding the terms of (63) from (A1.241), the update in (65) is given in terms of the factorization

$$\bar{\mathbf{\Omega}} \bar{\mathbf{\Omega}}^H = \omega_p \omega_p^H + \mathbf{\Omega}_p \mathbf{\Omega}_p^H - \frac{\omega_p \omega_p \omega_p^* \omega_p^H}{\omega_p \omega_p^*} \quad (\text{A1.242})$$

$$= \mathbf{\Omega}_p \mathbf{\Omega}_p^H \quad (\text{A1.243})$$

As one notes,  $\mathbf{\Omega}_p$  can be extracted by simply dropping the first row and column of  $\mathbf{W}_p$  giving (73). The components of the inverse covariance matrix for the next time instant are expressed with the components of the inverse factorization as

$$\begin{pmatrix} \mathbf{U}_f & \mathbf{u}_f \\ \mathbf{u}_f^H & u_f \end{pmatrix} \quad (\text{A1.244})$$

$$= \begin{pmatrix} \mathbf{\Omega}_f & \mathbf{0} \\ \omega_f^H & \omega_f^* \end{pmatrix} \begin{pmatrix} \mathbf{\Omega}_f^H & \omega_f \\ \mathbf{0}^H & \omega_f \end{pmatrix}$$

$$= \begin{pmatrix} \mathbf{\Omega}_f \mathbf{\Omega}_f^H & \mathbf{\Omega}_f \omega_f \\ \omega_f^H \mathbf{\Omega}_f^H & \omega_f^H \omega_f + \omega_f^* \omega_f \end{pmatrix}. \quad (\text{A1.245})$$

With these, a factorization that fulfills the recursion update equations (66),(67) and (68), expressed in terms of the factorization as

$$u_f = \left( \sigma_f - \sigma_f^H \bar{\Omega} \bar{\Omega}^H \sigma_f \right)^{-1} \quad (\text{A1.246})$$

$$\mathbf{u}_f = -u_f \bar{\Omega} \bar{\Omega}^H \sigma_f \quad (\text{A1.247})$$

$$\Omega_f \Omega_f^H = \bar{\Omega} \bar{\Omega}^H + u_f \bar{\Omega} \bar{\Omega}^H \sigma_f \sigma_f^H \bar{\Omega} \bar{\Omega}^H, \quad (\text{A1.248})$$

must be derived. In (A1.246),  $u_f$  is defined, and then  $\mathbf{u}_f$  in (A1.247). The equation for the matrix  $\Omega_f$  is derived from (68) as in (A1.248). With these expressions, a pre- and a post-array that fulfill the matrix factorization lemma [110, p. 590] are defined as

$$\begin{pmatrix} \bar{\Omega} & -\sqrt{u_f} \bar{\Omega} \bar{\Omega}^H \sigma_f \\ \mathbf{0}^H & \sqrt{u_f} \end{pmatrix} \quad (\text{A1.249})$$

$$\times \begin{pmatrix} \bar{\Omega} & \mathbf{0} \\ -\sqrt{u_f} \bar{\Omega} \bar{\Omega}^H \sigma_f \sigma_f^H \bar{\Omega}^H & \sqrt{u_f} \end{pmatrix} \quad (\text{A1.250})$$

$$= \begin{pmatrix} \Omega_f & \mathbf{0} \\ \omega_f^H & \omega_f^* \end{pmatrix} \begin{pmatrix} \Omega_f^H & \omega_f \\ \mathbf{0}^H & \omega_f \end{pmatrix} \quad (\text{A1.251})$$

$$= \mathbf{W}_f \mathbf{W}_f^H. \quad (\text{A1.252})$$

The pre-array can be converted into the post-array through a sequence of unitary rotations and, thus, compute  $\mathbf{W}_f$ . In (A1.249) the rotations  $\Theta$  should be defined to annihilate all but the last element in the last column of the pre-array, while preserving the triangular structure of the array. Unitary Givens rotations are a standard tool to perform this operation. It should be noted that the square root of (A1.246) can produce an unwanted imaginary element into the last diagonal position of the pre-array, the rotation matrix  $\Theta_p$  should be defined to produce a real element on the diagonal by utilizing an additional rotation. As a summary, the factorization of the new covariance matrix inverse can be computed with the rotation matrix  $\Theta$  as

$$\mathbf{W}_f = \begin{pmatrix} \bar{\Omega} & -\sqrt{u_f} \bar{\Omega} \bar{\Omega}^H \sigma_f \\ \mathbf{0}^H & \sqrt{u_f} \end{pmatrix} \Theta. \quad (\text{A1.253})$$

## Convergence set

For transmission  $k$ , the iterations begin with no prior information. In a  $K$ -dimensional system, this is expressed as the  $K - 1$ -dimensional set

$$\mathcal{C}_k^0 = \{\mathbf{I}_d \in \mathbb{E}^{K-1}, I_{d,k} = 0\} \subset \mathbb{E}^K. \quad (\text{A2.254})$$

Correspondingly, a successful decoding of transmission  $k$  is equivalent to reaching the  $K - 1$ -dimensional set

$$\mathcal{C}_k^1 = \{\mathbf{I}_d \in \mathbb{E}^{K-1}, I_{d,k} = 1\} \subset \mathbb{E}^K. \quad (\text{A2.255})$$

The convergence constraint set of each transmission  $k$  is defined by

$$\tilde{\mathcal{C}}_k = \{\mathbf{I}_d \in \mathbb{E}^2, f_{e,k}(\mathbf{I}_d) > f_{d,k}(I_{d,k})\} \subset \mathbb{E}^K, \quad (\text{A2.256})$$

which constitutes the “tunnel” between the equalizer and the decoder EXIT functions. The  $k$  constraints defined by (A2.256) for each  $k$  define the subset of  $\mathbb{E}^K$  which the iterative process can reach. For the successful equalization and detection of transmission  $k$  there must exist a connected set

$$\mathcal{C}_k = \{\mathcal{C}_k^0 \cup \mathcal{C}_k^1 \cup \tilde{\mathcal{C}}_k\}. \quad (\text{A2.257})$$

For the successful equalization and decoding of *all* transmissions, there must be a set defined by (A2.257) for each  $k$ .

The detection begins with no prior information on any transmission and ends with full prior information on all transmissions. These are represented by the points

$$\mathcal{C}^0 = \{\mathbf{I}_d = \mathbf{0}^K\} \quad (\text{A2.258})$$

$$\mathcal{C}^1 = \{\mathbf{I}_d = \mathbf{1}^K\}. \quad (\text{A2.259})$$

However, there is no guarantee of reaching the points in the full set of  $\mathcal{C}_k^0$  for any  $k$  (except for the point  $\mathcal{C}^0$ ), unless it is permitted by some of the  $\tilde{\mathcal{C}}_k$ . If all the  $k$  sets  $\tilde{\mathcal{C}}_k$  are disconnected from  $\mathcal{C}^0$ , no convergence can take place. Thus, at least one  $\tilde{\mathcal{C}}_{k'}$  for some  $k'$  must be connected to  $\mathcal{C}^0$ . If further convergence is to take place, there must be another  $\tilde{\mathcal{C}}_k$  which is

connected to  $\mathcal{C}^0 \cup \tilde{\mathcal{C}}_{k'}$  and so on. Thus, for a successful convergence and decoding of all transmissions and reaching  $\mathcal{C}^1$ , the union

$$\mathcal{C}^0 \cup \mathcal{C}^1 \bigcup_{k=1}^K \tilde{\mathcal{C}}_k \tag{A2.260}$$

must be a connected set.

## 1st derivative of eigenvalues

The vector of eigenvalues of the sum of hermitian matrices  $\mathbf{C} = (1 - a)\mathbf{A}\mathbf{A}^H + \mathbf{B}\mathbf{B}^H$ , where  $a \in [0, 1]$  is a real scalar, has the first derivative

$$\frac{d\zeta(\mathbf{C})}{da} = \lim_{\Delta a \rightarrow 0} \frac{\zeta(\mathbf{C} - \Delta a \mathbf{A}\mathbf{A}^H) - \zeta(\mathbf{C})}{\Delta a} \quad (\text{A3.261})$$

$$= - \lim_{\Delta a \rightarrow 0} \frac{\zeta(\mathbf{C} + \Delta a \mathbf{A}\mathbf{A}^H) - \zeta(\mathbf{C})}{\Delta a}, \quad (\text{A3.262})$$

which can be bounded from below by

$$\frac{d\zeta(\mathbf{C})}{da} \geq - \lim_{\Delta a \rightarrow 0} \frac{\Delta a \max\{\zeta(\mathbf{A}\mathbf{A}^H)\}}{\Delta a} \quad (\text{A3.263})$$

$$= - \max\{\zeta(\mathbf{A}\mathbf{A}^H)\}, \quad (\text{A3.264})$$

and from above by

$$\frac{d\zeta(\mathbf{C})}{da} \leq - \lim_{\Delta a \rightarrow 0} \frac{\Delta a \min\{\zeta(\mathbf{A}\mathbf{A}^H)\}}{\Delta a} \quad (\text{A3.265})$$

$$= - \min\{\zeta(\mathbf{A}\mathbf{A}^H)\}. \quad (\text{A3.266})$$

If  $\mathbf{A}$  and  $\mathbf{B}$  commute, i.e., they have the same eigenbasis, then  $\mathbf{C}$  has the eigenvalues

$$\zeta(\mathbf{C}) = (1 - a)\zeta(\mathbf{A}\mathbf{A}^H) + \zeta(\mathbf{B}\mathbf{B}^H), \quad (\text{A3.267})$$

so that

$$\frac{d\zeta(\mathbf{C})}{da} = -\zeta(\mathbf{A}\mathbf{A}^H). \quad (\text{A3.268})$$

## Maximum sum rate path

Consider an arbitrary point  $\mathbf{I}'_d \in \mathbb{E}^2$  and the corresponding points  $\mathbf{f}_e(\mathbf{I}'_d)$ . Two tangent planes can be defined for the EXIT functions, defined by the Jacobian

$$\mathbf{J} = \frac{\partial \mathbf{f}_e}{\partial \mathbf{I}_d} \quad (\text{A4.269})$$

$$= \begin{bmatrix} \frac{\partial f_{e,1}}{\partial I_{d,1}} & \frac{\partial f_{e,1}}{\partial I_{d,2}} \\ \frac{\partial f_{e,2}}{\partial I_{d,1}} & \frac{\partial f_{e,2}}{\partial I_{d,2}} \end{bmatrix}. \quad (\text{A4.270})$$

In Fig. 68, the following definition is made for the direction vector

$$\mathbf{a} = [a_1, a_2] \quad (\text{A4.271})$$

$$\mathbf{a}^T \mathbf{a} = 1 \quad (\text{A4.272})$$

and the following distances are defined

$$d_{1,1} = a_1 |dg_p| \frac{\partial g_p}{\partial I_{d,1}} \quad (\text{A4.273})$$

$$d_{1,2} = a_2 |dg_p| \frac{\partial g_p}{\partial I_{d,2}}. \quad (\text{A4.274})$$

The incremental increase in  $R_1$  can then be expressed as

$$dR_1 = \frac{1}{2} |dg_p|^2 a_1 \left( a_1 \frac{\partial f_{e,1}}{\partial I_{d,1}} + a_2 \frac{\partial f_{e,1}}{\partial I_{d,2}} \right), \quad (\text{A4.275})$$

and an equivalent expression for the incremental increase in  $R_2$  is given by

$$dR_2 = \frac{1}{2} |dg_p|^2 a_2 \left( a_1 \frac{\partial f_{e,2}}{\partial I_{d,1}} + a_2 \frac{\partial f_{e,2}}{\partial I_{d,2}} \right). \quad (\text{A4.276})$$

The sum rate function to be maximised is defined by

$$R(\mathbf{a}) = \frac{1}{2} |dg_p|^2 \mathbf{a}^T \frac{\partial \mathbf{f}_d}{\partial \mathbf{I}_d} \mathbf{a}. \quad (\text{A4.277})$$

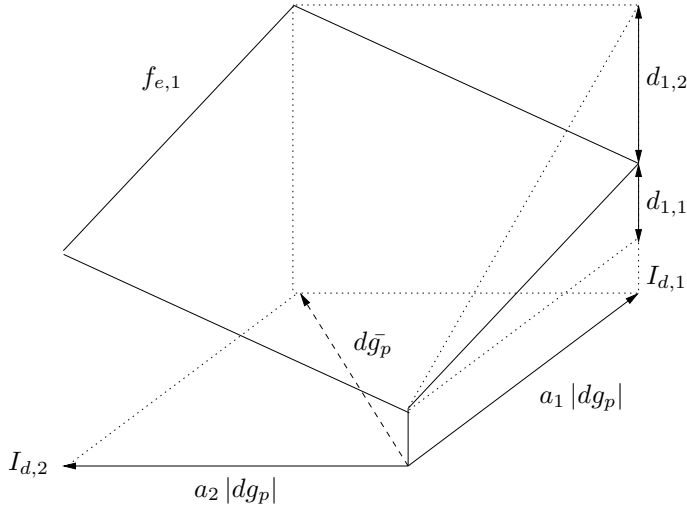


**Fig. 68.** Tangent plane of EXIT function  $f_{e,1}(I'_d)$ .

The quadratic form (A4.277) assumes its maximum value for the two equivalent forms

$$\mathbf{a}^T \mathbf{J} \mathbf{a} = \frac{1}{2} \mathbf{a}^T (\mathbf{J} + \mathbf{J}^T) \mathbf{a}, \quad (\text{A4.278})$$

and the path direction vector of the maximum sum rate increment is given by the eigenvector corresponding to the maximum eigenvalue of the (symmetric) Jacobian. The maximum sum rate path resulting in the optimal code design follows the eigenvector of the maximum Jacobian eigenvalue, starting from the point  $\{0, 0\}$  and finishing at the point  $\{1, 1\}$ .

In the generic case of  $K$  transmissions, each rate increment can be extended into

$$dR_k = \frac{1}{2} |dg_p|^2 a_k \left( \sum_{k'=1}^K a_{k'} \frac{\partial f_{e,k}}{\partial I_{d,k'}} \right), \quad (\text{A4.279})$$

and the corresponding point-wise sum rate maximiser expression is given by the already generic expression (A4.277). Geometrically, the eigenvalue following the optimal path steers the path towards the highest slope of the EXIT function, i.e., the highest turbo gain.

Two special cases are of special interest. Firstly, when the diagonal elements of the Jacobian are all equal, the eigenvalues of the (symmetric) Jacobian are all equal, and the optimal direction vector has its length evenly distributed to all  $K$  directions. In the two-by-two case, the optimal path is given by the diagonal  $g_d$ , the optimal rate allocation gives  $R_1 = R_2$ , and the points A and B in Fig. 24 have equal sum rates. Secondly, an optimal direction pointing to a single direction is possible when  $\mathbf{a} = [a_1, 0, \dots, 0]^T$ , so that

$$\mathbf{J} \mathbf{a} = \zeta (\mathbf{J}) \mathbf{a}, \quad (\text{A4.280})$$

which is equivalent to

$$a_1 \mathbf{J} = \zeta(\mathbf{J}) \mathbf{a}. \quad (\text{A4.281})$$

In the above  $\mathbf{J}$  can be considered to be the symmetric Jacobian, so that (A4.281) implies the first Jacobian row and column must contain zeros except for the diagonal term. In practice, such a situation where prior knowledge of a transmission does not have any effect on the detection of other transmissions is when the transmissions in question are orthogonal or otherwise non-interfering. The latter case is realized when full prior information is available of a signal, and its effect can be totally removed. Furthermore, a zero component  $a_k$  in the optimal direction vector implies the corresponding row sum of off-diagonal elements of the Jacobian is zero, i.e.,

$$\sum_{\substack{k'=1 \\ k \neq k'}}^K \frac{\partial f_{e,k}}{\partial I_{e,k'}} = 0, \quad (\text{A4.282})$$

but since all the Jacobian elements are non-negative, (A4.282) means all the off-diagonal terms must be zero and the orthogonality result between the transmission  $k$  and the other transmissions follows.